DAG BJERKETVEDT

RE-INITIATION OF DETONATION ACROSS AN INERT REGION

NTH
UNIVERSITETET I TRONDHEIM
NORGES TEKNISKE HØGSKOLE

N-7034 Trondheim-NTH Norway

Telephone: (+ 47 7) 593720 Telex: 55637 NTHAD-N
Telefax   : (+ 47 7) 935550 (att : Termisk energi)

Title of report	Date
RE-INITIATION OF DETONATION ACROSS AN INERT REGION	Aug. 1985
	No. of pages/appendices 230

Author(s)	Prosject manager (sign.)
Dag Bjerketvedt	O.K. Sønju

Division	Thermal Energy Division / Mechanical Engineering Department	Project no. —

ISBN no.

Client/sponsor of project	Clients ref.
Dr. Ing. Thesis	—

Abstract Re-initiation of gaseous C-J detonation waves across a region of air has been studied experimentally. The experimental apparatus consisted of a 9 meter long square tube with internal dimensions of 125 mm. The Random Choice Method (RCM) was used to predict the non-isentropic expansion behind a detonation wave and the shock transmission into an inert gas. Good agreement between numerical and experimental results was obtained. With an inert air gap of 0.1-0.2 m, detonation re-initiation occured in acetylene-air. However, under similar conditions detonation failed to re-initiate in ethylen-air. The re-initiation process did not occur instantaneously, but was characterized by a delay. The governing parameters for re-initiation were the C-J properties in the donor section, width of the inert region and the reactivity of the gas mixture in the acceptor section. The re-initiation process was also influenced by the sharpness of the inert region boundary, heat transfer and friction to the tube wall and by some other wall efect, likely due to soot on the tube wall.

Indexing terms: English	Norwegian
Explosion	Eksplosjon
Gas Detonation	Gass-detonasjon
Re-initiation	Transmisjon
Inert Gas Region	Inert gass-sone
Extinction of Detonation	Stopping av detonajon

Key terms selected by author(s)

Division Director O.K. Sønju

RE-INITIATION OF DETONATION ACROSS AN INERT REGION

by

Dag Bjerketvedt

**A thesis submitted to
the Norwegian Institute of Technology
for the degree of**

Doctor Ingeniør

August 1985

Revised version

Division of Heat and Combustion Engineering
Norwegian Institute of Technology
Trondheim, Norway

ABSTRACT

Re-initiation of gaseous C-J detonation waves across a
region of air has been studied experimentally. The
experimental apparatus consisted of a 9 meter long square
tube with internal dimensions of 125 mm. The Random Choice
Method (RCM) was used to predict the non-isentropic
expansion behind a detonation wave and the shock
transmission into an inert gas. Good agreement between
numerical and experimental results was obtained. With an
inert air gap of 0.1-0.2 m, detonation re-initiation
occurred in acetylene-air . However under similar
conditions detonation failed to re-initiate in ethylen-air
. The re-initiation process did not occur instantaneously,
but was characterized by a delay. The governing parameters
for re-initiation were the C-J properties in the donor
section, width of the inert region and the reactivity of the
gas mixture in the acceptor section. The re-initiation
process was also influenced by the sharpness of the inert
region boundary, heat transfer and friction to the tube wall
and by some other wall effects, likely due to soot on the
tube wall.

ACKNOWLEDGEMENTS

TABLE OF CONTENTS

7   REFERENCES

8   APPENDICIES

    A : Nomenclature
    B : Riemann Problem.
    C : Mixing at the Inert Region Boundary.
    D : Wave Interaction with the Interfaces.
    E : Use of Data Reduction Programs
    F : List of Experimental Results.

TABLES   **PAGE**

CHAPTER 1

INTRODUCTION

1.1   BACKGROUND

Accidental gas explosions such as that at Flixborough in
1974 shows the seriousness of such incidents. At
Flixborough a process plant was destroyed and 28 people were
killed. The losses were estimated at £36 million (Langseth,
1980).

The increase in the frequency of accidental explosions over
the past decades and the potential for accidents such as
that at Flixborough have made society conscious of the
danger associated with handling, storing and transporting
large quantities of potentially explosive fuels. As a
result, great efforts are being made to lower the hazard
potential. To lower the frequency and the impact of gas
cloud explosions in the future a better theoretical and
practical understanding of the phenomena involved is
required.

Detonation of gas clouds is one area where better
understanding is required. Detonations are the most
devastating form of gas explosions. In many scenarios
detonations have been regarded as not likely to happen.
However, some recent experiments have clearly shown that
occurrence of detonations are much more likely than
previously assumed (Geiger, 1983; Pförtner et al., 1984;
Moen et al., 1985b). The damage potential of a gas cloud is
strongly related to the possibility of initiation and
propagation of a detonation wave in the cloud.

It is therefore important to establish the conditions for detonation to initiate and to propagate. These phenomena are not fully understood at the present time.

Studies of gaseous detonation also have military relevance. Fuel-Air Explosive (FAE) weapons disperse the fuel to create an explosive gas cloud which is subsequently detonated. To protect against such FAE weapons, the conditions for propagation and quenching of detonations must be characterized.

This study is a fundamental study of detonation propagation in gas clouds with concentration variations. Specifically, re-initiation of detonation across an inert region is investigated experimentally and theoretically.
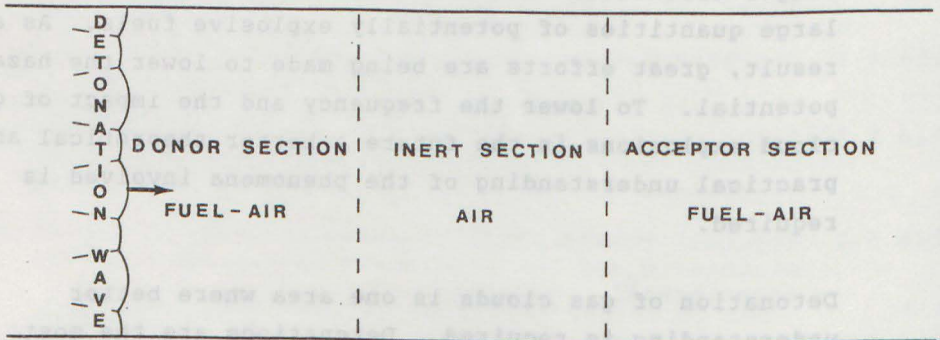
Figure 1.1

Illustration of the geometrical configuration for re-initiation of detonation across and inert region.

The geometrical configuration which is studied in the
present work is illustrated in Figure 1.1. Two sections,
the donor and acceptor sections,both containing a detonable
fuel-air mixture, are separated by a section of air. A
detonation wave is initiated in the donor section. Since
the detonation wave is a supersonic combustion wave, the gas
ahead of the wave is not disturbed. When the detonation
wave reaches the air interface, a shock wave is transmitted
into the inert section. When this shock wave propagates
into the detonable mixture in the acceptor section, the
mixture is ignited, and under certain conditions, the
detonation is re-established.

The aim of this study is to determine the effect of a sudden
disturbance, in the form of an inert region in the cloud, on
the propagation of a detonation wave. The main question to
be answered is, for what conditions will a detonation
transmit through an inert region and re-initiate in a
neighbouring detonable cloud. An experimental study is
required because at the present time the effect of such a
disturbance on a detonation wave cannot be predicted
theoretically.

The present investigation is related to practical situations
such as detonation propagation in a real gas cloud and as
means of stopping detonations. In a real gas cloud there
will be inhomogenities in the fuel concentration due to the
dispersion process. Parts of the cloud will consist of
regions where the mixture is too lean or too rich in fuel to
detonate. These inhomogenities may prevent a detonation
from propagating through the cloud and thereby reduce the
damage potential of the cloud. Although the experiments are
done under idealized conditions and in a simple geometric
configuration, the results are of practical importance. It
is necessary to understand the transmission process under
such idealized conditions in order to be able to determine
the effect of inhomogenities in real clouds.

4577Q

Gas clouds are able to diffuse into installations via
ventilation systems, tunnels, etc. When the gas cloud
detonates, it can destroy the installations by an internal
explosion. One suggested method to stop a detonation in an
installation or other confined situations, is to use an
artifical inert plug. The concept is that the inert plug
stops the detonation so that other more conventional means
such as water sprays can be used to quench the flame. The
present investigation on re-initiation of detonation across
inert regions is directly applicable to this method of
stopping detonations from penetrating protected
installations.

This program started in 1981. An experimental apparatus was
designed based on a proposal from Prof. R.A. Strehlow
(1980). The apparatus was installed in the laboratory of
Division of Heat and Combustion Engineering at The Norwegian
Institute of Technology (NIT) in Trondheim.

1.2   OBJECTIVES

The objectives of this investigation is to study
experimentally re-initiation of detonation using the
configuration shown in Figure 1.1, and then to analyze the
results using numerical and analytical calculations and
empirical correlations.

The investigation is mainly of an experimental nature. The
experiments were performed in a detonation tube and the
experimental conditions were varied by changing the width of
the inert section and the reactivity and detonation
properties of the gas mixture in the donor and acceptor
sections.

To get an overview of the different processes involved in
re-initiation of detonation across an inert region, it is
necessary to characterize the following phenomena; a)
detonation propagation in the donor section, b) transmission
of the shock wave into the inert region and decay of the
shock wave, c) re-establishment of detonation in the
acceptor section. To achieve these objectives, three
different experimental investigations are undertaken:

- detonation propagation in a homogeneous gas mixture,
- detonation propagation into an inert gas,
- re-initiation of detonation across an inert region.

The first two experimental test series are performed in
order to characterize the conditions in the donor section
and the strength of the shock wave entering the neighbouring
explosive cloud. These studies were supported by numerical
and analytical calculations. Detailed comparisons between
experimental results and theoretical calculations provided a
good characterization of the experimental conditions, in
particular the relevant wall effects were determined.

The re-initiation experiments were conducted to establish
the influence of the following parameters on the
re-initiation process:

- Detonation structure and the average properties of
  detonation in the donor section.
- Width of the inert section.
- Reactivity of the gas in the acceptor section.

1.3   ORGANIZATION OF REPORT

In Chapter 2 related literature and previous investigations
are reviewed. Theories and fundamental concept used in this
investigation are analysed, and the requirements for the
present investigation are discussed. The numerical codes
used in this study is described in Chapter 3. The
experimental test facility and test program are described in
Chapter 4. The experimental results are discussed and
compared with numerical results in Chapter 5. Chapter 6
contains the conclusions and recommendations for further
work.

CHAPTER 2

REVIEW OF RELATED MATERIAL AND STRATEGY FOR PRESENT

INVESTIGATION

2.1   INTRODUCTION

The purpose of this chapter is to give a description of the
phenomena involved in re-initiation of detonation across an
inert region based on previous related experiments and known
theories about detonations and further to describe various
definitions and expressions to be used later in this report.

Figure 2.1 shows an illustration of re-initiation of
detonation across an inert region on a time-distance
diagram. The test sections with the different gas mixtures,
as shown in Figure 1.1, are named donor section, inert
section and acceptor section. In a re-initiation
experiment, the donor and acceptor sections are filled with
an explosive fuel-air mixture and the inert section with
pure air. The interface between the donor and inert section
is referred to as Interface I, and the interface between the
inert and acceptor section is referred to as Interface II.

The detonation starts from the origin and propagates with
constant velocity through the donor section. The position
of the detonation front as a function of time is given by
the straight line. The velocity of the detonation is
inversely proportional to the slope of this line. The
nature of the detonation wave and its propagation in the
donor section are described in Sections 2.2 and 2.3,
respectively.
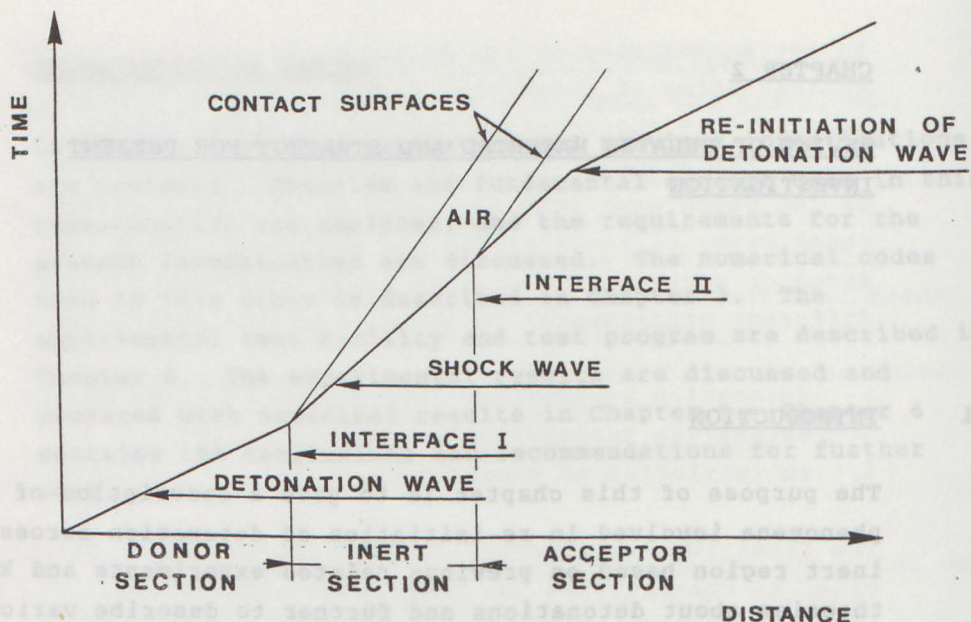
Figure 2.1
Time distance diagram showing the trajectories of the
wave front and contact surfaces for re-initiation of
detonation across an inert region.

When the detonation wave reaches Interface I, the chemical
reaction will end, and a shock wave will transmit into the
inert section. In Section 2.3, the refraction of the
detonation into the inert region and the decay of the shock
wave in the inert section are discussed.

When the shock wave crosses Interface II, the shocked gas is
again chemically reactive. The increase in temperature
caused by shock compression will therefore trigger the
chemical reactions if the shock wave is strong enough.
Depending on the strength of the shock wave, the reactivity
of the gas mixture and the boundary conditions, the
detonation wave may be re-established in the acceptor
section. This means that the chemical reaction zone and the
shock wave couple to form a new detonation wave.

In Section 2.5 a mechanism for onset of detonation is described. This mechanism is relevant to the reinitiation process in the acceptor section.

Section 2.6 gives an overview of previous experiments concerned with detonation transmission across an inert region.

The motivation and investigation strategy for this investigation are discussed in Section 2.7.

2.2   GASEOUS DETONATIONS

This section gives a general description of detonation waves. Properties and expressions used later are defined. Two one dimensional models are described, namely C-J and ZND models. The structure of the detonation wave is discussed and related to other detonability parameters such as critical tube diameter and induction time.

2.2.1   One-dimensional models

The propagation velocity of detonation can be predicted based on the one-dimensional Chapman-Jouguet (C-J) theory. The C-J theory treats the detonation wave as a steady mathematical discontinuity with infinite reaction rate. The conservation equations for mass, momentum and energy across a steady wave gives a unique solution for the detonation velocity, known as the C-J velocity. An approximate expression for the detonation velocity D is (Fickett and Davis, 1979):

$$D = \sqrt{2(\gamma^2-1)Q} \qquad\qquad (2.1)$$

where γ is the ratio of the specific heats and Q the heat of reaction. For stoichiometric fuel-air mixtures, the detonation velocity is about 1800 m/s.

The C-J theory assumes that the detonation velocity is independent of chemical reaction rates and that the chemical energy is released instantaneously. When the wave propagates at C-J velocity, the velocity of the reaction products relative to the wave, is equal to the local speed of sound. The properties of the reaction products are known as C-J properties. Numerical codes are available for calculating the C-J properties (Gordon and McBride, 1976). The pressure ratio across a C-J wave is about 18 for stoichiometric fuel-air. In the C-J solution it is assumed that the wave is not supported from behind. For unsupported detonation waves not influenced by physical boundaries, the measured detonation velocities agree within a few percent with the C-J values (Strehlow, 1984).

For a detonation velocity larger than the C-J velocity, there exists two solutions of the conservation equations, the weak and strong solutions. The strong solutions is also known as an overdriven detonation. The flow behind an overdriven wave is subsonic and the pressure is higher than C-J pressure. The wave is supported from behind. An overdriven detonation is of practical interest, since a detonation is normally overdriven in the first stage after initiation.

The weak solutions gives supersonic velocities behind the wave and the pressure is lower than the C-J pressure. Some experiments indicate that weak solutions exists for unsupported detonation waves (Fickett and Davis, 1979). Since the weak solution is very close to the C-J solution, it is difficult to draw any definite conclusion on the existence of weak detonations from availiable experimental results.

The Zeldovich, von Neumann and Doering model or the ZND model (Zeldovich and Kompaneets, 1960; Strehlow, 1984) describes a detonation wave as a shock wave followed by a reaction zone. The chemical reaction is triggered by the

increas in temperature due to shock compression. This is a
more physically correct view than the assumption of infinite
reaction rate made in the C-J theory. The thickness of the
shock wave is about one mean free path, however, the
chemical reaction requires a large number of collisions to
be completed (Zeldovich and Kompaneets, 1960). The shock
wave propagates at C-J velocity and the pressure behind the
shock wave is known as the von Neumann spike. For
stoichiometric fuel-air the von Neumann spike is about twice
the C-J pressure. The ZND model gives the same solution as
the C-J theory for the detonation velocity and the end state
of reaction products. The only difference between the two
models is the thickness of the wave. The plane where the
reaction is completed and the flow relative to the wave
front is sonic, is called the C-J plane. The thickness of
the wave, the distance from shock wave to the C-J plane,
depends on chemical kinetics of gas mixture. For most
fuel-air mixures, the reaction zone consists of a long
induction zone where pressure and temperature are nearly
constant followed by a short recombination zone where the
chemical energy is released. The structure of the ZND wave
is shown schematically in Figure 2.2.

C-J PLANE   SHOCK WAVE

DIRECTION OF PROPAGATION
OF DETONATION

INDUCTION LENGTH Δ

REACTION ZONE
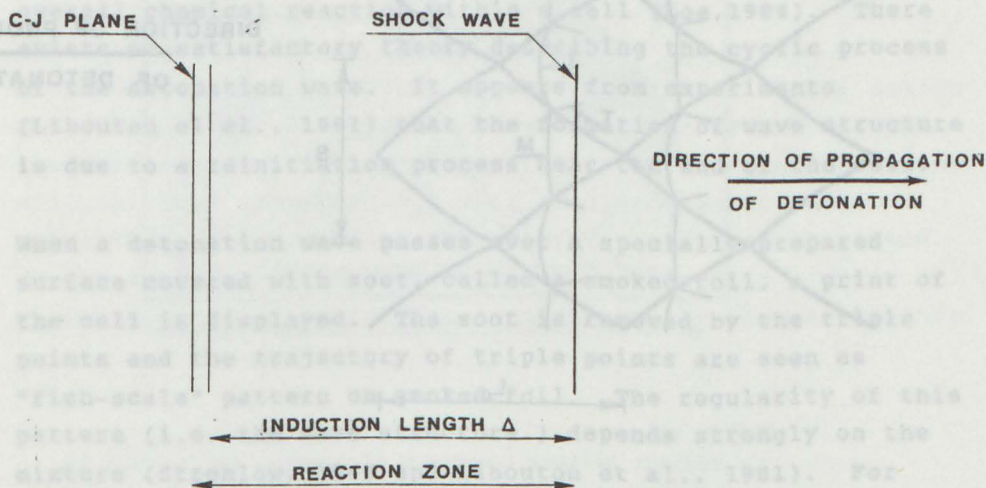
Figure 2.2
Sketch illustrating the ZND-wave structure.

Westbrook and Urtiew (1984) used numerical calculations of
chemical kinetics to calculate induction time τ and the
induction length Δ. They used the ZND model to obtain
post shock condition (von Neumann spike) and assumed
constant volume process over the reaction time. The
induction length ,Δ, can be considered as a characteristic
length scale for the idealized one-dimensional detonation
wave. It decreases with increasing chemical reactivity.

2.2.2   Detonation structure

Experiments have shown that a real detonation wave has a
three-dimensional wave structure. The leading shock
consists of curved shock segments. At the detachment lines
between these shock segments, three shock waves interact in
a Mach stem configuration. The wave structure is
illustrated in Figure 2.3.
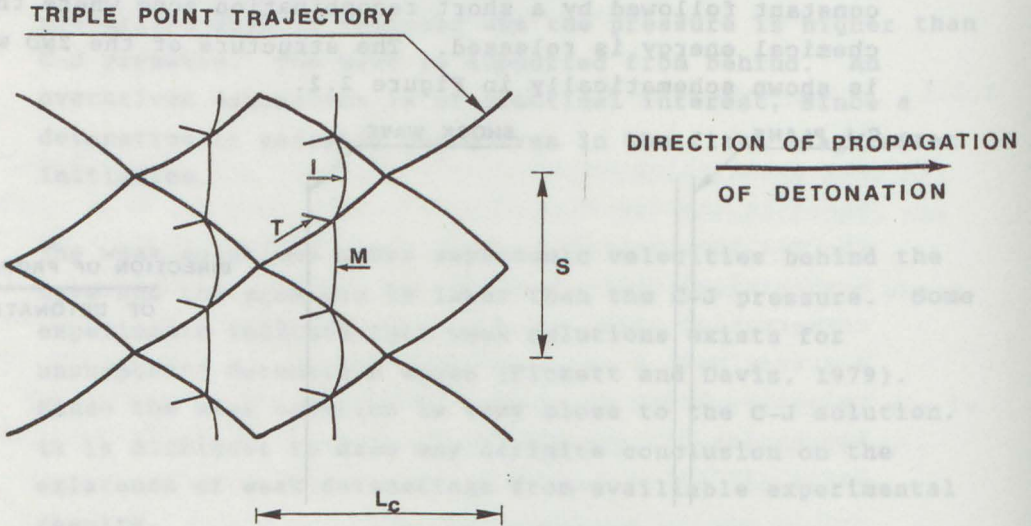
Figure 2.3
2-dimensional illustration of the detonation wave
structure. The incident shocks I, the Mach stems M and
the transverse waves T formes tripel points.

In this two-dimensional illustration, the detachment lines
between shock segments are seen as triple points. The waves
in a Mach stem configuration are the incident shock I, the
Mach stem M and the transverse wave T. The shock segments
have cyclic behaviour. They start out as Mach stems with a
velocity which is initally about 1.6 times the C-J
velocity. As the shock segments move ahead, their strength
decreases and the waves become incident waves. At the end
of a cycle, the wave velocity is about 0.6 times the C-J
velocity (Lee, 1984). The average leading shock velocity is
equal to the C-J velocity. The volume swept over by a shock
segment in one cycle is called a cell. The characteristic
lengths of the cell are the cell size S (i.e., transverse
wave spacing) and the cell length L_c as shown in the
figure.

The cell size is approximately 0.6 times the cell length
(Lee, 1984). The cell size depends on the chemical kinetics
and decrease with increasing reactivity. The induction zone
length,Δ, based on the ZND model, are proportional to the
cell size (Westbrook and Urtiew, 1984). It is likely that
cell size represent a length scale characterizing of the
overall chemical reaction within a cell (Lee,1984). There
exists no satisfactory theory describing the cyclic process
of the detonation wave. It appears from experiments
(Libouton el al., 1981) that the formation of wave structure
is due to a reinitiation process near the end of the cell.

When a detonation wave passes over a specially prepared
surface covered with soot, called a smoked foil, a print of
the cell is displayed. The soot is removed by the triple
points and the trajectory of triple points are seen as
"fish-scale" pattern on smoked foil. The regularity of this
pattern (i.e. the wave structure) depends strongly on the
mixture (Strehlow, 1969 and Libouton et al., 1981). For
fuel-air mixture the wave structure is irregular with a
substructure of weak transverse waves (Moen et al., 1985).

A typical example of a smoke foil with irregular cell
pattern and substructure is shown in Figure 2.4 a) (Moen et
al., 1982). To measure the cell size from irregular cell
patterns involves some judgement, since there is
considerable variations of the cell size on a smoked foil.
Interpretation of a smoked foil record is shown in
Figure 2.4 b)
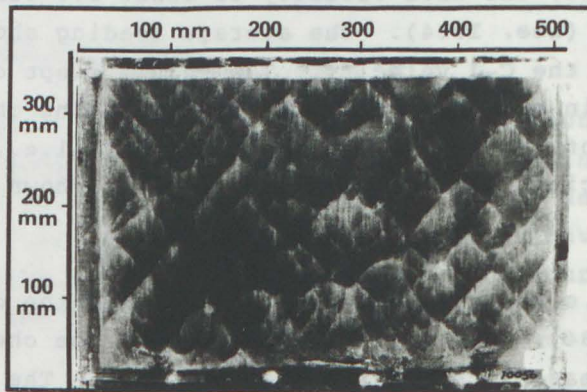
a) SMOKED FOIL RECORD
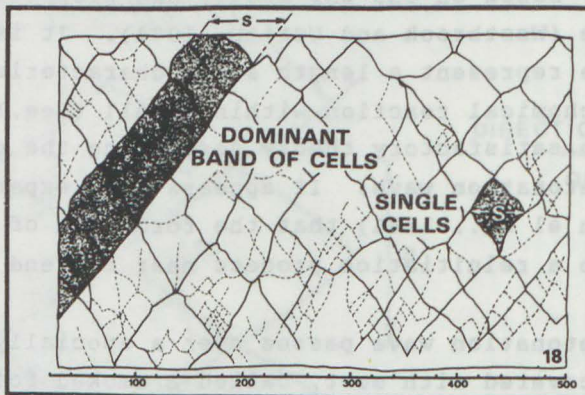
b) INTERPRETATION OF SMOKED FOIL RECORD

Figure 2.4
        Typical celluar structure of detonations in fuel-air
        mixtures (4.6 % C_2H_4-Air).
        a)   Smoked foil record.
        b)   Interpretation of smoked foil record.
             (Moen et al., 1982.)

Figure 2.5 (Moen, 1985) shows cell size measurements in acetylene-air and ethylene-air from several investigations. The cell size is plotted as a function of the equivalence ratio Φ, where Φ is the actual fuel-air ratio divided by the stoichiometric fuel-air ratio. As seen from this figure there, are some scatter in the results. For stoichiometric acetylene-air ($\Phi = 1.0$) the results vary by about a factor of two. This scatter is most likely a result of the method and judgement used by the individual investigators when measuring the cell size from the smoked foil tracks.

Behind the wave front the transverse waves decay and the pressure becomes more uniform. Vasiliev et al. (1971) concluded from their experiments that there exists a sonic plane, i.e., C-J plane behind the the wave front. The C-J plane was found 3-10 cell lengths downstream from the front. Edwards et al. (1976) have investigated the decay of transverse waves behind the wavefront. The oscillation energy of transverse waves dissipated in about 2 to 4 cell lengths. They related this length to the thickness of the wave front.

2.2.3   Critical tube diameter

Previously in this section, two characteristic length scales were introduced; namely, the induction zone length, Δ, and the cell size S. Another characteristical length scale, the critical tube diameter, d_c, will be discussed in this subsection. The critical tube diameter will later be used in the analysis of the experimental results as a characteristic parameter for detonability of the gas mixture.
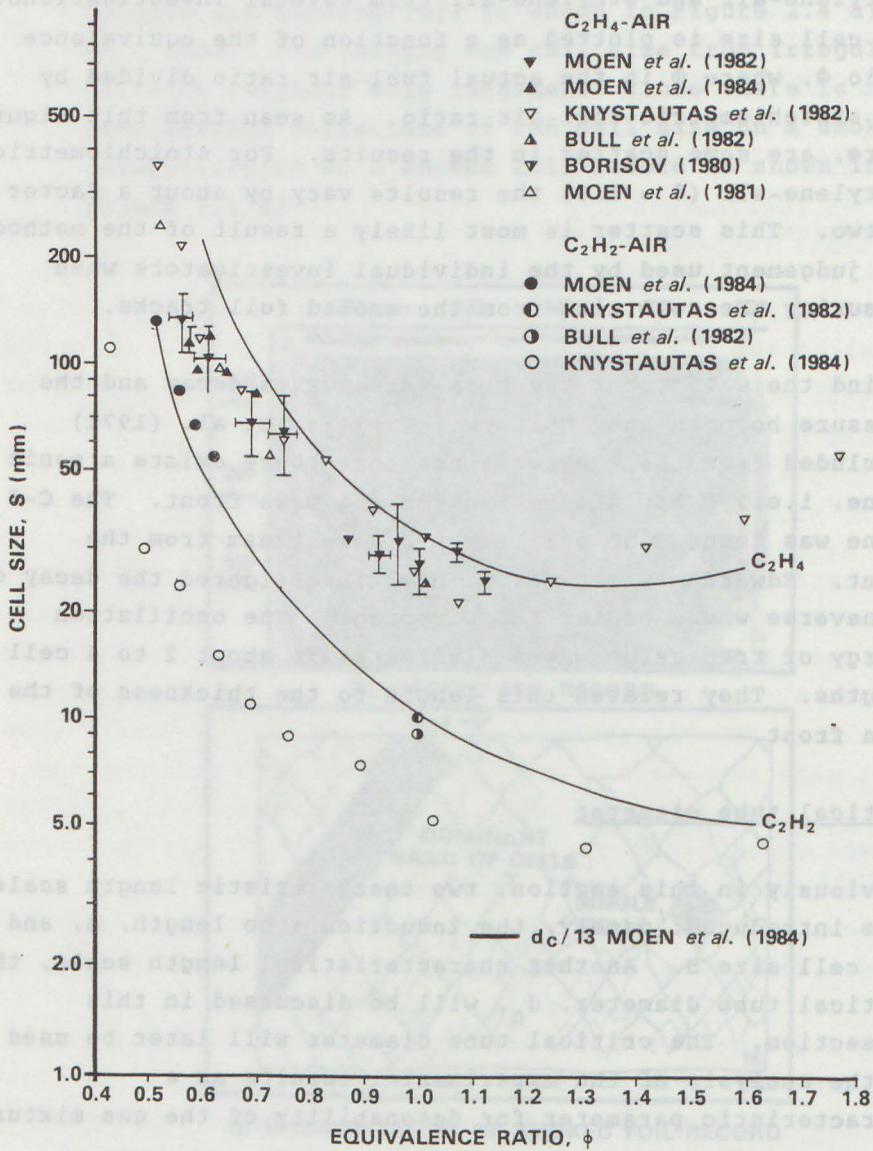
Figure 2.5
Measured cell size, s, versus equivalence ratio, Φ,
for acetylene-air and ethylene-air.
(Moen, 1985.)

The success of transmission of a detonation wave from the
opening of a tube into an unconfined cloud depends on the
gas mixture. The critical tube diameter for a gas mixture
is defined as the smallest tube diameter for which a
detonation wave successfully transmits into an unconfined
cloud from the tube. The critical tube diameter d_c is an
experimental parameter. A typical set-up for a large scale
critical tube experiment is shown in Figure 2.6. The tube
and the plastic bag are filled with the same gas mixture.
The detonation is initiated at the end of the tube and
propagates through the tube and expands into the bag. If
the tube diameter is too small, the detonation wave will not
be re-established in the bag. The shock wave and reaction
zone decouples. For tube diameters equal to or larger than
critical tube diameter d_c, the detonation wave
re-establishes itself as spherical detonation in the bag.

CRITICAL TUBE — D = 0.35 m
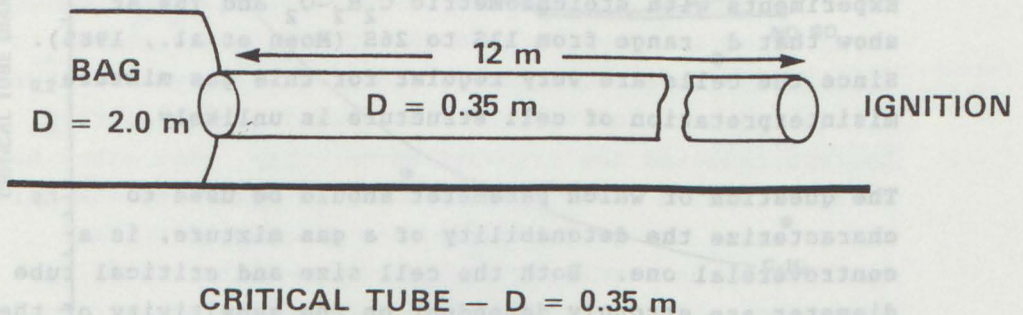
Figure 2.6
Set-up for a large scale critical tube experiment.

Critical tube results for acetylene-air and ethylene-air as a function of the equivalence ratio are shown in Figure 2.7. Acetylene (C_2H_2) which is the more sensitive of the two, has the smallest critical tube diameter. The results are mainly from large scale tests at The Defence Research Establishment Suffield (DRES), Canada (Moen, 1985) and at the Norwegian Defence Construction Service test site at Raufoss, Norway (Jenssen, 1985). These test programs have demonstrated that d_c is a reproducible parameter.

Mitrofanov and Soloukhin (1965) observed that $d_c \simeq 13$ S. Many experimental results (Knystautas et al., 1982 and 1984; Moen et al., 1982; Ungut et al., 1984) agree with this simple empirical correlation. For fuel-air mixtures some discrepancies have been observed (Moen et al., 1984). Some of these discrepancies can be explained by misinterpretation of the cell structure. However, recent results raise some futher questions regarding the 13 S-correlation. Experiments with stoichiometric $C_2H_2-O_2$ and 75% Ar show that d_c range from 13S to 26S (Moen et al., 1985). Since the cells are very regular for this gas mixture misinterpretation of cell structure is unlikely.

The question of which parameter should be used to characterize the detonability of a gas mixture, is a controversial one. Both the cell size and critical tube diameter are strongly dependent on the sensitivity of the gas mixture and represent characteristic length scales. The new observations by Moen et al. (1984 and 1985) indicate that the relationship between these two length scales is not as simple as previously assumed. The cell size seems to be a fundamental property of the detonation (Lee, 1984). The disadvantage of using the cell size is that it is not a well-defined parameter for less sensitive mixtures such as fuel-air mixtures. For the same gas mixture different cell sizes are measured in different investigations.

The critical tube diameter is more reproducible than the cell size and is therefore more practical to use for characterizing and comparing the sensivity of gas mixtures to detonation.
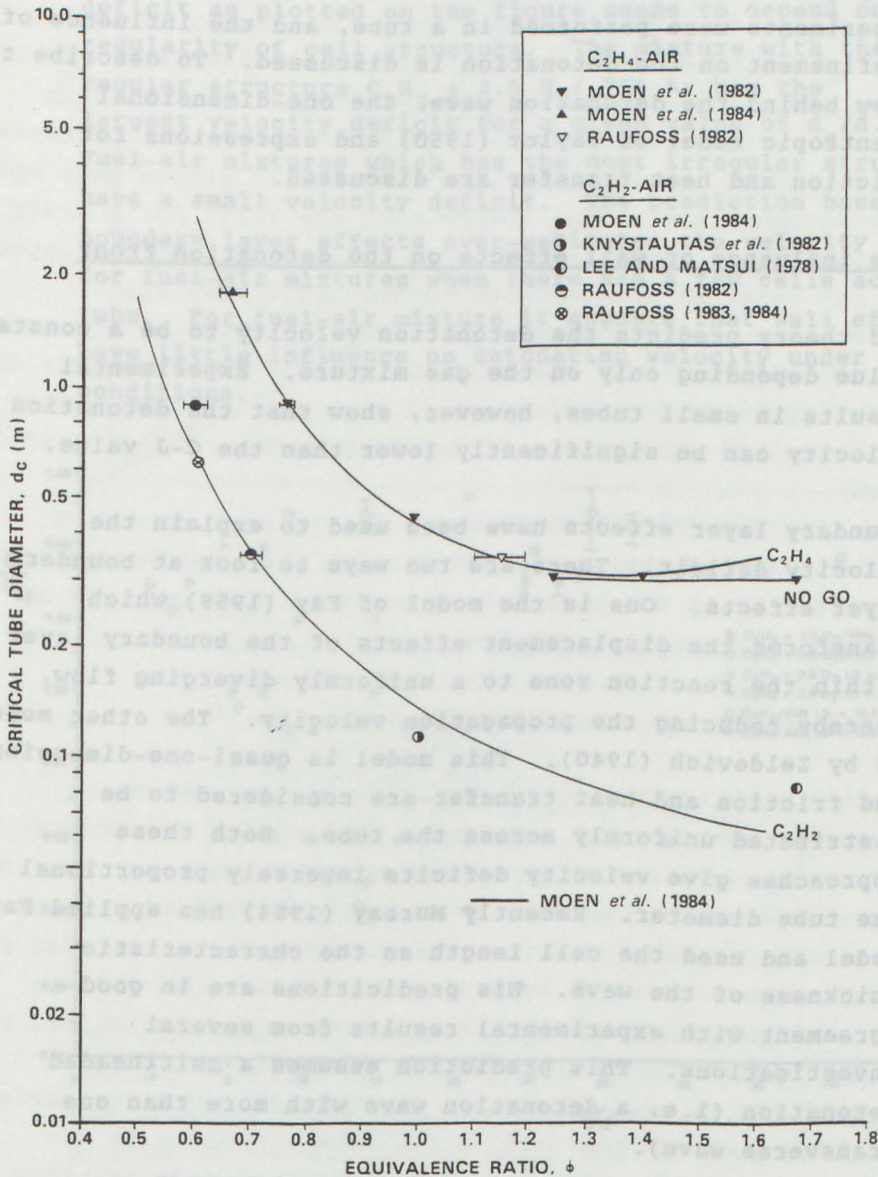
Figure 2.7
Critical tube diameter, d_c, versus the equivalence ratio, ϕ, for acetylene-air and ethylene-air.
(Moen, 1985.)

2.3   DETONATION PROPAGATION AND FLOW IN DONOR SECTION

This section describes the conditions when the detonation
propagates through the donor section. The present
experiments were performed in a tube, and the influence of
confinement on the detonation is discussed. To describe the
flow behind the detonation wave, the one-dimensional
isentropic model of Taylor (1950) and expressions for
friction and heat transfer are discussed.

2.3.1   The influence of wall effects on the detonation front

C-J theory predicts the detonation velocity to be a constant
value depending only on the gas mixture. Experimental
results in small tubes, however, show that the detonation
velocity can be significantly lower than the C-J value.

Boundary layer effects have been used to explain the
velocity deficit. There are two ways to look at boundary
layer effects. One is the model of Fay (1959) which
transforms the displacement effects of the boundary layer
within the reaction zone to a uniformly diverging flow,
thereby reducing the propagation velocity. The other model
is by Zeldovich (1940). This model is quasi-one-dimensional
and friction and heat transfer are considered to be
distributed uniformly across the tube. Both these
approaches give velocity deficits inversely proportional to
the tube diameter. Recently Murray (1984) has applied Fay's
model and used the cell length as the characteristic
thickness of the wave. His predictions are in good
agreement with experimental results from several
investigations. This prediction assumes a multiheaded
detonation (i.e. a detonation wave with more than one
transverse wave).

Moen et al. (1985) have investigated velocity deficits for
different gas mixtures and tube diameters. Their results

are shown in Figure 2.8. The ratio between the measured
detonation velocity, D, and C-J velocity, D_{C-J}, are
plotted versus the ratio between critical tube diameter,
d_c, and tube diameter of the test tube, d. The velocity
deficit as plotted on the figure seems to depend on the
regularity of cell structure. The mixture with the most
regular structure C_2H_2 + 2.5 H_2/ 75% Ar has the
largest velocity deficit for a given value of d_c/d.
Fuel-air mixtures which has the most irregular structure
have a small velocity deficit. The prediction based on
boundary layer effects over-estimates the velocity deficit
for fuel-air mixtures when there are a few cells across the
tube. For fuel-air mixture it appears that wall effects
have little influence on detonation velocity under these
conditions.
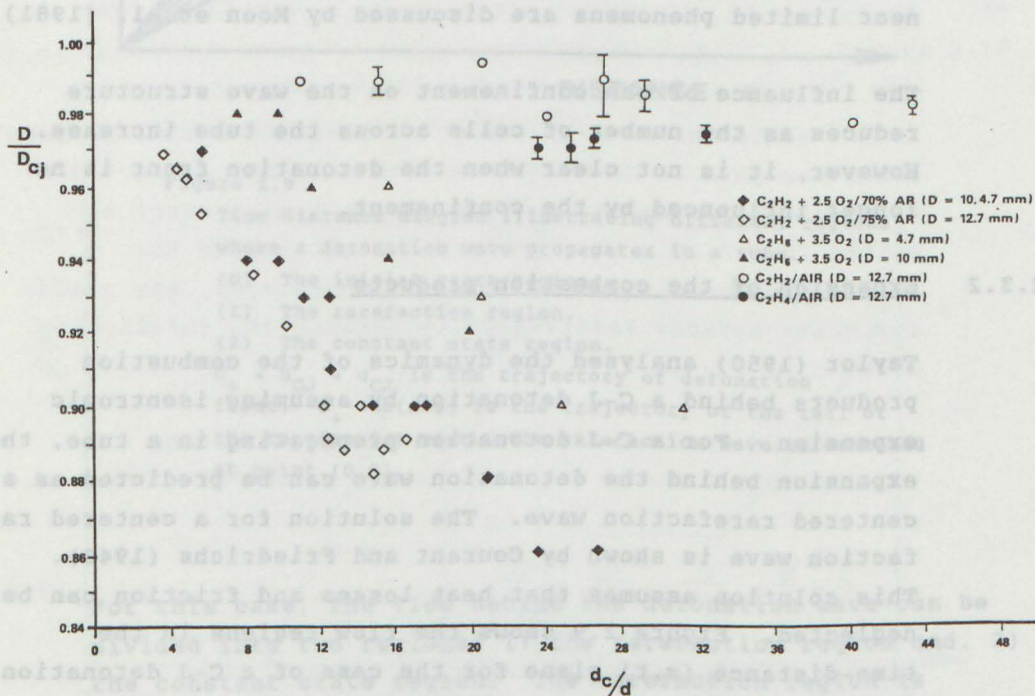
Figure 2.8
Ratio of measured detonation velocity to the theoretical
C-J velocity (D/D_{CJ}) versus ratio of critical tube
diameter of the mixture to the tube diameter, d_c/d,
for mixtures with different levels of cell regularity.

Confinement also influences the structure of the wave
front. Paillard et al. (1981) presented experimental data
showing that the cell size depends on the tube diameter.
The cell size for the same gas mixture increases with
decreasing tube diameter when there are just a few cells
across the tube. By decreasing the tube diameter, with the
same gas mixture, the structure of the detonation front
reaches a limit where front consists of only one transverse
wave. Such a detonation wave is known as single head spin
detonation. Lee (1984) states that the limit for a truly
selfsustained detonation wave in a circular tube corresponds
to the onset of single-headed structure. When the
detonation is a single-headed detonation wave the structure
of the wave front is given by the size of the tube, not the
coupling between gasdynamics and chemical kinetics. Such
near limited phenomena are discussed by Moen et al. (1981).

The influence of the confinement on the wave structure
reduces as the number of cells across the tube increase.
However, it is not clear when the detonation front is no
longer influenced by the confinement.

2.3.2   Expansion of the combustion products

Taylor (1950) analysed the dynamics of the combustion
products behind a C-J detonation by assuming isentropic
expansion. For a C-J detonation propagating in a tube, the
expansion behind the detonation wave can be predicted as a
centered rarefaction wave. The solution for a centered rare
faction wave is shown by Courant and Friedrichs (1948).
This solution assumes that heat losses and friction can be
neglected. Figure 2.9 shows the flow regions in the
time-distance (x,t) plane for the case of a C-J detonation
initiated at the rear end of the tube. Where x is the
distance from the rear end of the tube and t is the time.
The rear end of the tube is blocked so that the particle
velocity u (x = 0) = 0.
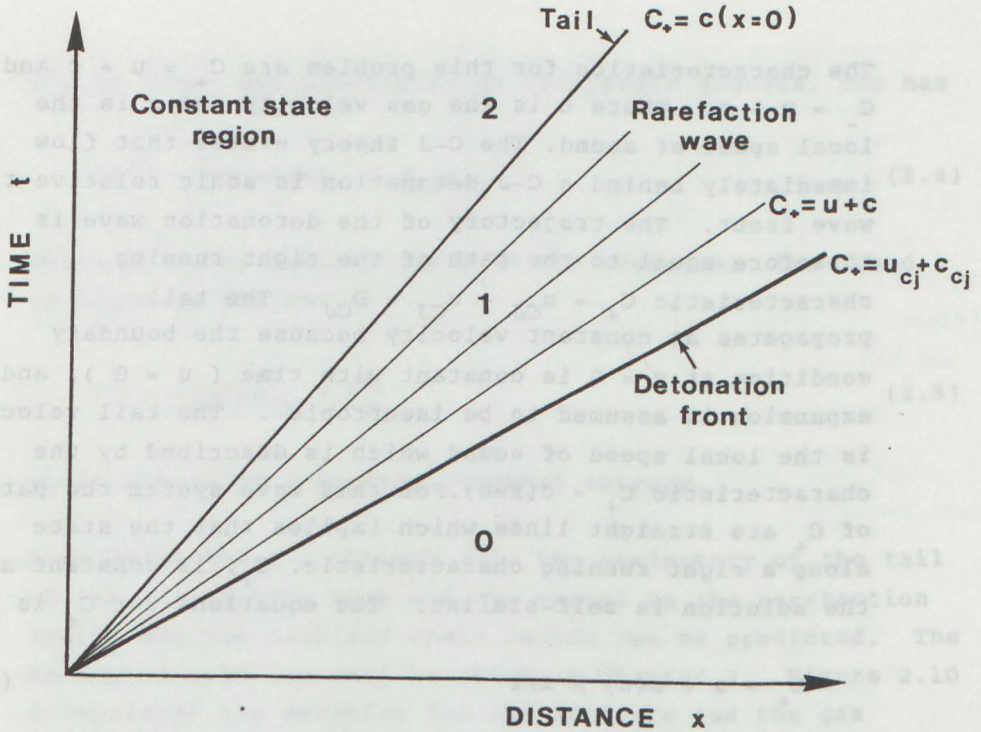
Figure 2.9

Time distance diagram illustrating different regions where a detonation wave propagates in a tube.

(0) The initial state region.

(1) The rarefaction region.

(2) The constant state region.

$C_+ = u_{CJ} + c_{CJ}$ is the trajectory of detonation front. $C_+ = c(x=0)$ is the trajectory of the tail of the rarefaction wave. The rarefaction wave is centered at point (0,0).

For this case, the flow behind the detonation wave can be divided into two regions; 1) the rarefaction region and, 2) the constant state region. The rarefaction region is bounded by the detonation front and the tail of the rarefaction wave. This is a hyperbolic problem, and the characteristics C_- and C_+ represent the path of the sound waves (i.e. the disturbance waves).

The characteristics for this problem are $C_+ = u + c$ and
$C_- = u - c$. Where u is the gas velocity and c is the
local speed of sound. The C-J theory states that flow
immediately behind a C-J detonation is sonic relative to the
wave front. The trajectory of the detonation wave is
therefore equal to the path of the right running
characteristic $C_+ = u_{CJ} + c_{CJ} = D_{CJ}$. The tail
propagates at constant velocity because the boundary
condition at x = 0 is constant with time (u = 0), and the
expansion is assumed to be isentropic . The tail velocity
is the local speed of sound which is described by the
characteristic $C_+ = c(x=0)$. For this wave system the paths
of C_+ are straight lines which implies that the state
along a right running characteristic, C_+, is constant and
the solution is self-similar. The equations for C_+ is :

$$C_+ = u + c(u) = x/t \qquad (2.2)$$

If the state is known at one point this state will propagate
along the path of the right running characteristic. All
C_+-characteristics in the rarefaction region start at
origin (x = 0, t = 0). The state right behind the
detonation wave is the C-J state. Thereafter, the gas at
C-J state expands isentropically through the rarefaction
wave.

The Riemann variant, r, along C_- gives the second
relationship between u and c. It is given by:

$$r = \frac{u}{2} - \frac{c}{\gamma-1} = \frac{u_{CJ}}{2} - \frac{c_{CJ}}{\gamma-1} \qquad (2.3)$$

where γ is the ratio of the specific heat.

Since this is a one-wave problem, the Riemann invariant is
constant in both the constant state region and the
rarefaction region. The value of r is given by the C-J
conditions as shown in Equation 2.3.

For an ideal gas undergoing an isentropic process, one has

$$p\rho^{-\gamma} = \text{constant} = p_{CJ}\rho_{CJ}^{-\gamma} \tag{2.4}$$

where ρ is the density and p is the pressure. The speed of sound is defined as

$$c^2 = (\delta p/\delta \rho)_s = \gamma\frac{p}{\rho} \tag{2.5}$$

where subscript s denotes constant entropy.

From Equations 2.2 through 2.5, the trajectory of the tail of the rarefaction wave and the states in the rarefaction region and the constant state region can be predicted. The method of solution will be shown in Chapter 3. Figure 2.10 illustrates the solution for the pressure and the gas velocity behind a C-J detonation.
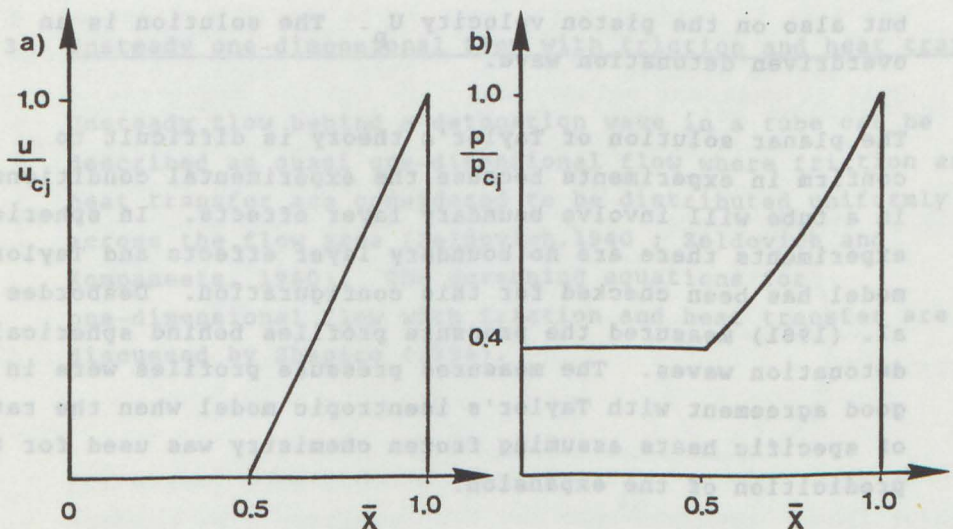
Figure 2.10
Illustration of the flow behind a detonation wave.
(a) Gas velocity profile.
(b) Pressure profile.

The solution is self-similar, with $\bar{x}$ is a dimensionless
distance scaled with distance from origin to the position of
the detonation wave. Normally the velocity of the tail is
about half the velocity of the detonation wave and therefore
$\bar{x} \simeq 0.5$ at the position of the the tail. As seen in the
figures, the gas velocity decreases linearly from the
detonation front to the tail of the rarefaction wave, and
the pressure expands from the C-J state to about 0.4 p_{CJ}.

Fickett and Davis (1979) discuss the same problem, but they
consider different boundary conditions at the rear end of
the tube. Instead of having the rear end blocked, they have
a piston moving with constant velocity, U_p, starting from
$x = 0$ at $t = 0$. When the piston velocity is less than the
gas velocity at the C-J plane, u_{CJ}, the method of solution
is the same as for the blocked end solution ($U_p = 0$). The
position of the tail and the state in the constant state
region will depend on U_p. If U_p is larger than the gas
velocity predicted by the C-J theory, u_{CJ}, then the
detonation velocity, D, depends not only on the gas mixture,
but also on the piston velocity U_p. The solution is an
overdriven detonation wave.

The planar solution of Taylor's theory is difficult to
confirm in experiments because the experimental conditions
in a tube will involve boundary layer effects. In spherical
experiments there are no boundary layer effects and Taylor's
model has been checked for this configuration. Desbordes et
al. (1981) measured the pressure profiles behind spherical
detonation waves. The measured pressure profiles were in
good agreement with Taylor's isentropic model when the ratio
of specific heats assuming frozen chemistry was used for the
predicition of the expansion.

However, in a tube, the boundary layer can significantly
affect the wave expansion following the front. Edwards et
al. (1959) show that the pressure profile behind a $2H_2 +$
O_2 detonation at 1 atm agrees with isentropic expansion
for a 50 mm tube. The measurements are only made close to
the detonation front. For narrow tubes, the wall effects
are significant even close to the front and the experimental
pressure profiles differ from the isentropic expansion model
by Taylor, (Edwards et al., 1959 and 1970; and Paillard et
al., 1979 and 1981).

The experiments by Bazhenova et al. (1981) show that the
thermal conductivity of the wall material also influence the
expansion.

All these experiments show that wall heat transfer and
friction do influence the flow behind a detonation in a
tube. Unfortunatly, little information is currently
availiable in the literature concerning pressure profiles
behind detonation waves in larger tubes.

2.3.3   Unsteady one-dimensional flow with friction and heat transfer

Unsteady flow behind a detonation wave in a tube can be
described as quasi one-dimensional flow where friction and
heat transfer are considered to be distributed uniformly
across the flow area (Zeldovich,1940 ; Zeldovich and
Kompaneets, 1960). The governing equations for
one-dimensional flow with friction and heat transfer are
discussed by Shapiro (1954).

For a control volume as shown in Figure 2.11, one has the
following conservation equations:

Continuity :

$$\frac{\delta}{\delta t}(\rho) + \frac{\delta}{\delta x}(\rho u) = 0 \tag{2.6}$$

Momentum :

$$\frac{\delta}{\delta t}(\rho u) + \frac{\delta}{\delta x}(\rho u^2 + p) = \frac{dA}{A_x dx} \tau_w \tag{2.7}$$

Energy :

$$\frac{\delta}{\delta t}[(\rho A_x dx)(c_v T + \frac{u^2}{2})] + \frac{\delta}{\delta x}[\rho u A_x(c_v T + \frac{p}{\rho} + \frac{u^2}{2})]dx = -\dot{q}'' dA \tag{2.8}$$

A_x is the flow area, dA is the area where friction acts
and heat is conducted through, τ_w is the wall friction, q
is the heat transfer rate to the wall, c_v is the specific
heat at constant volume, and T is the gas temperature.

Figure 2.11
    Quasi one-dimensional control volume illustrating flow
    through area A_x in a tube with wall friction τ_w
    and heat transfer $\dot{q}''$ to the tube wall area dA.

In terms of the internal energy e, defined by:

$$e = \rho c_v T + \frac{1}{2}\rho u^2 = \frac{1}{\gamma-1}p + \frac{1}{2}\rho u^2 \qquad (2.9)$$

The energy equation becomes

$$\frac{\delta e}{\delta t} + \frac{\delta}{\delta x}((e+p)u)) = - \frac{dA}{A_x dx} \cdot \dot{q}'' \qquad (2.10)$$

The complete set of equations can now be written in the following form:

$$\frac{\delta}{\delta t}\begin{bmatrix} p \\ \rho u \\ e \end{bmatrix} + \frac{\delta}{\delta x}\begin{bmatrix} pu \\ \rho u^2 +p \\ (e+p)u \end{bmatrix} = - \frac{dA}{A_x dx}\begin{bmatrix} 0 \\ \tau_w \\ \dot{q}'' \end{bmatrix} \qquad (2.11)$$

When the inhomogeneous terms on the right hand side are zero, the solution becomes the same as the Taylor's isentropic expansion model.

The boundary layer behaviour behind a detonation wave are very difficult to model accurately because of the three-dimensionality of the wave front, the expansion of the combustion products and the chemical reactions. The simplest way to estimate τ_w and $\dot{q}''$ is to use a one-dimensional approximation. For flow in tubes, it is common to define the friction coefficient C_f as:

$$C_f = \frac{\tau_w}{\frac{1}{2}\rho u^2} \qquad (2.12)$$

For steady tube flow, C_f is a function of the Reynolds number, wall roughness and the tube diameter (Schlicting, 1976). For high Re-number the friction factor depends only on the wall roughness and the tube diameter. The flow behind a detonation wave have local Reynold numbers in this high Re-number regime and C_f is therefore approximately a constant.

For a non-reacting gas, the heat transfer rate $\dot{q}''$ is given by:

$$\dot{q}'' = h \ (T_r - T_w) \tag{2.13}$$

where h is the heat transfer coefficient, T_r is the recovery temperature and T_w is the wall temperature (Eckert and Drake, 1972). By applying Reynold's analogy (Kays and Crawford, 1980), the heat transfer coefficient can be estimated by:

$$h = \frac{C_f}{2} \cdot u\rho c_p \tag{2.14}$$

where c_p is the specific heat at constant pressure. These relationships (2.13 and 2.14) for the heat transfer rate give a very simplified description of the heat transfer process behind a detonation wave. Effects of variation of properties through the boundary layer, development of the boundary layer, three dimensional effects caused by transverse waves and effects due to chemical reactions in the boundary layer are neglected.

Sichel and David (1966) have applied Mirels' (1957) expression for $\dot{q}''$ to calculate the heat transfer rate immediately behind detonations in H_2-O_2 mixtures. They assume a turbulent boundary layer and use both enthalpy and temperature differences as the driving potential for $\dot{q}''$. The chemical reactions in the boundary layer can be taken into account by assuming chemical equilibrium in the boundary layer and use the enthalpy difference as the driving potential. For stoichiometric H_2-O_2 the calculated heat transfer rate using enthalpy difference is about 60% higher than the heat transfer rate using temperature differences.

Edwards et al. (1970) have measured heat transfer rates
behind detonation waves in 16 mm and 50 mm tubes. The
experimental values agree well with the calculated values of
Sichel and David (1966) using enthalpy differences. By
using Reynolds analogy and temperature differences, Edwards
et al. found that an average value of the friction factor
C_f of 0.005 corresponds to the experimental value of the
heat transfer rate.

2.4   TRANSMITTED SHOCK WAVE FROM A DETONATION

When the detonation wave reaches the inert interface the
shock wave will continue to propagate through the inert
region. The energy release by chemical reaction will end
and the shock wave must adjust to the new conditions. The
combustion products are pushing the inert gas forward and
drive the shock wave into the inert region. In the case of
a second interface (Interface II), there will also be a
transmission and reflection of the wave at the contact
dicontinuity. In this section the simple-one dimensional
model of Paterson (1953) for refraction of the detonation
will be presented. The decay and nature of the transmitted
shock will also be discussed.

2.4.1   A simple model for refraction of a detonation wave at an
inert interface

When a detonation wave in a fuel-air mixture propagates into
an inert gas mixture, the transmission process is very
complex. The structure of the wave involves
three-dimensional phenomena. In order to model this
transmission process in detail, it would be necessary to use
a numerical analysis similar to what Hiramatsu et al. (1984)
use for a numerical simulation of transmission of a gaseous
detonation from a confined to an unconfined space. To
estimate the strength of the transmitted shock wave, the
one-dimensional model of Paterson (1953) can be used.

This simplified one-dimensional model assumes that the detonation wave has zero thickness as in the C-J theory, that the properties behind the wave have C-J values, and that there is no expansion of the products. This is then a typical Riemann problem. On one side of an interface one has a gas in the C-J state, and on the other side, an inert gas with zero velocity and with the initial pressure and density. The solution to the Riemann problem is discussed in Appendix B.

The solution must satisfy the continuity conditions such that the velocity, u, and pressure, p, are the same for the combustion products and the inert gas after being crossed by the respective waves. In a p-u diagram, the solution (p*,u*) is found at the interception of the curves for the right and left running waves. The two possible types of solutions are shown in Figures 2.12a) and 2.12b). The arrow gives the direction of the wave. S stands for shock wave and R for rarefraction wave. The waves for the respective situations are shown in Figures 2.13a)and 2.13b). In case a), a rarefaction wave propagates back into the combustion products whereas in case b) a shock wave propagates into the combustion products. The type of solution depends on the properties of the gases and the initial conditions.

Lee et al. (1977) have calulated the strength of the refracted shock waves for C-J detonations into air. The calculations were done for common hydrocarbons and H_2, and for air and O_2 as oxidizer. Only for H_2-O_2 detonations the situation shown in Figure 2.13b) was predicted. For all the other gas mixtures, a rarefaction wave propagates back into the combustion products.
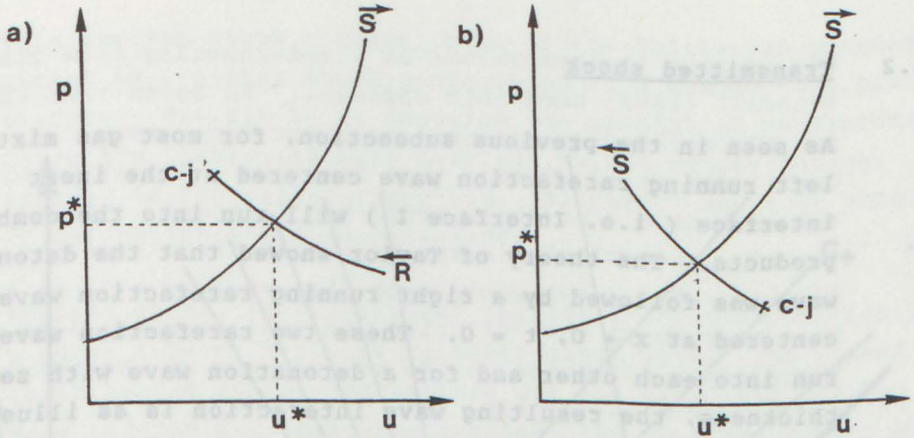
Figure 2.12
p-u diagram showing the possible solutions p* and u*
behind a transmitted shock wave $\vec{S}$ when a C-J detonation
refracts at an inert interface.
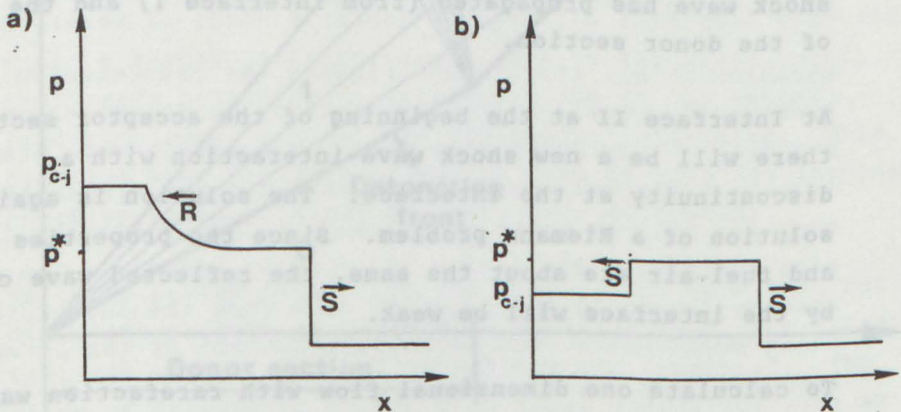
Figure 2.13
Pressure profiles illustrating the two possible
solutions of figure 2.13 when a C-J detonation refracts
at an inert interface.
a) a rarefaction wave, $\vec{R}$, propagates back into the
combustion products.
b) a shock wave, $\vec{S}$, propagates back into combustion
products.

2.4.2   Transmitted shock

As seen in the previous subsection, for most gas mixtures, a
left running rarefaction wave centered at the inert
interface (i.e. Interface I) will run into the combustion
products. The theory of Taylor showed that the detonation
wave was followed by a right running rarefaction wave
centered at x = 0, t = 0. These two rarefaction waves will
run into each other and for a detonation wave with zero
thickness, the resulting wave interaction is as illustrated
in Figure 2.14. The thin lines represent characteristics.
The flow behind the transmitted shock wave is not able to
support a shock wave with the strength that was transmitted
at the interface. The transmitted shock will therefore
decay in strength as it propagates into the inert gas. The
rate of decay depends on the ratio between the distance the
shock wave has propagated (from Interface I) and the length
of the donor section.

At Interface II at the beginning of the acceptor section,
there will be a new shock wave interaction with a
discontinuity at the interface. The solution is again the
solution of a Riemann problem. Since the properties of air
and fuel-air are about the same, the reflected wave caused
by the interface will be weak.

To calculate one dimensional flow with rarefaction waves,
interface interaction and shock decay, is today relatively
simple using numerical programs like the Random Choice
Method (RCM) code (Saito and Glass, 1979) or the Flux
Corrected Transport (FCT) code (Boris, 1976). There are no
simple analytical solutions for this problem like the
self-similar solution for shock decay from a point charge
(Taylor, 1950b). In the present case (i.e. gaseous
detonations), the charge is distributed. In a numerical
code the Taylor expansion profile, as shown in Figure 2.10
can be used as input in order to simulate the distributed
charge.
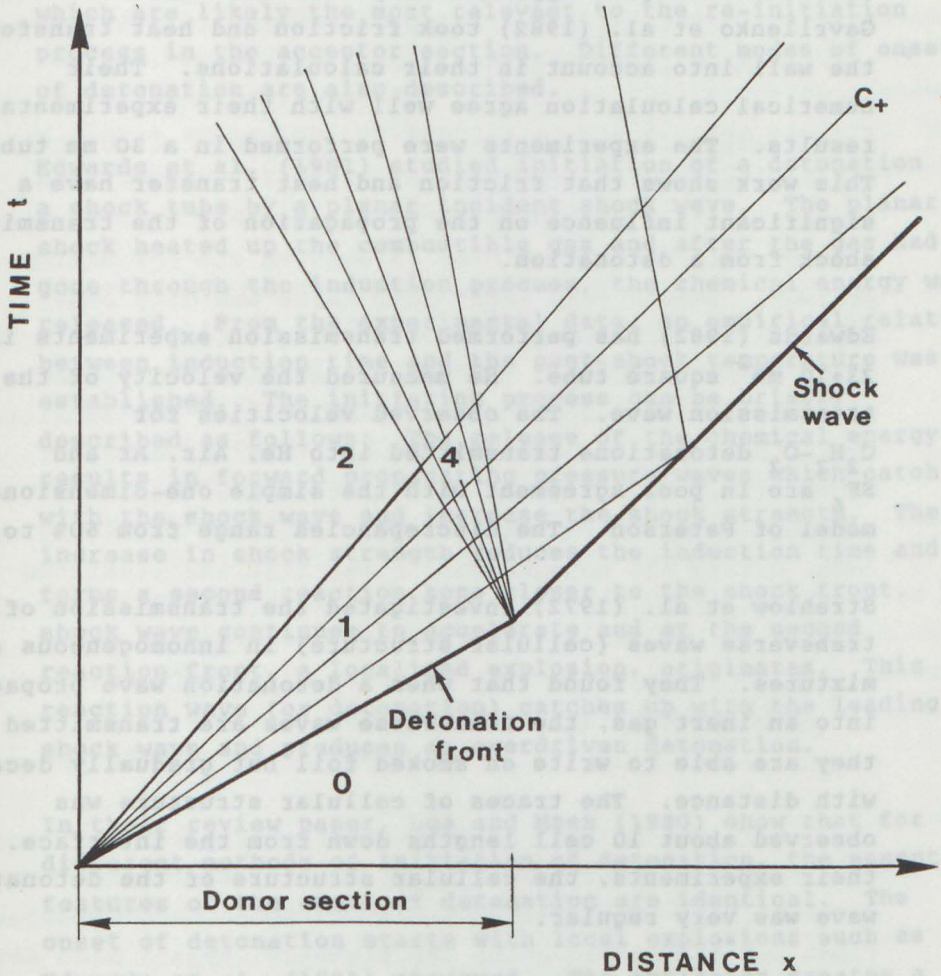
Figure 2.14
Time distance diagram illustrating wave motion when a
shock wave is transmitted into an inert gas region.
In region (4) two rarefaction waves interacts.

The problem is then solved as a non-reacting flow problem.
Thibault (1983) used this approach. He found that the FCT
and RCM codes gave approximately the same answer.
Gavrilenko et al. (1982) took friction and heat transfer to
the wall into account in their calculations. Their
numerical calculation agree well with their experimental
results. The experiments were performed in a 30 mm tube.
This work shows that friction and heat transfer have a
significant influence on the propagation of the transmitted
shock from a detonation.

Edwards (1982) has performed transmission experiments in a
$23 \cdot 10$ mm^2 square tube. He measured the velocity of the
transmission wave. The observed velocities for
$C_2H_2-O_2$ detonations transmitted into He, Air, Ar and
SF_6 are in poor agreement with the simple one-dimensional
model of Paterson. The discrepancies range from 60% to 75%.

Strehlow et al. (1972) investigated the transmission of
transverse waves (cellular structure) in inhomogeneous gas
mixtures. They found that when a detonation wave propagates
into an inert gas, the transverse waves are transmitted and
they are able to write on smoked foil but gradually decay
with distance. The traces of cellular structure was
observed about 10 cell lengths down from the interface. In
their experiments, the cellular structure of the detonation
wave was very regular.

2.5   INITIATION OF DETONATION BY A SHOCK

As discussed by Lee (1982) there are many mechanisms that
can accelerate a flame and thereby cause onset of
detonation. At the present time the mechanisms involved in
initiation of a detonation are not understood in detail,
however, qualitative descriptions are available.

This section gives a description of the initiation process
caused by a planar shock propagating in a combustible gas
mixture. The aim is to describe the initiation mechanisms
which are likely the most relevant to the re-initiation
process in the acceptor section. Different modes of onset
of detonation are also described.

Edwards et al. (1981) studied initiation of a detonation in
a shock tube by a planar incident shock wave. The planar
shock heated up the combustible gas and after the gas had
gone through the induction process, the chemical energy was
released. From the experimental data, an empirical relation
between induction time and the post-shock temperature was
established. The initiation process can be briefly
described as follows: The release of the chemical energy
results in forward propagating pressure waves which catch up
with the shock wave and increase the shock strength. The
increase in shock strength reduces the induction time and
forms a second reaction zone closer to the shock front. The
shock wave continues to accelerate and at the second
reaction front, a localized explosion, originates. This
reaction wave (or detonation) catches up with the leading
shock wave and produces an overdriven detonation.

In their review paper, Lee and Moen (1980) show that for the
different methods of initiation of detonation, the essential
features of the onset of detonation are identical. The
onset of detonation starts with local explosions such as
Edwards et al. (1981) observed. The explosion creates a
shock wave. This shock wave propagates in an unburnt
mixture and accelerates to a detonation wave. It is
necessary that the unburnt mixture is pre-conditioned to get
the shock wave to accelerate. Pre-conditioning means that
the gas has gone through a part of the induction process.
As pointed out by Lee and Moen, a local explosion alone will
not result in the onset of a detonation; the pre-conditioned
gas has to release its chemical energy in such a way that
the shock wave is amplified. This amplification of the
shock wave

from the localized explosion, caused by the induction time
gradient ahead of shock, is referred to as the SWACER (Shock
Wave Amplification by Coherent Energy Release) mechanism
(Lee et al., 1978). The SWACER mechanism is discussed by
Lee and Moen (1980) and Strehlow (1984).

A very enlightening experiment on the onset of detonation
was done by Urtiew and Oppenheim (1966). They studied
transition from deflagration to detonation. A stroboscopic
schlieren technique was used to observe the transition
process. Before this experiment there was only some
hypothesis of the events leading to development of
detonations. However, in their experiment, the process of
onset of detonation was clearly exhibited. The localized
explosion phenomena was a major event in the onset of
detonation, and was either a consequence of turbulent flame
propagation or shock induced ignition. For the turbulent
mode, Urtiew and Oppenheimer showed that the localized
explosion could start off at:

-   the flame front,
-   between shock and flame front,
-   the shock front.

From their photographs it is clear that the boundary layer
and the boundary conditions play an important role. When a
detonation is initiated at the shock front, the turbulent
flame has propagated along the boundary layer. Also for the
other cases, the local explosion is first observed in the
boundary layer possible due to some irregularity at the
surface and weak transverse waves. As shown in a later
paper by Meyer et al. (1970), it was not the gas dynamical
process that triggered the explosion in these cases. At the
time when the local explosion takes place, the gas has only
undergone about 4 percent of the induction process. The
explosion must be due to a turbulent flame process, which is
closely linked to the boundary conditions.

Urtiew and Oppenheim (1966) also observed transition to
detonation caused by gasdynamic processes. When two shock
waves merge, they create a regime with high temperature
behind the transmitted shock. When the gas at the contact
surface, which is the first shocked gas in the high
temperature region, has gone through the induction process,
a planar explosion is observed at the contact surface. The
experimental induction time agrees with calculations of the
induction time (Urtiew and Oppenheim, 1967).

Urtiew and Oppenheim's experiments show that detonation can
be initiated by different modes, and that the transition
process can either be a result of turbulent flame
propagation or shock induced ignition. The localized
explosions and the acceleration of the shock wave result in
strong transverse waves. In photographs by Urtiew and
Oppenheim (1966), transverse wavefronts can be seen. They
propagate at constant velocity which is close to the
predicted velocity of sound. Edwards et al. (1981) also
measured pressure oscillations indicating the presence of
strong transverse waves. Because the onset of detonation is
normally a non-planar phenomena, transverse waves appear
during the initiation process.

2.6 OVERVIEW OF PREVIOUS EXPERIMENTS WITH RE-INITIATION OF DETONATION ACROSS AN INERT REGION

One has to go back to 1892 to find the first reported
experiments on the transmission of explosions across an
inert region. These experiments were done by Lean and Dixon
(1892). Since then, just a few more experiments of this
kind have been reported.

They are given below in chronological order:

- Lean and Dixon (1892)
- Bone, Fraser and Wheeler (1935)
- Bull, Elsworth, McLeod and Huges (1981)
- Gavrilenko, Krasnov and Nikolaev (1982 b)
- Edwards, Thomas and Sutton (1983)
- Bjerketvedt and Sonju (1983)

All of these studies are quite limited in scope and cover only a small range of the very complex problem. In this section, a short summary of these investigations is given.

The apparatus used by Lean and Dixon (1892) consisted of two lead tubes, which could be connected together by an inert section consisting of glass tubes of varying lengths. The lead tubes were 880 mm long and 17.5 mm in internal diameter. Glass tubes were also placed at each end of the lead tubes. The lead tubes were filled with $2H_2 + O_2$. The inert section was filled with air. The gas mixtures were separated by two valves. Just before ignition, the valves were opened. The gas was ignited by a spark and probably detonated, although detonation was not mentioned by Lean and Dixon. For similar conditions as Lean and Dixon, Bollinger et al. (1961) observed transition to detonation after 750 to 900 mm. It is, therefore, likely that detonation waves also were initiated in Leon and Dixon's experiments. Another uncertainty with Lean and Dixon's experiment is that the flame acceleration may have created a flow which could have destroyed the inert region.

Lean and Dixon's only diagnostic were a visual observations through the glass tube at the end of the acceptor section. A flash indicated that the explosion had been transmitted. They observed a flash when the length of the air gap was 192 mm or less. Today it is obvious that visual observation is insufficient to distinguish between different complex explosion phenomena, such as re-initiation caused by reflection of the shock at the end of the acceptor glass tube section.

The paper by Bone et al. (1935) describes a photographic
investigation of detonations. Among the experiments
reported, there were some tests with re-initiation of
detonation across a N_2-gap. These experiments were
carried out in a tube with 13 mm internal diameter. A
spinning detonation in $2CO + O_2$ was temporarily suppressed
by a 6.4 mm N_2-gap. The detonation wave re-initiated 1.4
to 3.0 msecs after the detonation had reached the gap.
Tests with the more reactive gas mixture of $2H_2 + O_2$ and
6.4 mm and 26.4 mm N_2-gap, were performed. The N_2-gap
seems to have no effect on the speed an character of the
detonation. The detonation wave transmitted straight
through the gap. The transmission process was not observed
on the photographs because the valve creating the inert
region was made with opaque material. These experiments
show that an inert gap can supress a detonation, but that
the detonation can also be reinitiated. As expected,
detonations in more reactive mixtures re-initiated more
easily after the inert region.

Bull et al. (1981) performed some relatively large scale
experiments. Their apparatus consisted of two plastic bags
with 0.75 m diameter which were mounted on two steel hoops.
The bags had a common longitudinal axis. The spacing
between knife edges attached to the steel hoops made up the
inert gap. The gap distance was adjustable, and the
explosive gas mixture in the bags was separated from the air
region by diaphragms. The diaphragms were removed less than
0.2 sec before the mixture in the donor section was
detonated. This short time was necessary to avoid the
mixing of the gas mixtures in the donor and acceptor
sections. The difference in the molecular weights of the
air and of the fuel-air mixtures causes a density
difference. Buoyancy forces will, therefore, induce a flow,
which can partially mix the different gas regions. The
detonation was initiated by high explosives. Stoichiometric
ethylene-air and propane-air mixtures were used. For the
ethylene experiments, the donor section was 1.35 m long and

the acceptor section was 1.5 m long. For propane, these
lengths were 3.0 m and 2.1 m, respectively. The experiments
were instrumented with pressure transducers and microwave
radar doppler equipment.

In Bull's experiments, the detonation wave re-established
itself when the air gap was less than 0.15 m for
ethylene-air and less than 0.12 m for propane-air. The
re-initiation occurred within the first 0.26 m of the
acceptor section. In this experimental apparatus the
rarefraction wave from the sides will propagate into the
center of the bag and presumably make reinitiation further
downstream less likely since the expansion will reduce the
temperature and thereby slow down the induction process.
This effect would not be present in a confined tube
experiment. The observed reinitiation cannot be explained
by one-dimensional shock wave decay and chemical induction
time considerations. In their conclusions, Bull et al. say
that their results indicate that transverse components of
the decaying shock wave contribute to the re-initiation
process.

The advantage of doing large scale tests is that wall
effects are minimized, but the problem of mixing the gas in
the donor and acceptor sections gets amplified when scale is
increased.

Gavrilenko et al. (1982b), performed experiments in a tube.
The tube diameter was 30 mm. The different sections were
separated by thin rubber membranes. The gas in the donor
and acceptor sections was stoichiometric mixture of
acetylene-oxygen at 1 atm. The inert section was filled
with air. The length of the donor section was only 105 mm,
the inert section was 460 or 880 mm long, and the acceptor
section was 1.5 m long. Before ignition, the membranes were
ruptured using needles. The detonation was initiated using
a spark. The gas mixture used in the acceptor section in
these experiments was so detonable that when it was ignited,

the flame more or less immediately transited to a
detonation. The transfer of the detonation was therefore a
matter of sufficient strength of the transmitted shock wave
so the gas in the acceptor section was ignited. These
experiments are therefore quite different from experiments
in weaker mixtures such as fuel-air mixtures. It is
believed that transition to detonation is one of the
controlling processes for re-initiation of detonation across
an inert region in fuel-air mixtures. In the experiments of
Gavrilenko et al the critical Mach number for the shock to
ignite the mixture in the acceptor section was 2.3. For the
inert region to stop a detonation, the inert section had to
be about six times longer than the donor section. The
effects of some wall irrelugarities were also investigated
and discussed. In some of the experiments, the acceptor
section had an annular groove of 1.5 mm width and 5 mm
depth. This irregularity always led to re-initiation of the
detonation.

Edwards et al. (1983) presented some preliminary data from
laboratory experiments. They also showed how regions with
different densities quickly form layers and destroy a
distinct interface between the two regions. It is clear
that it is necessary to control the interface mixing in
order to perform reproducible experiments.

Bjerketvedt and Sonju (1983) presented some preliminary
experimental results from the program described in this
report.

In summary, a few preliminary experiments have been
performed, but a complete understanding of re-initiation of
detonation across inert regions has not yet been established.

2.7   <u>MOTIVATION AND INVESTIGATION STRATEGY FOR PRESENT WORK</u>

In the summary remarks of the proceedings of the
International Specialist Meeting on Fuel-Air Explosions at
McGill University ·in 1981, gas phase detonation in
inhomogeneous mixtures was identified as one of four areas
worth further intensive study (Bull, 1982). The motivation
was the concern for detonations in real gas clouds. There
is a need for some quantitative knowledge in this area,
especially to ascertain the effects of inhomogeneties in
fuel concentration on propagation of detonation waves in a
real cloud. This is a complex problem since the conditions
(i.e., fuel conditions) cannot be described exactly, and the
propagation of detonation waves in inhomogeneous mixtures is
not well understood. A first step to try to understand this
phenomena is to investigate an idealized geometrical
configuration where a detonation wave in a homogeneous cloud
propagates across an inert region into another detonable
homogeneous cloud. Such an investigation also has
application to methods of stopping detonations in confined
situations. There is a need for practical devices to stop
detonations in such geometries. Using an inert plug is one
device which needs to be evaluated.

As shown in the literature review, re-initiation of
detonation across an inert region involves phenomena such as
detonation propagation in homogeneous mixtures, transmission
of shock waves into an inert mixture and re-initiation of
detonation.

The velocity of a detonation wave propagating in a
homogeneous mixture is known to be close to the C-J value .
The expansion of combustion products after the detonation
has only been investigated close to the wave front and in
small tubes (Edwards et al., 1970 and Paillard et al., 1979
and 1981). There have been some experimental investigations

of detonation wave propagation into an inert gas (Edwards et
al., 1981; Strehlow et al., 1972 and Gavrilenko et
al.,1982). These experiments were performed in small
apparatus in mixtures more sensitive than fuel-air
mixtures. One-dimensional codes can be used to predict the
transmitted shock wave (Thibault, 1983 and Gavrilenko et
al., 1982). Comparison with experimental results shows that
wall effects have to be taken into account. The behaviour
of transverse waves transmitted into inert gas have only
been investigated experimentally (Strehlow et al., 1972),
and numerical predictions are not available.

The re-initiation process is of interest not only for
re-initiation of detonation across an inert region, but also
for other transition and transmission processes. At the
present this phenomena is only described qualitatively
(Urtiew and Oppenheim, 1966; Lee and Moen, 1980). The
critical conditions for the onset of detonation cannot be
predicted at the present time.

The lack of methods for predicting the transmitted shock
wave and the critical condition for the onset of detonations
makes it difficult to predict conditions for the
re-initiation of detonation across an inert region. The
experiments reported so far (Lean and Dixon, 1892; Bone et
al., 1935; Bull et al., 1981; Gavrilenko et al., 1982b;
Edwards et al., 1983; Bjerketvedt and Sonju, 1983) are
limited and they were mainly performed in quite small scals
apparatus. Only Bull et al. (1981) performed experiments in
fuel-air mixtures in a relatively large scale apparatus.
From these experiment it is not clear what mechanism caused
the re-initiation of the detonation. None of the reported
experiments have investigated the influence of gas mixture
and width of inert region over a wide range. The influence
of these experimental conditions on the transmission process
has not yet been established. There was therefore a need
for further investigation of this problem and after

consultation with Prof. R.A. Strehlow at the University of
Illinois, an experimental study was initiated at the
Norwegian Institiue of Technology.

The investigation strategy was to perform experimental
investigations on re-initiation of a stabilized detonation
wave across a distinct inert region of air in order to
determine under what experimental conditions a detonation
wave re-initiated across the inert air gap. The width of
the inert region and the properties of the gas mixture were
the variable experimental conditions. The goal was to
obtain quantitative information on detonation propagating in
inhomogeneous gas mixtures, and to obtain a qualitative
understanding of the re-initiation process. The ultimate
objective was to be able to scale these results to other gas
mixtures and to inert pockets in unconfined situations. It
was expected that the detonation wave would transmit rather
easily through the inert region and then re-initiate within
a short distance in the acceptor section. The experiments
showed that this did not occur. Therefore, it became
important to carefully characterize the experimental
conditions. In the latter part of this investigation
experiments were performed to characterize the experimental
conditions, and the results were compared with numerical
calculations. To ascertain the effect of heat transfer and
friction on the experimental conditions, tests with
detonation propagation in homogeneous mixtures and
transmission of shock waves into an inert region were also
performed.

CHAPTER 3

NUMERICAL METHODS AND CALCULATIONS

3.1   INTRODUCTION

The purpose of this chapter is to give an overview of the
numerical calculations which have been performed. The aim
of these numerical calculations was to estimate the
influence of the confinement caused by tube walls and to
calculate the flow field. The flow field was calculated in
order to obtain the pressure histories, the time of arrival
for the shock waves and the contact surfaces, and to
estimate the induction time. The calculations are only
gasdynamical calculations. Chemical reactions are not
treated. An ideal gas with constant ratio of specific heat
and molecular weight is assumed. The combustion products
are assumed frozen at C-J concentrations.

The application of the isentropic expansion model of Taylor
(1950) for predicting the expansion process behind a
detonation wave are explained in Section 3.2. The remaining
sections decribes the Random Choiche Method (RCM) and its
use. A general description of this code is given in
Section 3.3. The operator splitting method, is also
discussed in Section 3.3. This method is used in the RCM
code in order to take heat transfer and friction into
account. In Section 3.4 the modelling of heat transfer and
friction are explained and the procedure for including these
effects in the RCM calculations is described. Section 3.5
describes a modified version of the RCM code, which can be
used to predict an non-isentropic expansion of combustion

products behind a detonation wave. Using this code the
effects of heat transfer and friction on the expansion
process can be evaluated. Section 3.6 gives an overview of
how the RCM code was applied to predict the trajectory of
the shock wave and flow field behind this shock wave for the
case of a C-J detonation propagating into an inert gas.
Induction time calculations, based on flow field from the
transmitted shock wave calculations, are described in
Section 3.7.

3.2   ISENTROPIC EXPANSION OF COMBUSTION PRODUCTS

In Chapter 2 the isentropic model of Taylor (1950) for
expansion of combustion products behind a C-J detonation was
described and the equations (Eqs. 2.2 to 2.4) governing this
problem were given. In this section these equations are
applied to calculate pressure histories for comparison with
experimental results and to obtain input pressure profiles
for subsequent numerical calculations.

The equations for the Taylor model can be written as follows:

$$u + c = x/t \tag{3.1}$$

$$r = \frac{u}{2} - \frac{c}{\gamma-1} = \frac{u_{CJ}}{2} - \frac{c_{CJ}}{\gamma-1} \tag{3.2}$$

Assuming ideal gas and isentropic expansion of the
combustion products one obtain:

$$p\rho^{-\gamma} = p_{CJ} \cdot \rho_{CJ}^{-\gamma} \tag{3.3}$$

The speed of sound c_{CJ} is related to the ratio of specific
heats γ, pressure p and density ρ by the standard ideal
gas relation:

$$c^2 = \gamma \frac{p}{\rho} \tag{3.4}$$

and L is defined as:

$$L = 2r = u_{CJ} - \frac{2c_{CJ}}{\gamma-1} \qquad (3.5)$$

The first step in solving the pressure profile is to
calculate the velocity of the tail (c_{tail}) of the
rarefaction wave (see Figure 3.1) so the time t_{tail} when
the tail of the rarefaction wave reaches position x is known
or the position of the tail x_{tail} at time t.
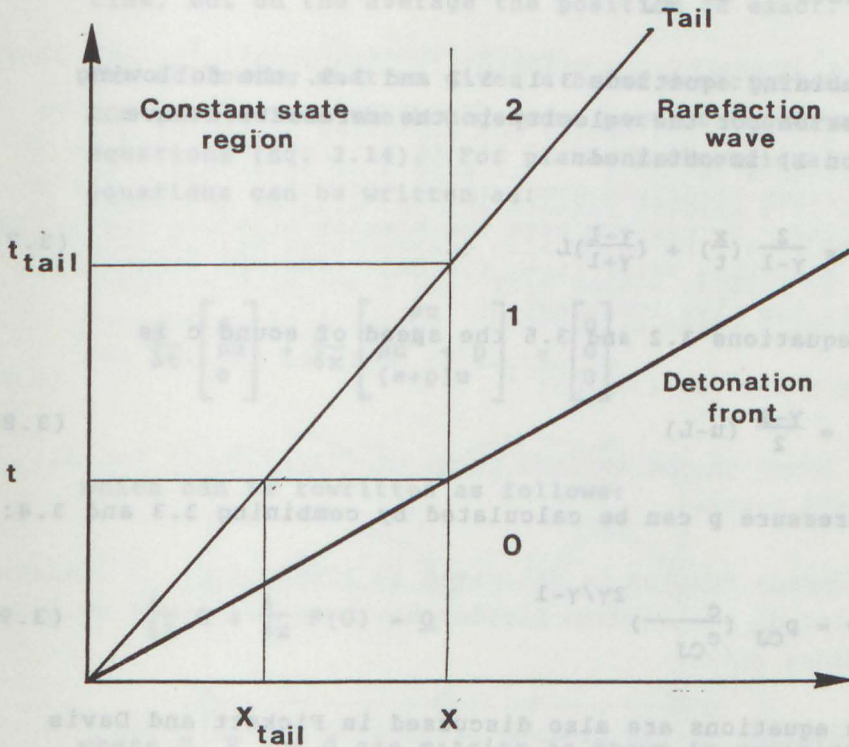
Figure 3.1
    Time distance diagram illustrating the trajectory of
    detonation wave and the regions for constant state and
    rarefaction wave.

This velocity is found from equation 3.2 by setting u = 0.

$$c_{tail} = \frac{\gamma-1}{2}L = -\frac{\gamma-1}{2}(u_{CJ} - \frac{2u_{CJ}}{\gamma-1})$$

The pressure, p_{tail}, in region (2) on Figure 3.1 is found by combining 3.3 and 3.4:

$$p_{tail} = p_{CJ}(\frac{c_{tail}}{c_{CJ}})^{2\gamma/\gamma-1} \tag{3.6}$$

By combining equations 3.1, 3.2 and 3.5, the following expression for the velocity in the rarefaction wave (region 1) is obtained:

$$u = \frac{2}{\gamma-1}(\frac{x}{t}) + (\frac{\gamma-1}{\gamma+1})L \tag{3.7}$$

From equations 3.2 and 3.5 the speed of sound c is

$$c = \frac{\gamma-1}{2}(u-L) \tag{3.8}$$

The pressure p can be calculated by combining 3.3 and 3.4:

$$p = p_{CJ}(\frac{c}{c_{CJ}})^{2\gamma/\gamma-1} \tag{3.9}$$

These equations are also discussed in Fickett and Davis (1979).

3.3   GENERAL DESCRIPTION OF RANDOM CHOICHE METHOD (RCM).

Saito and Glass (1979) gave a general description of the RCM code, including applications and a listing of the code. The code used in this investigation is basically the RCM code from Satio and Glass (1979). The algorithm was developed by

Glimm (1965), Chorin (1976) and Sod (1977). This code
solves the non-stationary gasdynamical equations for a ideal
gas in problems where shock waves, rarefaction waves and
contact surfaces are involved. The RCM code divides the
problem into many Riemann problems and the new solution is
chosen from the solutions of the Riemann problems at random
positions. This method does not use artificial viscosity,
so that shock waves and contact surfaces remain as
discontinuities and are not artificially smeared. The
position of a discontinuity may not be exact at a given
time, but on the average the position is exact.

The following section gives a brief description of how the
RCM code solves the homogeneous part of conservation
equations (Eq. 2.14). For planar 1-dimensional flow these
equations can be written as:

$$\frac{\delta}{\delta t} \begin{bmatrix} \rho \\ \rho u \\ e \end{bmatrix} + \frac{\delta}{\delta x} \begin{bmatrix} \rho u \\ \rho u^2 + p \\ (e+p)u \end{bmatrix} = \begin{bmatrix} 0 \\ 0 \\ 0 \end{bmatrix} \qquad (3.10)$$

which can be rewritten as follows:

$$\frac{\delta}{\delta t} G + \frac{\delta}{\delta x} F(G) = \underline{0} \qquad (3.11)$$

where G, F and $\underline{0}$ are matrixs as shown in equation 3.10.

Equation 3.11 is solved by dividing time, t, and distance,
x, into intervals, where G is piecewise constant and solve
the Riemann problem for each distance interval.

Let Δx and Δt be length and time increments and i and n integers. The values of G at time $n\Delta t$ on the interval $[i\Delta x, (i+1)\Delta x]$ are given by:

$$G(x, n\Delta t) = \begin{cases} g_{i+1}^n & x \geq (i+1/2)\Delta x \\ \\ g_i^n & x < (i+1/2)\Delta x \end{cases} \qquad (3.12)$$

Where g_i^n approximates $G(i\Delta x, n\Delta t)$. The problem is now divided into many Riemann problems. The Riemann problems on the intervals between the grid points have exact solutions if the Courant-Fredrichs-Lewey (CFL) criterion (Smith, 1978) is satisfied. In the RCM code the Riemann problems are solved every half time step, (i.e. 0.5 Δt). The CFL criteria specify the time increment as:

$$\Delta t \leq \max \, [\Delta x / (|u| + c)] \qquad (3.13)$$

Δt is based on the maximum value of $[\Delta x / (|u| + c)]$ for all the grid points.

The Riemann problem is discussed in Appendix B. A numerical solution of the Riemann problem has been described by Saito and Glass (1979).

The solution of the Riemann problem on the interval $[i\Delta x, (i+1)\Delta x]$ at time $(n+1/2)\Delta t$ has an exact solution $V(x, (n+1/2))$. The value for $g_{i+1}^{n+\frac{1}{2}}$ is defined as:

$$g_{i+1}^{n+\frac{1}{2}} = V[(i+\xi)\Delta x, (n+\frac{1}{2})\Delta t] \qquad (3.14)$$

Where ξ is a random number on the interval $[0,1]$. ξ is
a constant for each step in time .

To advance the next half time step the initial data are
assumed again to be piecewise constant and the Riemann
problems are solved. For the last half time step
g_i^{n+1} is defined as:

$$g_i^{n+1} = V[(i+\xi)\Delta x,(n+1)\Delta t] \qquad (3.15)$$

where ξ is a new random number.

The method of selecting the values for G in the grid points
is illustrated in Figure 3.2 . P is the sampling point
where the solution of the Riemann problem V is chosen. V is
used in the neighbouring grid point as prescribed by
equation 3.14 and 3.15. This method results in some
randomness in solution; however, as shown by Glimm (1965),
the average solution is correct.
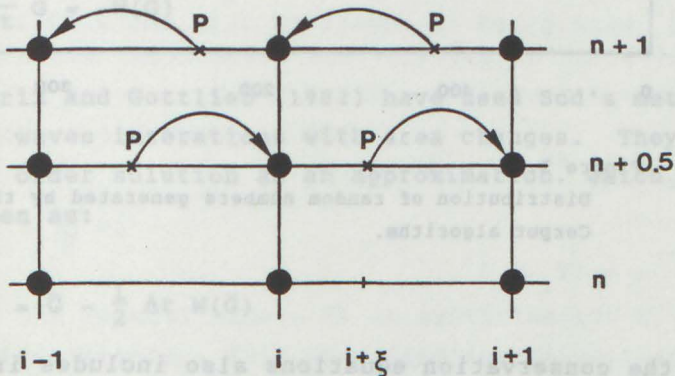
Figure 3.2
    Illustration of how the solution for a grid point is
    selected.

Gottlieb (1983) has used different algorithms for generating random numbers ξ. He found that the numerical results in terms of quality and noiseness depend on the random number alorithm. The Van der Corput algorithm gave the best results and that algorithm was used in this work. Figure 3.3 shows the random numbers generated by Van der Corput's algorithm.
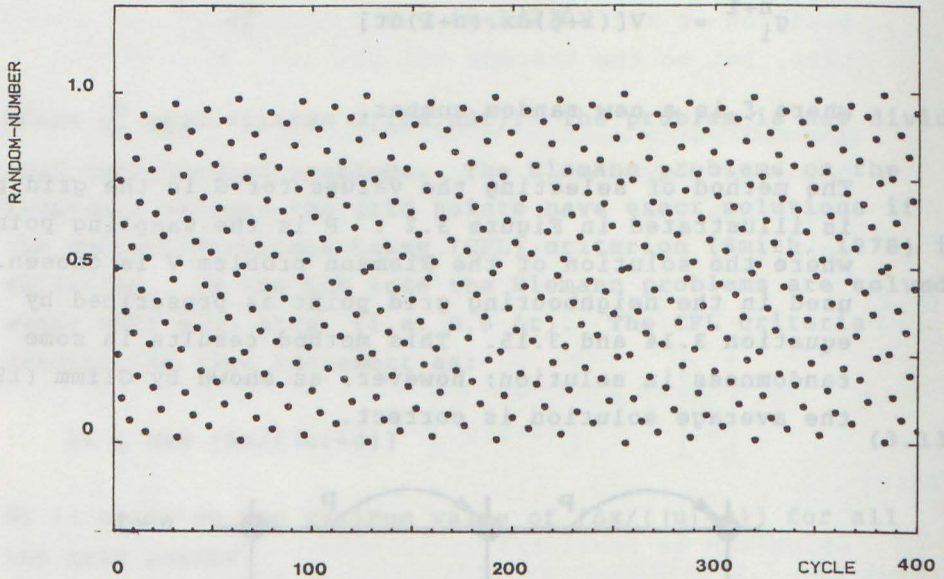
Figure 3.3
Distribution of random numbers generated by the van der Corput algorithm.

When the conservation equations also includes inhomogeneous terms the conservation equations can be written as:

$$\frac{\delta}{\delta t}G + \frac{\delta}{\delta x}F = -W \qquad (3.16)$$

where $W(G)$ is a matrix which includes the inhomogeneous terms.

In Chapter 2 the conservation equations for planar one dimensional flows, including friction and heat transfer, were given in equation 2.11. The inhomogeneous term W(G) from equation 2.11 is:

$$W = \frac{dA}{A_x dx} \begin{bmatrix} 0 \\ \tau_w \\ \dot{q}'' \end{bmatrix} \qquad (3.17)$$

Sod (1977) applied the RCM to solve the gasdynamical equations for cylindrical and spherically symmetric flows. In a cylindrical and spherical symmetric flow, the inhomogeneous term W(G) arises from the volume expansion in radial direction. Sod (1977) solved equation 3.16 in two steps also known as an operator splitting method. First the homogeneous part of the equation was solved using the RCM. Then he corrected for the inhomogeneous term by solving the following equation:

$$\frac{\delta}{\delta t} G = -W(G) \qquad (3.18)$$

Greatrix and Gottlieb (1982) have used Sod's method to study shock waves interations with area changes. They used a first order solution as an approximation, which can be written as:

$$G = \bar{G} - \frac{1}{2} \Delta t \; W(\bar{G}) \qquad (3.19)$$

where $\bar{G}$ is the homogeneous solution of conservation equation 3.16 solved by RCM for every half time step (i.e. 0.5 Δt).The value of W is obtained from the value of $\bar{G}$. The same approach has been applied in this work to correct for friction and heat transfer by using equation 3.17 and 3.19.

Satio and Glass (1979) have modified RCM to handle flow
field, which involves different gases with different
specific heat ratios γ. In these calculations the
position of the contacts surface, which divides the
different gases, have to be known. The same approach as
Saito and Glass (1979) used for determining the trajectory
of the contact surface has in this work been applied to
estimate the particle trajectory in flow field. The
trajectory of particles in one grid point (i,n) is
approximated by the trajectory of the contact surface
between the two grid points (i,n,) and (i-1,n).

3.4   MODELLING OF HEAT TRANSFER AND FRICTION

This section describes how the operator-splitting method
(Sod, 1977) was applied to take the inhomogeneous terms
caused by heat transfer and friction into account in the RCM
code. The equations for modelling the heat transfer rate $\dot{q}''$
and the wall friction τ_w are also described. The
relations for the wall friction τ_w and the heat transfer
rate $\dot{q}''$ were given in equations 2.12 and 2.13 by:

$$\tau_w = C_f \frac{\rho u^2}{2} \qquad (3.19)$$

$$\dot{q}'' = h \ (T_r - T_w) \qquad (3.20)$$

where C_f is the friction factor, h the heat transfer
coefficient, T_r the recovery temperature and T_w the wall
temperature. Using the temperature differences to estimate
the rate of heat transfer is a rather crude approximation
when gas is reacting in the boundary layer. However, due to
the uncertainties in other factors such as h, improvements
to this approach will not significantly increase the
reliability of the heat transfer estimate. Heat transfer

coefficients are empirical correlations, and behind a
detonation wave the only expressions available are based on
modified versions of the Reynolds analogy (Sichel and Davis,
1966). Also in the present modelling, the Reynolds analogy
has been applied. Reynolds analogy is a relation between
the friction factor C_f and the heat transfer coefficient h
(Schlicthing, 1979). From the Reynolds analogy the heat
transfer coefficient can be written:

$$h = \frac{C_f}{2} u \cdot \rho \cdot C_p \qquad (3.21)$$

The heat transfer is then given by:

$$\dot{q}'' = \frac{C_f}{2} u \rho C_p (T_r - T_w) \qquad (3.22)$$

where the recovery temperature is

$$T_r = T + r \frac{u^2}{2C_p} \qquad (3.23)$$

T and u are temperature and velocity in the core stream and
r is the recovery factor. In a turbulent boundary layer r
is (Eckert and Drake, 1972):

$$r = \sqrt[3]{Pr} \qquad (3.24)$$

where the Prandtl number Pr is approximately 0.7 for gases
of interest here. This approximation gives r equal 0.9.
The heat transfer rate can then be written:

$$\dot{q}'' = 0.45 \frac{C_f}{2} \rho u^3 + \frac{C_f}{2} \rho u C_p (T - T_w) \qquad (3.25)$$

The wall temperature T_w was assumed to be equal to the ambient temperature

$$T_w \simeq T_o = \frac{p_o}{R\rho_o} , \qquad (3.26)$$

and for an ideal gas:

$$\frac{p}{\rho} = RT \qquad (3.27)$$

$$C_p = \frac{\gamma}{\gamma-1} R \qquad (3.28)$$

By applying these equations, the heat transfer rate can be expressed as:

$$\dot{q}'' = 0.45 \frac{C_f}{2}\rho u^3 + \frac{\gamma}{\gamma-1} \frac{C_f}{2} u \ (p-\frac{\rho p_o}{\rho_o}) \qquad (3.29)$$

The areas in the term W(G) in equation 3.16 can for a square channel with internal dimension w be written as:

$$A_x = w^2 \qquad (3.30) \qquad\qquad dA = 4wdx \qquad (3.31)$$

The complete expression for W(G) can therefore be written in the form:

$$W(G) = \frac{4}{w} \begin{bmatrix} 0 \\ C_f \cdot \frac{\rho u^2}{2} \\ 0.45 \frac{C_f}{2} \rho u^3 + \frac{\gamma}{\gamma-1} \frac{C_f}{2} u \ (p-\frac{\rho p_o}{\rho_o}) \end{bmatrix} \qquad (3.32)$$

4621Q

This expression for W(G) was then used in the operator
splitting method. A solution for G was obtained using the
following first order approximation :

$$G = \bar{G} - \frac{1}{2} \Delta t \ W(\bar{G})$$ (3.33)

where $\bar{G}$ is the solution of the homogeneous part of the
conservation equations, which was solved by the RCM. In
terms of the individual conservation equations one has:

Continuity:

$$\rho = \bar{\rho}$$ (3.34)

Momentum:

$$u = \bar{u} - \frac{4\tau_w \ (\Delta t/2)}{w\rho}$$ (3.35)

where

$$\tau_w = \frac{1}{2} \ C_f \ \bar{\rho} \ \bar{u}^{\ 2}$$ (3.36)

Energy:

$$e = \bar{e} - \frac{4}{w} \cdot \dot{q}'' \cdot (\Delta t/2)$$ (3.37)

where

$$e = \frac{p}{\gamma - 1} + \frac{1}{2}u^2$$ (3.38)

and

$$\dot{q}'' = 0.45 \ \frac{C_f}{2} \ \rho\bar{u}^{\ 3} + \frac{\gamma}{\gamma - 1} \ \frac{C_f}{2} \ \bar{u} \ (\bar{p} - \frac{\bar{\rho} p_o}{\rho \ o})$$ (3.39)

The new value for p is obtained from the energy equation .
Equations, 3.34 to 3.39 show, in principle, how the
operator-splitting method was used.

3.5   NON-ISENTROPIC EXPANSION OF COMBUSTION PRODUCTS

In Section 3.2 the isentropic expansion model (Taylor, 1950)
for the combustion products behind a detonation wave was
described. As discussed Chapter 2, experimental results
have shown that the expansion behind a detonation wave is
not isentropic, but influenced by heat losses and friction.
In order to obtain an estimate of this effect on the
experimental conditions in the donor section, a modified
version of the RCM code was developed.

This RCM code is a standard RCM code, which includes heat
transfer and friction, as described in the previous section,
but the trajectory of the detonation wave is specified as a
boundary condition. Figure 3.4 illustrates the principle
for these calculations. The detonation front moved one
length increment Δx (i.e. one grid point) in a positive
direction for each Δt, i.e.,

$$\Delta t = \frac{\Delta x}{D_{CJ}} \tag{3.40}$$

Where D_{CJ} is the C-J detonation velocity. The C-J state
was imposed on the grid point where the detonation front was
located at each time step. The flow velocity behind a C-J
detonation is sonic relative to the wave front. The
detonation wave have therefore the same trajectory as the
right running characteristic, $C_+ = u_{CJ} + c_{CJ}$. The
above specification of Δt therefore satisfies the
Courant-Friedrichs-Lewy criterion (Eq. 3.13).

A Taylor profile was used as initial conditions to avoid numerical problems with the boundary conditions at the left side (i=0). The computation was carried out in the grid points between the left side boundary and the location of detonation wave, by the standard RCM, including heat transfer and friction.
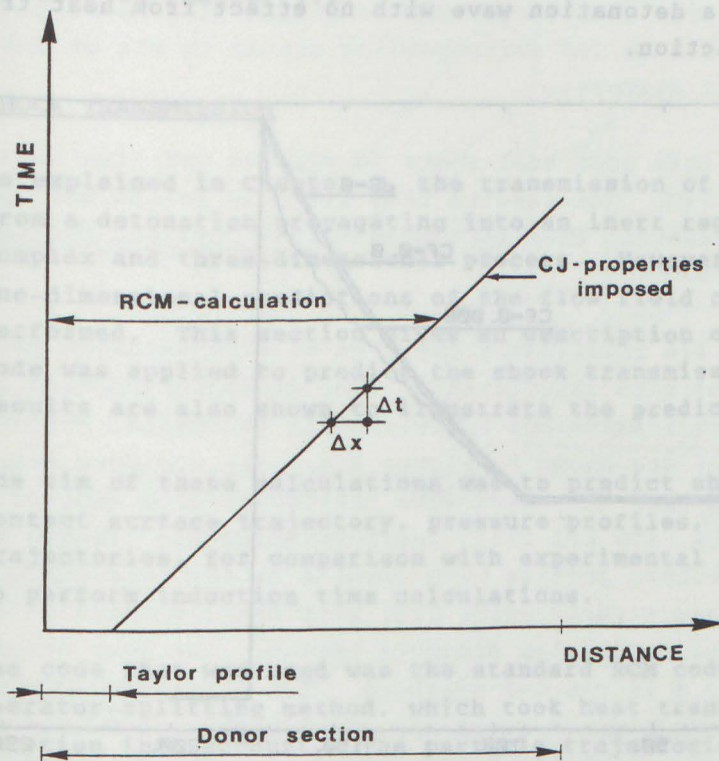
Figure 3.4
Time distance diagram showing the principle of the method of predicting non-isentropic expansion of combustion products by using the RCM-code.

In figure 3.5 pressure profiles from this modified RCM code (C_f =0 and 0.008) are compared with the isentropic pressure profile (ds = 0). When the friction factor, C_f, equals zero, heat transfer and friction are neglected in the RCM calculations. The results should in that case be identical to the isentropic result. Although there is a small difference between the two results it is seen that the calculation gives a good approximation for the flow field behind a detonation wave with no effect from heat transfer and friction.

RCM – INPUT PRESSURE PROFILE
7.73% C2H2-AIR
IDF-SINTEF 15
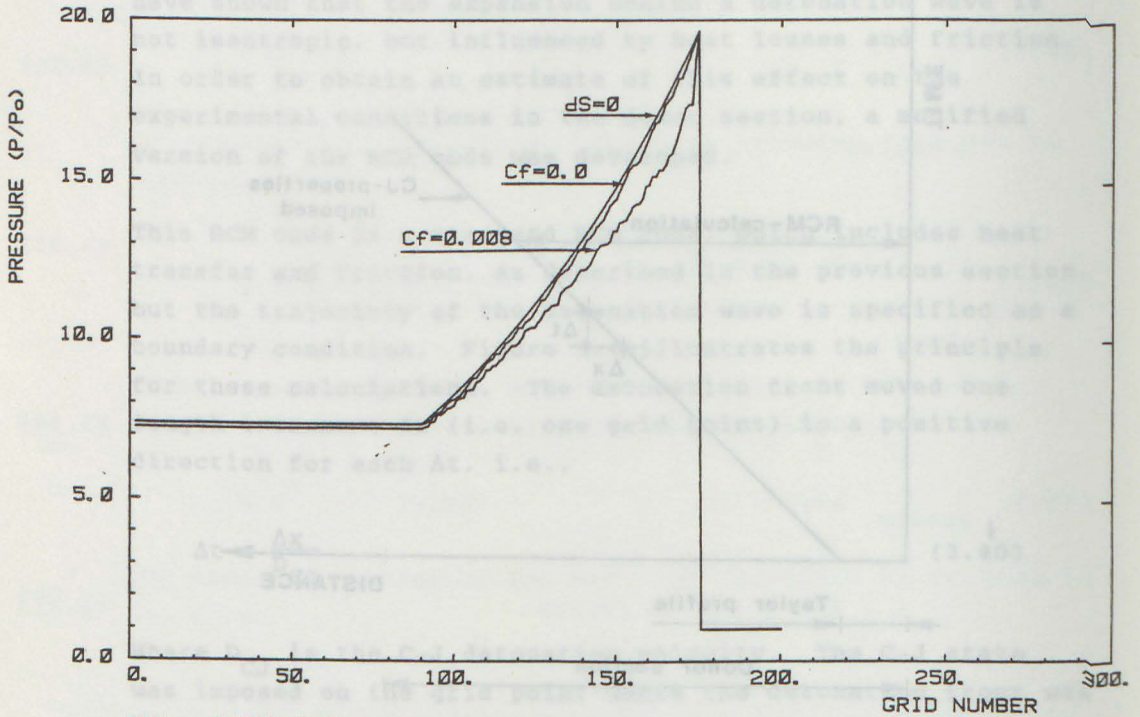
Figure 3.5
    Predicted pressure profiles versus distance behind a C-J
    detonation wave. ds = 0 marks the profile from the
    isentropic expansion model (Taylor, 1950). C_f = 0
    marks the profile from the RCM calculation without wall
    effects and C_f = 0.008 when heat transfer and friction
    is taken into account.

When heat transfer and friction are included (C_f = 0.008) the pressure behind the front is reduced relative to the isentropic pressure profile. The pressure profile on the figure is the predicted pressure profile in donor section when the detonation front reaches Interface I. These profiles are used as input to calculate the transmission and decay of the shock wave in an inert gas region. These type of profiles are also compared with experiment pressure records in chapter 5.2.

3.6   SHOCK TRANSMISSION

As explained in Chapter 2, the transmission of a shock wave from a detonation propagating into an inert region is a complex and three-dimensional process. However, one-dimensional predictions of the flow field can be performed. This section gives an description of how RCM code was applied to predict the shock transmission. Typical results are also shown to illustrate the predictions.

The aim of these calculations was to predict shock and contact surface trajectory, pressure profiles, and particle trajectories, for comparison with experimental results and to perform induction time calculations.

The code that was used was the standard RCM code, including operator-splitting method, which took heat transfer and friction into account. The particle trajectories were also predicted. The effect of heat transfer and friction could be varied, depending on the input value of the friction factor C_f. The calculations were performed with a total of 300 grid points in the distance coordinate, with 175 of these grid points in the donor section. The non isentropic expansion of combustion products behind a detonation wave, as described in the previous section, was used as the initial conditions in the donor section (i.e., for grid points 1 to 175).

Since the resolution was rather low, it was not possible to
do the predictions with different gas types in the inert and
acceptor section. An inert region of 100 mm would consist
of 4 grid points. The inert region could disappear due to
randomess in the calculations and the compression across the
shock wave. Interface II was therefore neglected. This
approximation is discussed in Appendix D and it appears to
be a reasonable approximation for predicting the shock
decay. The calculation was performed with ideal gas in grid
points 176 to 300 corresponding either to air or unburned
fuel-air mixture .

To run this code took about 20 minutes CPU time on a
VAX 11/750. The results from all grid points were stored on
an unformatted file in dimensionless form for further
analysis.

Figure 3.6 illustrates the type of dimensionless data
obtained from calculations. The pressure profiles predicted
for a stoichiometric acetylene-air detonation propagating
into air are shown in Figure 3.6. The pressure profiles are
plotted when the shock wave arrives at grid numbers 200,
225, 250, 275 and 295. These profiles are labeled B to F.
The pressure profile with label A is the detonation front at
Interface I (grid point 175) with non-isentropically
expanded combustion products behind. The peak pressure in
profile A is the C-J pressure. The preak pressure of the
transmitted shock waves are considerably lower than the C-J
pressure. Profiles B and C clearly show the interaction
between a left running rarefaction wave, which propagates
into the combustion products and the right running
rarefaction wave, which follows the detonation wave in donor
section. When heat transfer and friction are taken into
account, the region following the right running rarefaction
wave is also expanded slowly. This expansion can be seen in
the figure as a small decrease in pressure in grid points
between 1 and about 100.

Figude 3C7 shows the predicted rate of heat transfer to the
at wyseeil for the same condition as the previous figured. The
vol hear thhmoordials at the detonation front is as high as 4.9
ehxxcimpls. As the combustion products exploder the ghex
ED sohledy. sOKK B throwingter 1A7 decreased. The graphics
etoronbelle'e and E show the heat transfer rate when ishhock is
aaddrizhhadrtted interthersott. There is a jump in heat transfer
late at the contact surface between the combustion products
and the compressed aib. This jump is mainly due to the
higher temperature of the combustion products.

PRESSURE (P/Po)

20.0

15.0

10.0

5.0

0.0

DONOR SECTION

A   B   C   D   E   F

0.   50.   100.   150.   200.   250.   300.

GRID NUMBER

RCM – Cf=0.008 – PRESSURE PROFILE
7.73% C2H2-AIR / AIR
IDF-SINTEF 15

Figure 3.6
    Predicted pressure profiles versus distance when a shock
    wave transmit into an inert gas. The donor section
    consists of grid points 0 to 175.

Figure 3.7 showes the predicted rate of heat transfer to the wall for the same condition as the previous figure. The heat transfer rate at the detonation front is as high as 4.8 kW/cm^2. As the combustion products expands the gas velocity and the heat transfer rate decrease. The profiles labelled C and E show the heat transfer rate when a shock is transmitted into the air. There is a jump in heat trensfer rate at the contact surface between the combustion products and the compressed air. This jump is mainly due to the higher temperature of the combustion products.
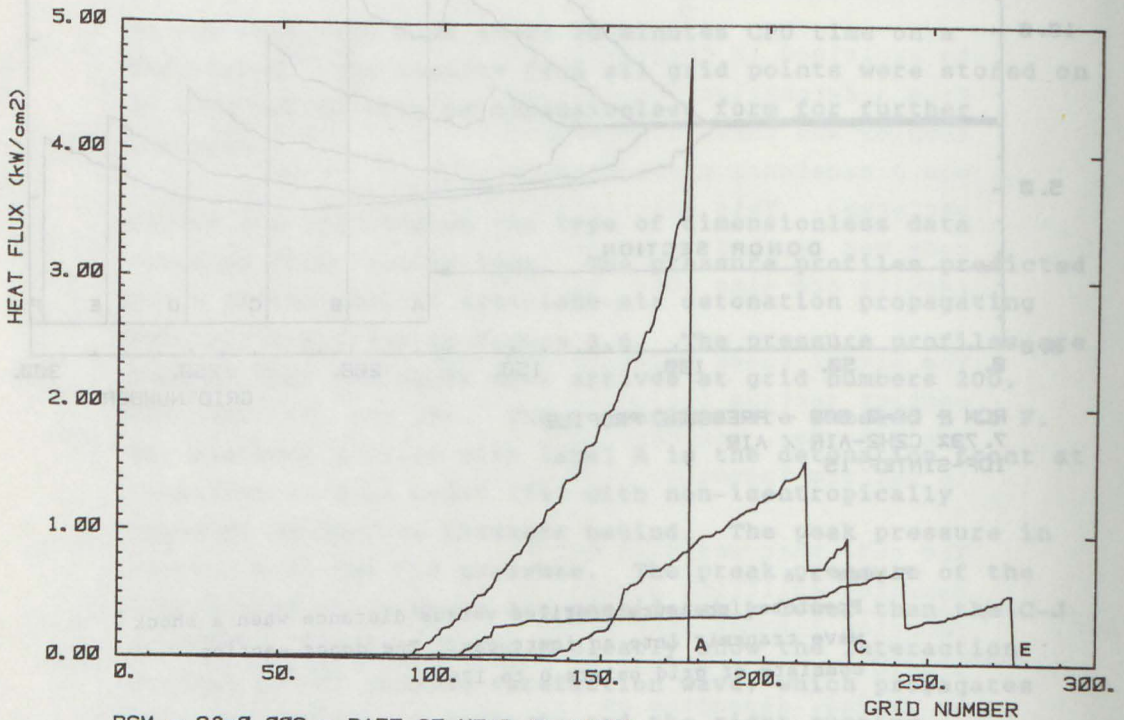
RCM – Cf=0.008 – RATE OF HEAT TRANSFER
7.73% C2H2-AIR / AIR
IDF-SINTEF 15

Figure 3.7
Rate of heat transfer when a shock wave transmit into an inert gas.

Figure 3.8 shows the particle trajectories and the
trajectory of the shock wave. The shock wave trajectory is
the continuous curve. As a result of the method used for
predicting the particle trajectory, the particles in the
grid point can move ahead of the shock wave. When the gas
is crossed by the shock wave, it is compressed. Therefore
the resolution the particle trajectories is reduced across
the shock wave.

RCM - Cf-0.008 - PARTICLE TRAJECTORY
7.73% C2H2-AIR / AIR
IDF-SINTEF 15
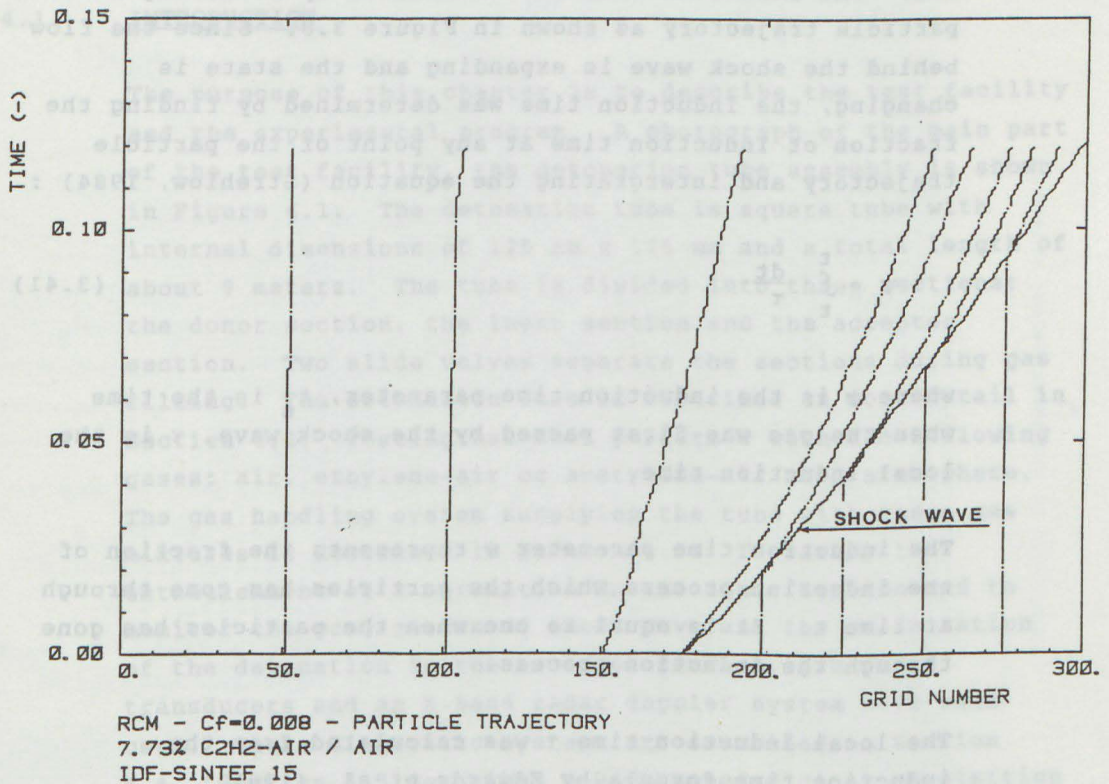
Figure 3.8
    Particle trajectories when a shock wave transmit into an
    inert gas.

The trajectory of the shock wave and contact surface as well
as the pressure profiles predicted are compared with
experimental results in Chapter 5.

3.7   INDUCTION TIME CALCULATIONS

The aim of the induction time calculation was to estimate
the effects of heat losses and friction on the chemical
induction process in the acceptor section.

The induction process was predicted for non-reacting ideal
gas corresponding to unburnt fuel-air in grid points 176 to
300. The induction time was calculated by following a
particle trajectory as shown in Figure 3.8. Since the flow
behind the shock wave is expanding and the state is
changing, the induction time was determined by finding the
fraction of induction time at any point of the particle
trajectory and intergrating the equation (Strehlow, 1984) :

$$\psi = \int_{t_s}^{t} \frac{dt}{\tau} \tag{3.41}$$

where ψ is the induction time parameter, t_s is the time
when the gas was first passed by the shock wave, τ is the
local induction time.

The induction time parameter ψ represents the fraction of
the induction process which the particles has gone through
at time t. It is equal to one when the particles has gone
through the induction process.

The local induction time τ was calculated from the
induction time formula by Edwards et al. (1981):

$$\log(\tau[O_2]) = - 10.48 + 101280/(19.14T) \tag{3.42}$$

where T is the temperature [K] and $[O_2]$ is the molar
concentration of oxygen [moles/liter].

Since the total induction time in some cases was longer than
the calculated time, the times for the gas to go through a
fraction ψ of its induction process were also calculated.

CHAPTER 4

TEST FACILITY AND EXPERIMENTAL PROGRAM

4.1   INTRODUCTION

The purpose of this chapter is to describe the test facility
and the experimental program. A photograph of the main part
of the test facility, the detonation tube assembly is shown
in Figure 4.1. The detonation tube is square tube with
internal dimensions of 125 mm x 125 mm and a total length of
about 9 meters. The tube is divided into three sections:
the donor section, the inert section and the acceptor
section. Two slide valves separate the sections during gas
filling. The detonation tube is described in more detail in
Section 4.2. Testing has been performed with the following
gases: air, ethylene-air og acetylene-air at 1 atmosphere.
The gas handling system supplying the tube with these gas
mixtures is described in Section 4.3. To verify the
establishment of a detonation in the donor section and to
monitor the progagation of shock wave and the re-initation
of the detonation in the acceptor section, pressure
transducers and an X-band radar doppler system have been
used. These diagnostic systems are described in Section
4.4. Section 4.5 describes a high speed digital acquisition
system, which has been developed for recording the signals
from the instruments. Section 4.6 explains the operating
procedure for the test facility. A computer has been used
to analyse the experimental data. Section 4.7 shows a
typical set of output data and explains the methods of
analysing the data. Section 4.8 describes the experimental
conditions and the purpose of the different types of tests.

The main events as far as the development and use of the
test facility are listed below in chronological order below:

Date: Event:

March 81   Start of program.
June 81   Fabrication of detonation tube parts.
Dec. 81   Design slide valves.
March 82   Test CJ-detonations.
Sept. 82   Test pressure diagnostics and a tape
               recording system.
Nov. 82   Preliminary test of re-initiation of a
               detonation across an inert region.
April 83   Design of high speed data logger.
Oct. 83   Checkout of high speed data logger.
Dec. 83   Microwave doppler system tested.
May 84   Main testing ended.

4.2   DETONATION TUBE

The design requirement for the experimental apparatus was to
create three regions with homogeneous gas mixtures in
various sections of the tube. The concentration gradients
at the interfaces should be as sharp as possible. The
dimension of the tube had to be large enough so that it
could support a multi-headed detonation wave and stabilize
the detonation wave in the donor section prior to
Interface I.

Figure 4.2 shows a schematic of the experimental apparatus.
The tube assembly consists of four sections: a booster
section, a donor section, an inert section and an acceptor
section. The booster section is circular while the other
sections are square. The donor and acceptor sections are
filled with a detonable mixture of acetylene-air or
ethylene-air. The inert section contains air. In order to
divide the three sections during gas filling, two slide
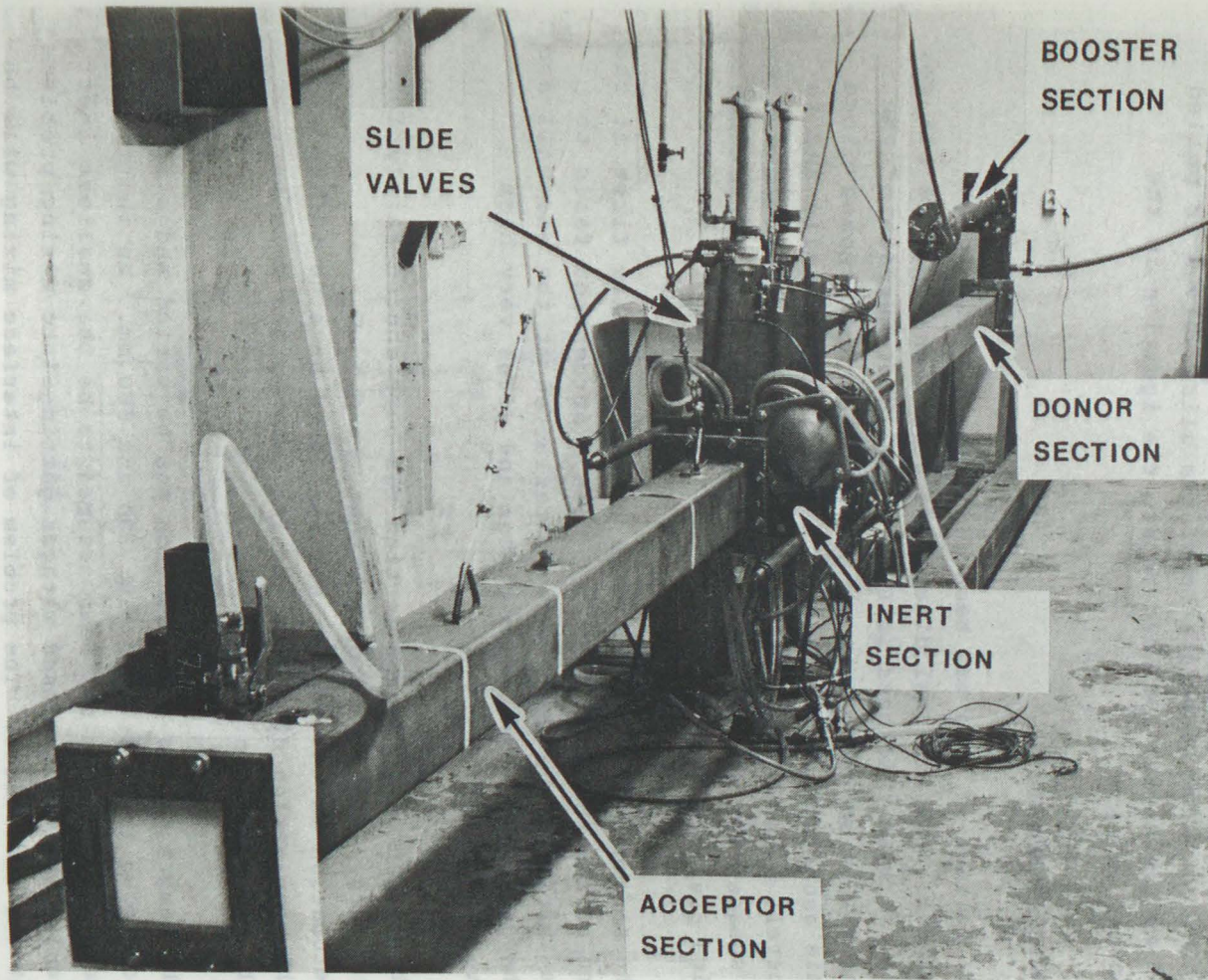
Figure 4.1
Photograph of the experimental apparatus.

valves are used. A slide valve consists of a steel plate
which can be pulled out rapidly through a pneumatic piston
arrangement. The booster section is filled with
acetylene-oxygen to initiate the detonation wave in the
donor section. The firing sequence is preprogrammed and
automated. The steel plates of the slide valves is pulled
out approximately 250 msec before the ignition in the
booster section.

4.2.1   Tube dimensions

The detonation tube has been made from a square steel
channel. The internal dimensions of the channel are 125 mm,
and the wall thickness is 6 mm. The inner surface of the
channel is untreated. A square tube has been chosen since
this geometry makes it simple to mount smoked foils and to
install windows for high-speed filming. The disadvantage of
a square tube is the relative low capability of withstanding
high pressures.

The strength problem with high pressure appears first at the
end of the acceptor section. When a detonation fails to
re-initiate, the shock wave is reflected at the end wall and
the compressed gas then explodes and gives very high
over-pressure.

The length of the donor section has been chosen fairly long,
5 meters, in order to ensure that the $C_2H_2-O_2$
detonation in the booster section would have no influence on
the propagation of the detonation wave in the main part of
the donor section.

The length of the inert section can be varied and attain
following lengths: 100, 150, 200 and 500 mm. An inert
section of 100 mm has been assumed to be the smallest inert
region that can be used without getting into mixing problems
at the interfaces. The problem of interface mixing will be
convered in more details later.
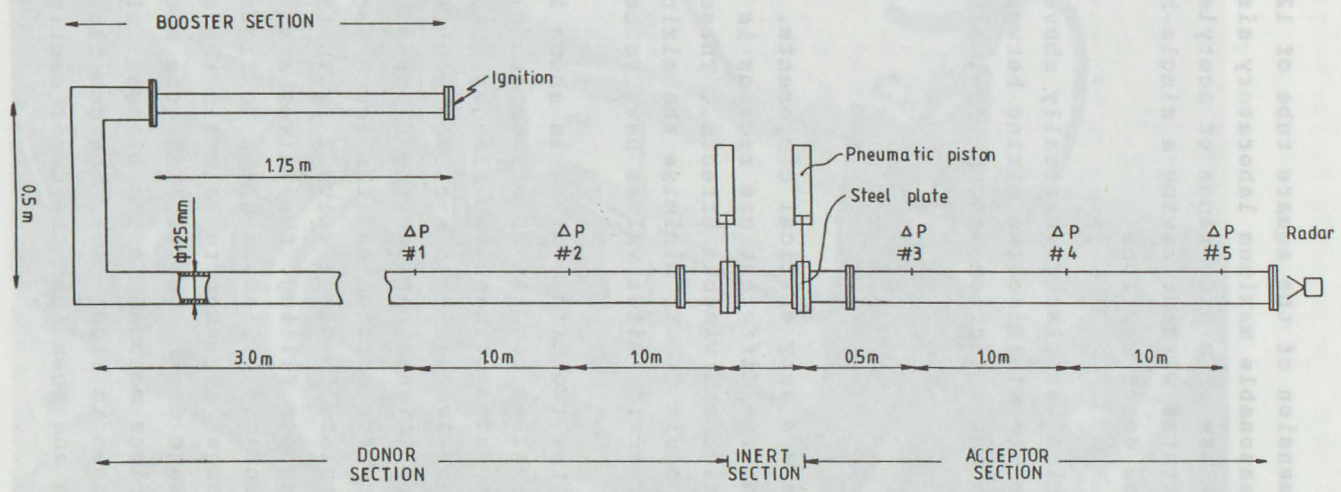
Figure 4.2
Experimental apparatus.

The length of the acceptor section is about 3 meters.

The internal dimension of the square tube of 125 mm was
selected as a reasonable maximum laboratory size, which
still allows the use of a wide range of acetylene or
ethylene-air mixtures without having a single-headed
detonation in the donor section.

The booster section was placed vertically above the other
sections in order to minimize the mixing between
$C_2H_2-O_2$ in the booster section and the fuel-air in the
donor section.

4.2.2   Slide valves

The slide valves are very critical components. The
interface between two different gas regions is influenced by
buoyancy, diffusion and viscous effects. These effects are
discussed in Appendix C. To minimize the mixing at the
interfaces, fast-acting slide valves have to be used.

A photograph of the two slide valves is shown in Figure
4.3. The slide valves consist of a 1 mm stainless steel
plate which is mounted between two flanges. In the
photograph slide Valve II is in a closed position, i.e.: the
steel plate is positioned between the flanges, thereby
dividing the acceptor section and the inert section. As
shown the steel plate in slide valve I is in the out or open
position. During gas filling, the valves are kept closed
and the four pneumatic cylinders shown in figure as cylinder
B, forcs the flanges together to maintain the seal. To
prevent gas leakage during gas filling, the steel plates are
sealed using O-rings mounted in the flanges. In the
configuration shown in Figure 4.3, the gas flows through the
acceptor section and then into the donor section.

CYLINDER A

SLIDE VALVE I

SLIDE VALVE II

CYLINDER B
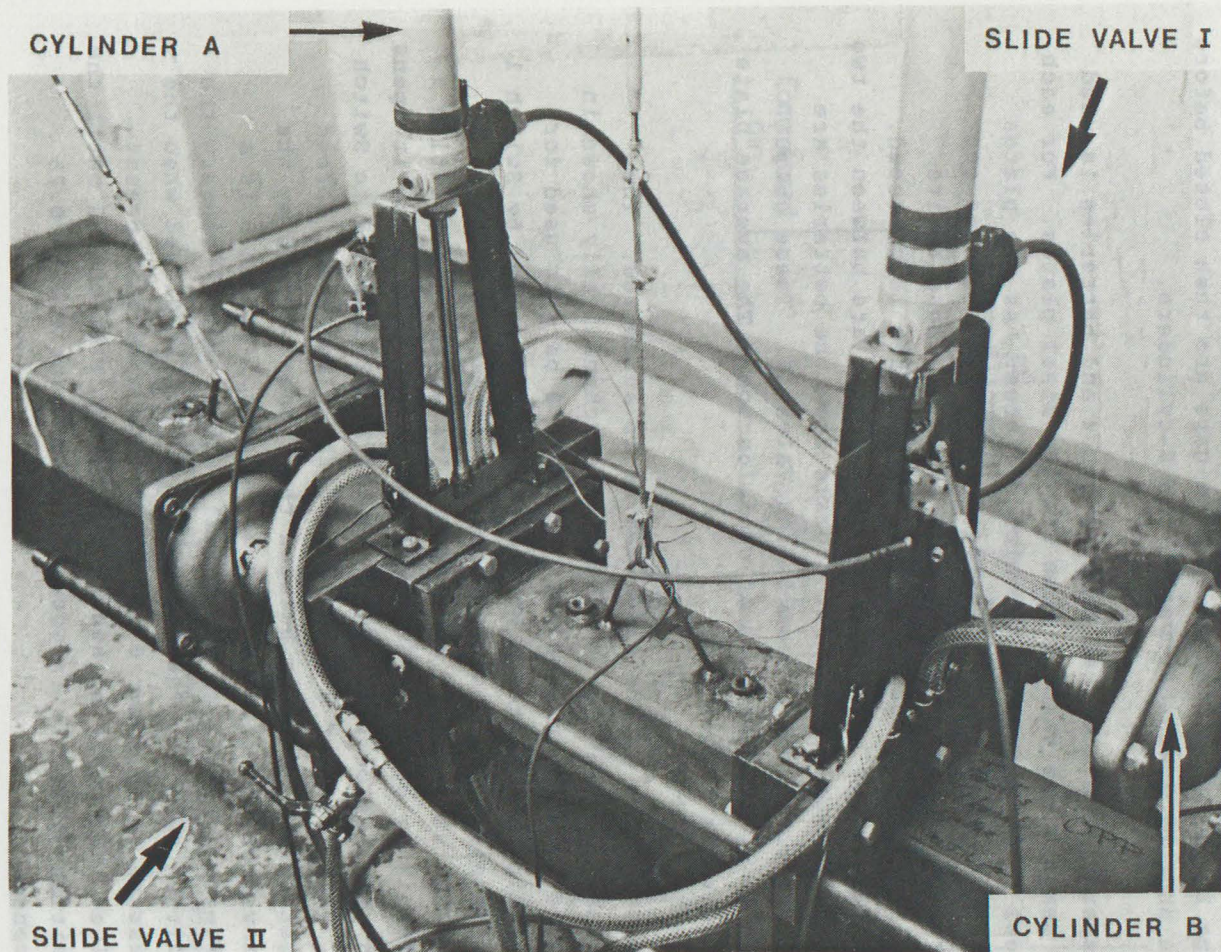
Figure 4.3
Photograph of the two slide valves. Slide valve I in
open position. Slide valve II in closed position.

The gas is flowed via eight 6 mm diameter holes in the flanges and the bypass hoses shown on the Figure 4.3. Just before each shot the pressure in the B-cylinders is released so that the steel plates can be pulled out by the two A-cylinders. The removal of the steel plates causes gaps between the flanges. These gaps are then closed before the shot by again activating the B-cylinders.

A system of electrical microswitches and batteries is used to measure the removal time for the steel plates. For each steel plate there are two microswitches. As the plates starts to move, the upper edge of the plate passes one microswitch and when the steel plate is close to its pulled-out position, a secound microswitch is contaced. When the upper edges of the steel plates are between the two microswitches, the output signals from the batteries are -3.0V for Valve I and +1.5V for Valve II. These output signals are recorded on an oscilloscope. The average plate velocity is 2 to 4 m/s.

The operation of the slide valves is automated. The pneumatic system for the valves is schematically shown in Figure 4.4. Compressed air at about 6 bars is used for operating the system. Cylinder A is controlled by Switch 1 and by opening Switch 1 the steel plates are pulled out. When the steel plate is close to its pulled-out position Switch 3 is opened. Switch 3 activates Valve 4, so it opens and supplies compressed air to the B-cylinder and to Switch 5. When cylinder B is activated the flanges are forced together and the gaps between the flanges caused by the removal of the steel plates are closed. Switch 5 is a pneumatic-controlled electrical switch, which triggers the ignition system. The electrical switch is closed when the pressure in Cylinder B is higher than a certain preset value. The whole sequence from Switch 1 is opened until the ignition system is triggered, takes about 0.2 to 0.25 seconds.
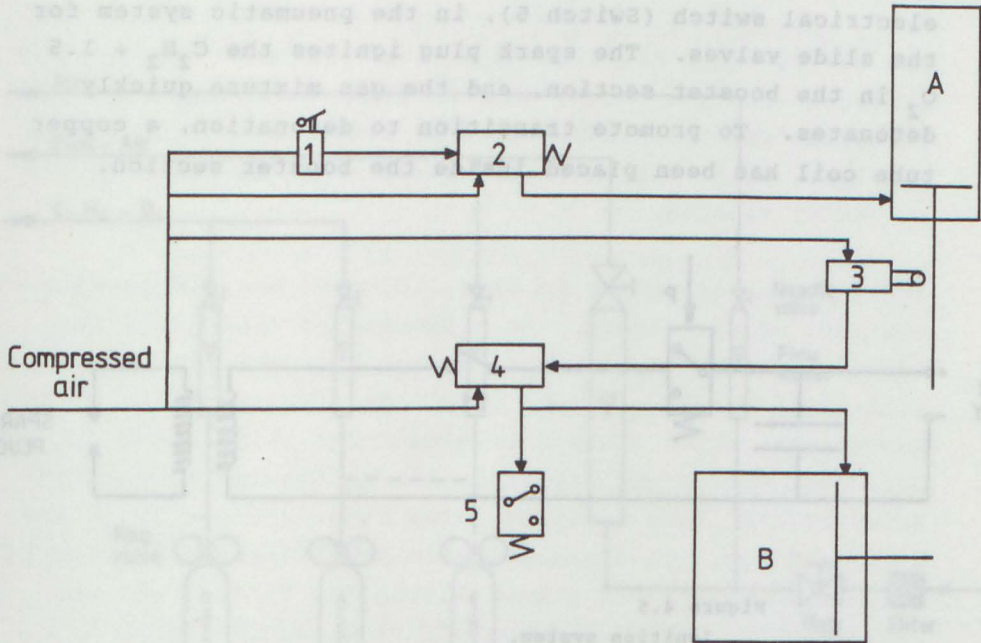
Figure 4.4
Schematic diagram of the pneumatic system for operating
the slide valves.

4.2.3   Ignition system

The ignition system is basically an automobile-coil circuit
as shown in Figure 4.5. It is powered by 35 VDC power
supply. First the Switch S1 is closed and then the system
is triggered by closing the pneumatical-controlled
electrical switch (Switch 5), in the pneumatic system for
the slide valves. The spark plug ignites the C_2H_2 + 1.5
O_2 in the booster section, and the gas mixture quickly
detonates. To promote transition to detonation, a copper
tube coil has been placed inside the booster section.
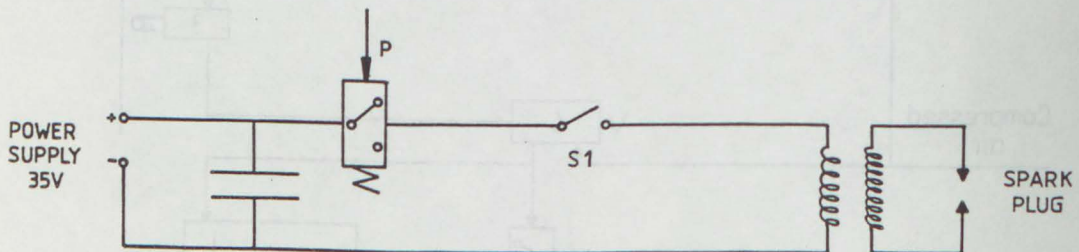
Figure 4.5
Ignition system.

4.3   THE GAS HANDLING SYSTEM

This section gives a description of the gas handling system
and how the tube is filled with different gas mixtures. The
gas handling system is capable of supplying the tube with
air, fuel-air and acetylene-oxygen mixtures. The fuel-air
mixtures used are either acetylene-air or ethylene-air. The
gas handling system is shown in Figure 4.6. The gas
mixtures are generated using compressed air, and bottles of
commercial grade acetylene, ethylene (99.7% pure) and

oxygen. The gas mixtures are supplied to the tube in a
continuous flow. The composition is monitored by calibrated
flow meters and regulated with needle valves. The gas
pressures are at a constant level after the regulator valves.
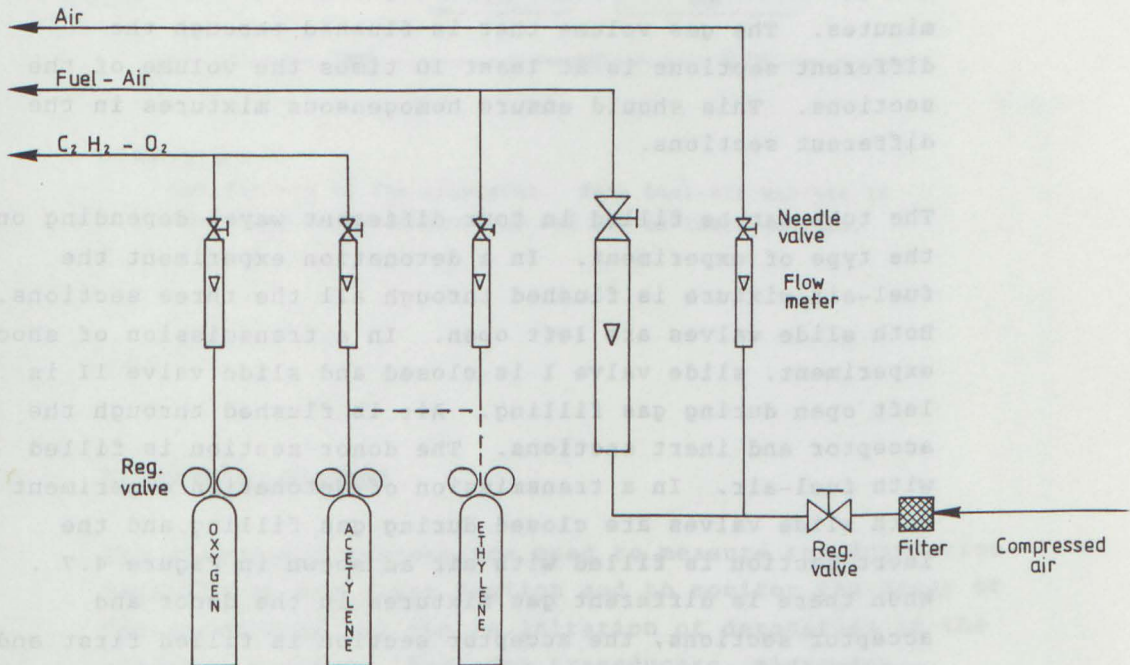
Figure 4.6
Gas handling system.

The flow meters have been calibrated using a gas meter type
Elster 02 H-D. The accurancy of the calibration for the
fuel-air mixture is estimated to be about $\pm$ 0.25% of the
fuel concentration. The relative accurancy of the fuel
concentrations between each experiment is expected to be
$\pm$ 0.1% of the fuel concentration.

The gas mixtures are flushed through the tube for about 20
minutes. The gas volume that is flushed through the
different sections is at least 10 times the volume of the
sections. This should ensure homogeneous mixtures in the
different sections.

The tube can be filled in four different ways, depending on
the type of experiment. In a detonation experiment the
fuel-air mixture is flushed through all the three sections.
Both slide valves are left open. In a transmission of shock
experiment, slide valve I is closed and slide valve II is
left open during gas filling. Air is flushed through the
acceptor and inert sections. The donor section is filled
with fuel-air. In a transmission of detonation experiment
both slide valves are closed during gas filling and the
inert section is filled with air as shown in Figure 4.7 .
When there is different gas mixtures in the donor and
acceptor sections, the acceptor section is filled first and
thereafter the donor section. In all the experiments the
booster section is filled at the same time as the donor
section.

After the sections are filled with the gas mixture the
pressure in the different sections are equalized by opening
valves to ambient pressure. These equalizer valves stays
open during a test. This is done to avoid enhanced mixing
at the interfaces caused by small differences in pressure
between the different sections.
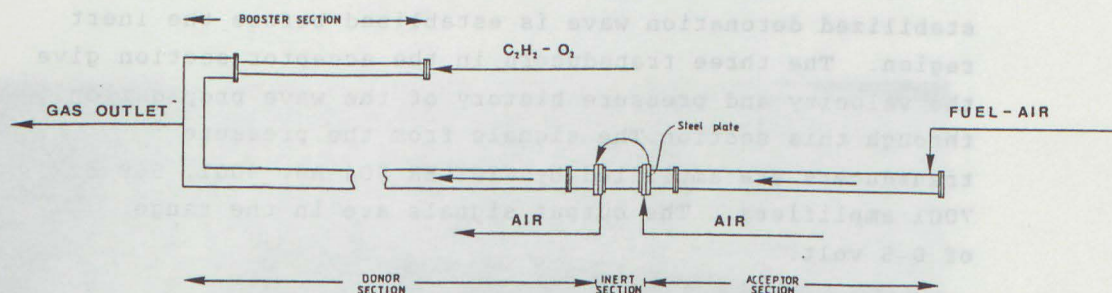
Figure 4.7
    Gas filling of the apparatus. Same fuel-air mixture in
    donor and acceptor sections and air in inert section.

4.4   DIAGNOSTIC SYSTEMS

The diagnostic systems are used to measure the detonation
velocity in the donor section and to monitor the decay of
the shock wave and the re-initation of detonation in the
acceptor section. Pressure transducers, microwave
radar-doppler equipment and smoked foils are used. In this
section these diagnostic system are described.

4.4.1   Pressure diagnostics

Kistler 603 B pressure transducers are used. The
transducers are mounted in plastic adaptors to reduce the
noise signal. The transducer diaphragm is covered with a
thin film of silicon (Silastic 732 RTV) to reduce the
thermal effect. The diameter of the transducer diaphragm is
5.55 mm. The positions of the pressure transducers are
shown in Figure 4.2.

Two pressure transducers are mounted in the donor section
1 m apart. These measurements are used to ensure that a
stabilized detonation wave is establised before the inert
region. The three transducers in the acceptor section give
the velocity and pressure history of the wave propagation
through this section.The signals from the pressure
transducers are amplified by KISTLER 504 A5, 5001, 568 or
7001 amplifiers. The output signals are in the range
of 0-5 volt.

4.4.2 Microwave radar-doppler system

An X-band (10.525 GHz) microwave radar-doppler system is
used to continuously measure the velocity of the detonation,
the reaction wave and the contact surface. The
radar-doppler system utilizes the fact that the microwaves
reflected by the moving ionized reaction zone or the region
of hot combustion products will result in a shift in
frequency. The shift in frequency is proportional to the
velocity of the reflecting target. The microwave Doppler
transceiver used is M/A-COM type MA 86656-D unit. The
output signal from the transceiver is the doppler shift
frequency. The scaling factor between the doppler frequency
and the target velocity is 70.2 Hz/(m/s).

The signal from the radar-doppler unit is filtered and
amplified before it is recorded. Two amplifiers were used
during the experiments. One of the amplifiers has an
amplification of about 100 and a band pass filter in the
range of 40 Hz - 400 kHz. This amplifier has been used in
most of the experiments. However, after test # 82 another
amplifier with an amplification of 1000 and a
20 Hz - 700 kHz band pass filter was used.

The radar-doppler unit is located at the end of the acceptor
section as shown in Figures 4.2 and 4.8. The microwaves are
transmitted into the detonation tube through a "window".
This "window" is made of a 40 mm thick high density
polyethylene plate.
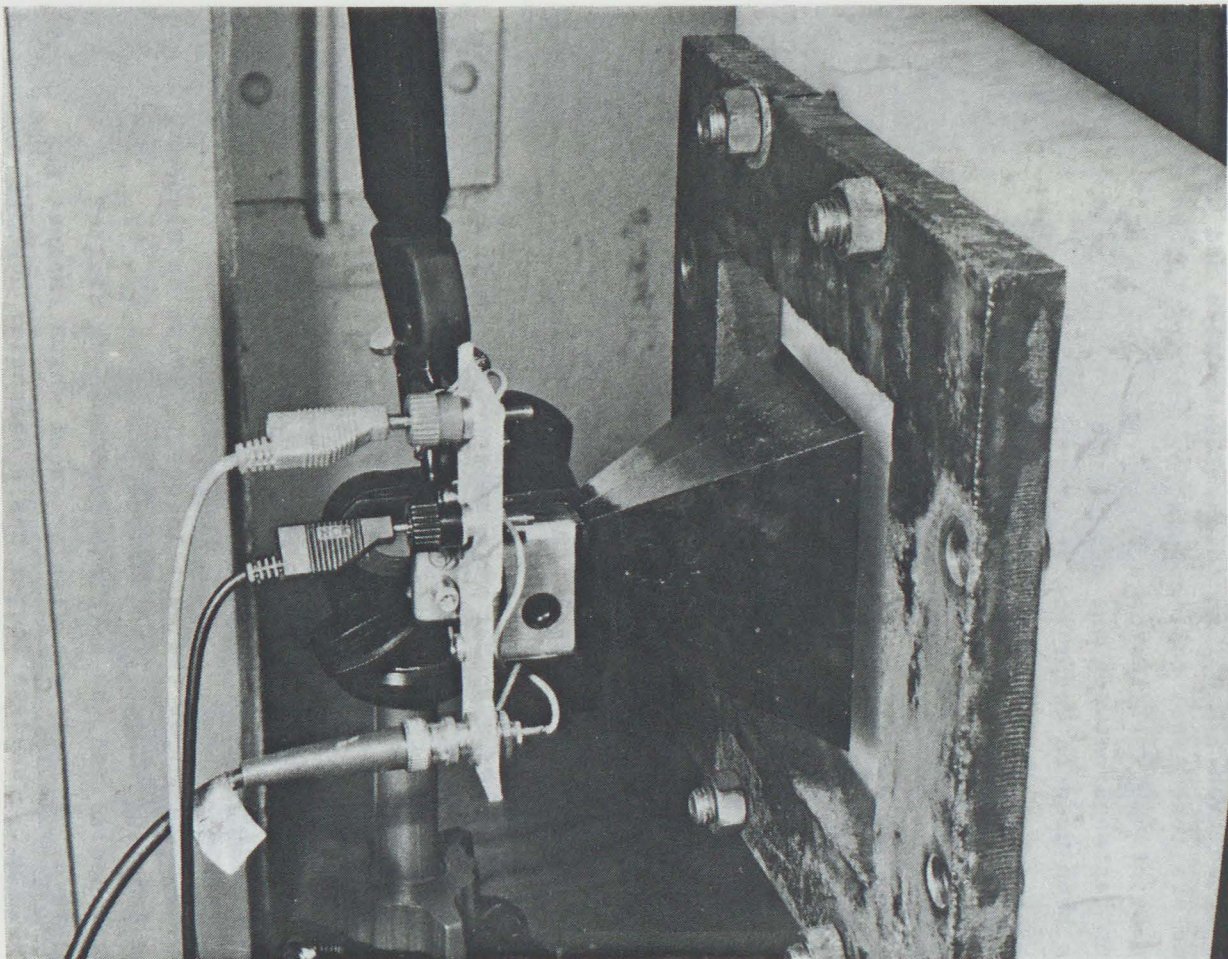
Figure 4.8
    Photograph of the microwave doppler unit and the 40 mm
thick high-density-polythylene "window" at the end of
acceptor section.

4.4.3   Smoked foil

In some experiments a smoked foil has been used in the
acceptor section to identify the location of the onset of
the detonation. A 0.1 mm thick, 100 mm wide and about
3 meters long metal foil covered by soot is placed along the
inside of one wall in the acceptor section. The foil is
then fastened between the end flanges. An acetylene torch
has been used to cover the foil with soot.

4.5   DATA ACQUISITION SYSTEM

This section describes the system used for recording the
signals from the pressure transducers and the radar-doppler
unit. In the early phases of this program a tape recorder,
Ampex-FP 1300, was used for data acquisition. The tape
recorder system was time-consuming to use and the resolution
of the results was not quite satisfactory.   To obtain a
more suitable system it was decided to build a high speed
digital data logger (transient recorder) based on a
concept developed by the firm Micro-Mathisen (Mathisen,1983).

A high speed data logger with relativily simple overall
performance, but with large memory and high sampling rate
was desired. The specification and design of the data
logger was done in cooperation with Micro-Mathisen.
Micro-Mathisen designed the electonic circuits. The system
was built in the electronic workshop at the Division of Heat
and Combustion Engineering at NIT.

The front panel of the data logger is shown on Figure 4.9.
The sampling interval and trigger delay is set by
thumbwheels, and the settings are shown on digital
displays. A two-digit display shows which channel is
displayed. The data logger has 6 channels; however, the
system can be expanded to 16 channels by plugging in new
A/D-boards. The data logger has been designed for input
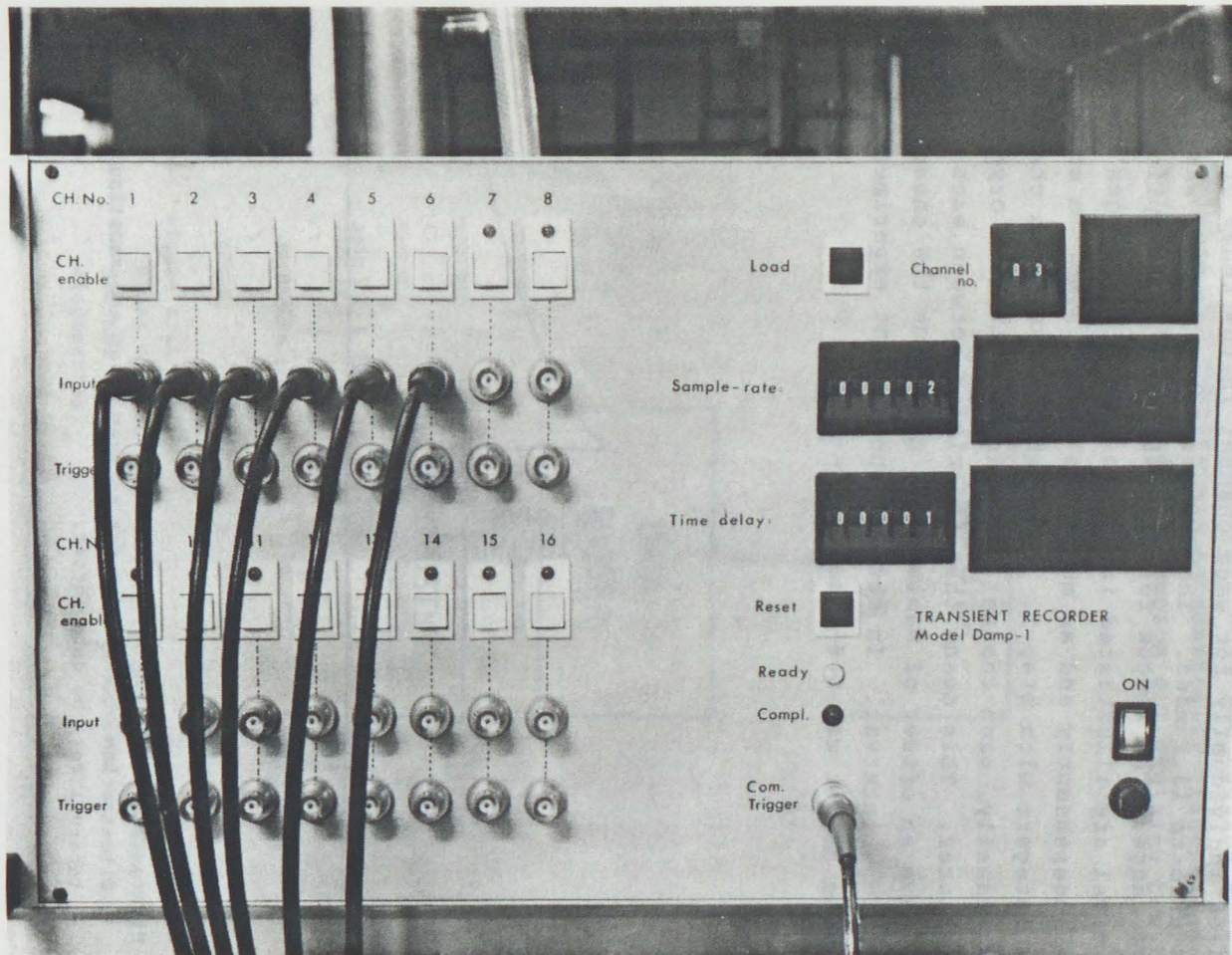
Figure 4.9
Photograph of the high speed digital data logger.

signals of 0–5 V. The analog signal is directly converted
to a 7 bit digital signal. The accuracy is ± 0.02 V. The
total storage for each channel is 16 Kbyte RAM
(16384 sampling points). The sampling interval can be
varied individually for each channel in the range of
0.2 μsec to 13.1 msec. The trigger delay has the same
time range. The ranges for trigger delay and sampling
interval are illustrated in Figure 4.10. The ranges can be
set independently and as multiples of 0.2 μsec. n and j
are integers with step 1. To be able to set each channel
individually, each channel A/D-board has its own crystal
oscillator. This means that the timing between each channel
can have an offset of maximum 0.2 μsec plus the chosen
samplings interval. In most of the present experiment this
maximum offset was 0.6 μsec.
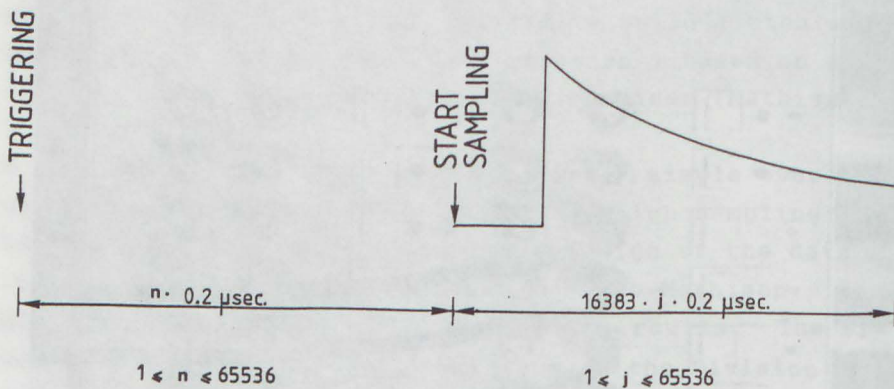
Figure 4.10
Illustration of the range for trigger delay and sampling
interval for the data logger.

The data logger is connected to a DEC LSI 11/03 computer as illustrated in Figure 4.11. The computer controls the operation of the data logger. It is also used to store and reduce the raw data. The data logger is triggered by a pressure transducer signal. When the logging sequence is finished the results are automatically transferred and stored in the computer. Section 4.7 explains how this raw data is reduced.

```
┌─────────────┐
│  COMPUTER   │
│    DEC      │
│   11 / 03   │
└─────────────┘
       ↑
       ↓
┌─────────────┐
│    DATA     │
│   LOGGER    │
└─────────────┘
       ↑
┌─────────────┐
│ DIAGNOSTICS │
└─────────────┘
```
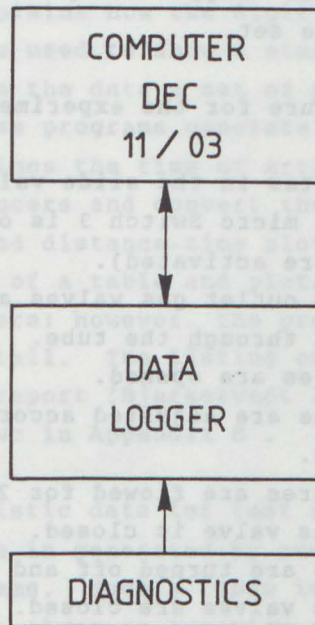
Figure 4.11
   Block diagram illustrating the coupling between the
   DEC LSI 11/03 computer, high speed data logger and
   diagnostics.

4.6   OPERATION PROCEDURE

The previous sections have contained descriptions of the operation of the individual sub-systems for the test facility. In this section the total operation procedure is explained.

First the flow settings are calculated. Then the communication line between the computer and the data logger is established. The trigger delay and sampling interval on the data logger are set.

The running procedure for the experiments is as follows:

1) The steel plates in the slide valves are installed.
2) The pneumatic micro Switch 3 is opened (i.e. B-cylinders are activated).
3) The inlet and outlet gas valves are opened.
4) Air is flowed through the tube.
5) The gas bottles are opened.
6) The flow rates are adjusted according to the calculated flow settings.
7) The gas mixtures are flowed for 20 minutes.
8) The outlet gas valve is closed.
9) The gas flows are turned off and the gas bottles closed.
10) The inlet gas valves are closed.
11) The outlet gas valve is opened for short periods to equalize the pressure to 1 atmosphere.
12) Equalizer valves are opened.
13) The radar-doppler unit is turned on.
14) The pressure amplifiers is reset.
15) Pneumatic microswitch 3 is opened.
16) Switch S1 in the ignition circuit is closed.
17) The data logger is set in the operation mode.
18) Switch 1 in pneumatic system for for the slide valves is opened and the ignition system is automatically activated.

The procedure from events 8 through 18 is carried out after
a preset time schedule and took about 2 min. and 10 sec. To
go through the whole procedure takes about 30 minutes.
After this procedure was carried out, the recorded results
are automatically transferred and stored on the
DEC LSI 11/03 computer.

4.7   DATA REDUCTION

This section explains how the digitized data are reduced.
Test #18 will be used to show a standard type of reduced
data. To reduce the data a set of programs have been
developed. These programs generate plots of pressure
records, determines the time of arrival of the wave at the
pressure transducers and convert the radar-doppler signal
into velocity and distance-time plots. The outputs from the
program in form of a table and plots of the reduced data
will be shown here; however, the programs will not be
discussed in detail. The listing of the programs is given
in a reference report (Bjerketvedt 1985). The use of the
programs is shown in Appendix E .

The characteristic data for test #18 are shown in Table
4.1. This table is generated by running one of the data
reduction programs. Such a table is generated for every
test. The table gives an overview of the experimental
conditions and the average velocity between the pressure
transducer measurement stations. In this table the test
number, the date, the time of day and the data for the
experimental conditions are given. It is seen that for test
#18 the gas mixtures in the donor and acceptor sections were
both stochiometric acetylene-air (7.75% C_2H_2-AIR).
Further more, a 100 mm long inert section filled with air
was used. The settings of the flow meters and the data for
the diagnostics and the data acquisition system are also
listed in the table.

TABLE 4.1 :

Table showing the characteristical data for test # 18.

DETONATION TRANSMISSION ACROSS AN INERT REGION
IDF-SINTEF 15

TEST NO.:018   DATE :01-MAR-84   TIME :09:45:39

TEMPERATURE :   18.0 C   PRESSURE : 737 Torr

		LENGTH (M)	GAS COMP.
DONOR SECTION	:	5.0	7.75%C2H2—AIR
INERT SECTION	:	.10	AIR
ACCEPTOR SECTION	:	3.0	7.75%C2H2—AIR
BOOSTER SECTION	:	1.75	C2H2+1.5 O2

FLOWMETERS :

		FUEL		OXIDIZER	
		RANGE (%)	PRES.(Ato)	RANGE (%)	PRES.(Ato)
DONOR SECTION	:	18.9	1.5	37.0	3.0
INERT SECTION	:			20.0	
ACCEPTOR SECTION	:	18.9	1.5	37.0	3.0
BOOSTER SECTION	:	14.0	1.5	20.0	1.5

	1	2	3	4	5	6
MEASURING POINT	1	2	3	4	5	6
TRANSDUCER	603B	603B	603B	603B	603B	RADAR
TRANSDUCER NO	50188	100590	100589	50187	123488	
TRANS. CALL. (pC/bar)	6.50	4.89	4.49	5.94	4.68	
AMPLIFIER MODEL	504A5	5001	568	568	5001	
AMPLIFIER NO	SN0554	SN17841	SN2164	SN2156	SN14948	
SENSITIVITY	5.0	8.00	3.5	5.0	8.0	
RANGE (bar/V)	5	5	10	10	5	
FILTER (kHz)	150	180	--	—	15	

	1	2	3	4	5
CHANNEL NO:	1	2	3	4	5
CHANNEL CALL (Vout/Vin)	0.9133	1.0116	1.0199	0.9894	.9033
TRANSDUCER POS. (M)	0.000	1.000	2.600	3.600	4.600
SAMPLE RATE	1	1	1	1	1
DELAY TIME	1	1	1	1	1
SCALING FACTOR (Bar/V)	4.794	8.136	7.643	8.508	9.462
TIME OF ARRIVAL (Mic.Sec.)	0.6	530.2	1570.6	2213.4	2729.0

VELOCITIES (M/S) :   CJ-INERT INTERFACE (M) :   2.00

         1 - 2 :1888.2
         2 -AIR :1888.2
        AIR- 3 :1174.6
         3 - 4 :1555.7
         4 - 5 :1939.5

TIME DELAY : .24 SEK   COUNT DOWN : 2.10

COMMENTS :

4.7.1 Pressure signal

The measured average velocities between the pressure
transducer are also given in Table 4.1. The time of arrival
of the pressure pulse at a transducer is defined as the time
when the sampling value for the first time exceeded a
certain specified value. The inaccuracy of this method is
expected to be less than twice the samplings interval (i.e.
< 0.8 μsec).

For each channel there is a total of 16.384 sampling
points. When plotting the pressure records, it is necessary
to reduce the number of data points considerably. This
reduction of points is achieved by averaging the sampling
values by the following formula:

$$\bar{y} = \frac{\sum\limits_{i=j}^{j+n-1} y_i}{n} \tag{4.1}$$

Where n is the number of sampling points. i, j and n are
integers. y_i is the sampling value at point i and y is
the average sampling value in the interval [j,j+n−1].

The pressure recordings can be plotted in two ways. First,
all five pressure profiles can be plotted on one figure as
shown in Figure 4.12.

This figure gives an overview of all the pressure profiles.
For this case the averaging is based on 100 samplings points
(i.e. n = 100). In this case channels 1 and 2 (CH 1 and CH
2) did not work properly. An overdriven detonation is
observed on CH 4. The detonation wave has been
reestablished before this transducer.

TEST NO.: 018   DATE : 01-MAR-84
7.75%C2H2-AIR /   AIR (.10 m) / 7.75%C2H2-AIR
IDF-SINTEF 15
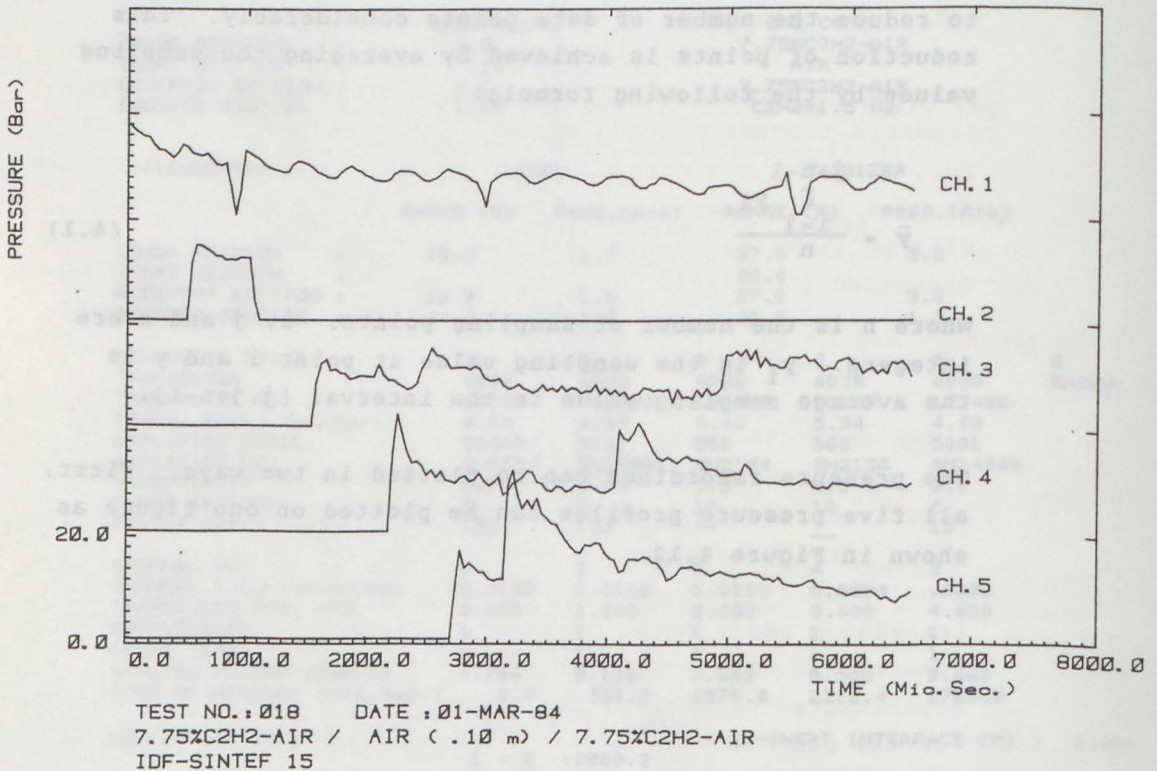
Figure 4.12
    Pressure time diagram for all the pressure profiles in
    test #18.

In the other type of plot, a more detailed view of the
pressure profiles can be obtained. A specified part of a
pressure record can be extracted from the memory and
plotted. Figure 4.13 shows an example of this type of
plot. In this case the pressure recording for channel 3
(CH 3) between the times of 1500 μsec and 3000 μsec is
plotted. The plotted values are here based on the averaging
of 5 sampling points (i.e. n = 5).

TEST NO.:018   DATE :01-MAR-84
7.75%C2H2-AIR / AIR (.10 m) / 7.75%C2H2-AIR
IDF-SINTEF 15
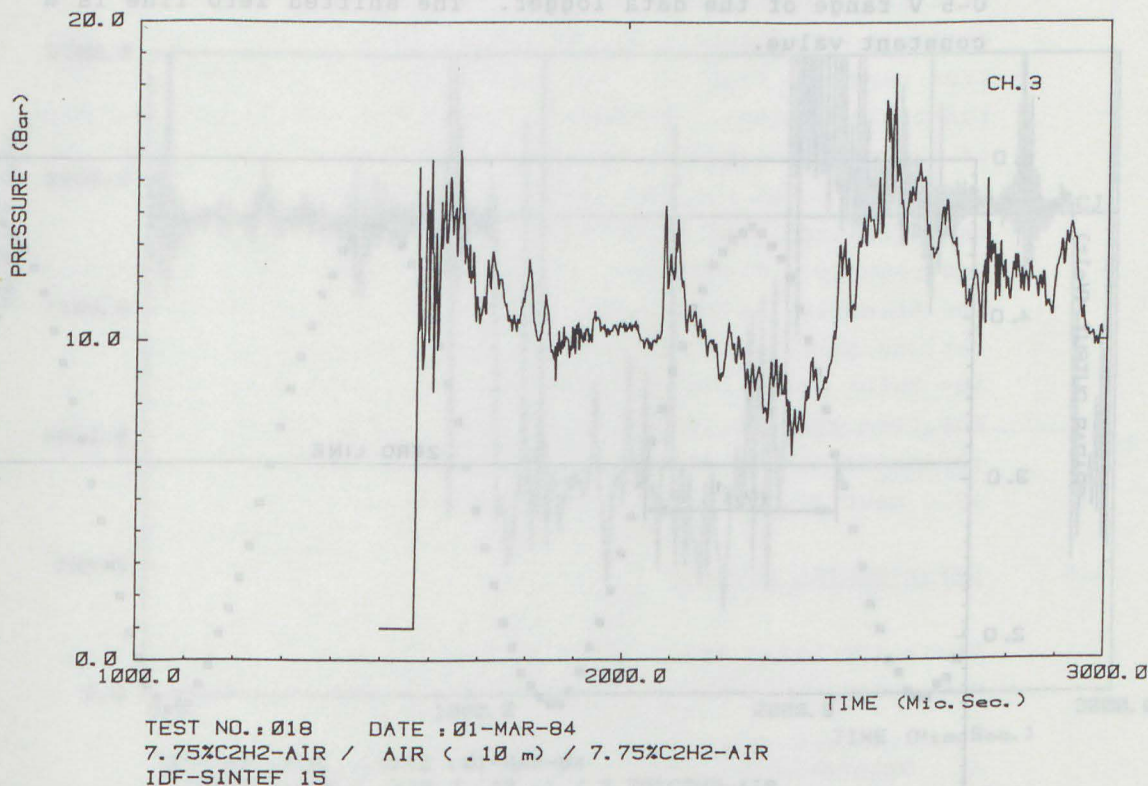
Figure 4.13
Pressure time diagram for a single pressure profile.

4514Q

4.7.2 Radar doppler signal

The frequency of the radar doppler signal is proportional to
the velocity of the target that reflects the microwaves.
Figure 4.14 illustrates how the frequency, f, is found. The
time when the radar doppler signal cross the shifted zero
line is estimated by linear interpolation between two
neighbouring sampling points with values on each side of the
shifted zero line. The value of the shifted zero line is
set by the amplifier to adapt the radar doppler signal to
0-5 V range of the data logger. The shifted zero line is a
constant value.
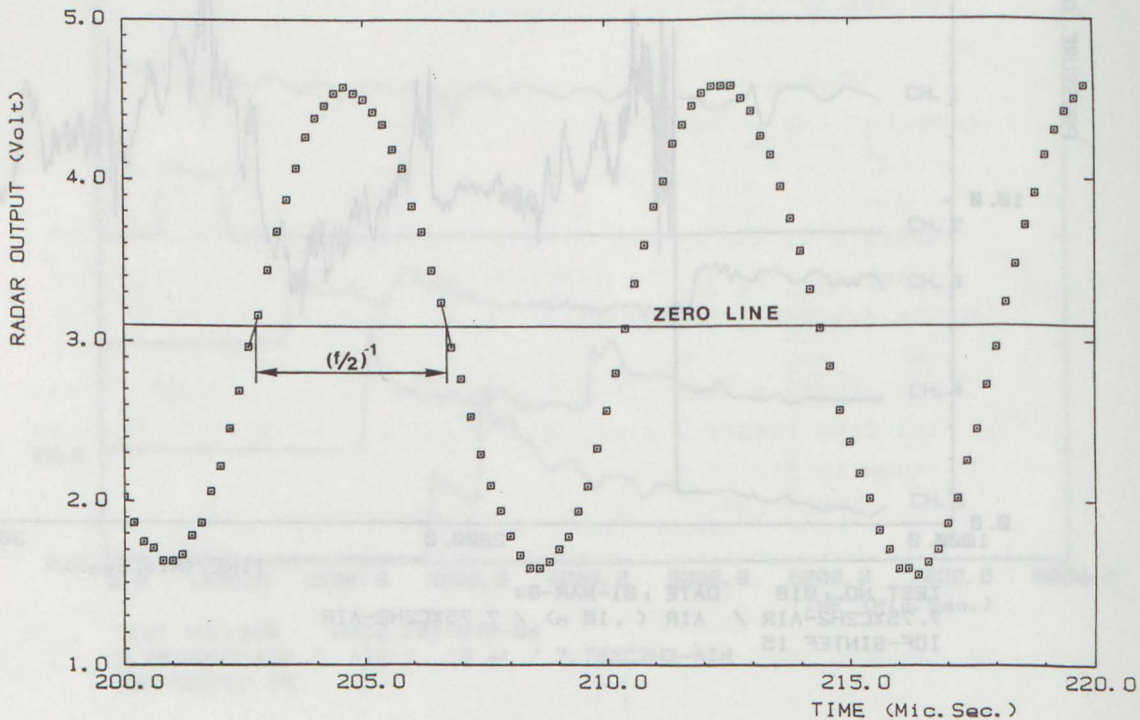
Figure 4.14
    Illustration of how the frequency, f, is obtained from
    the radar doppler signal.

For each half cycle a velocity V_r is calculated by the following formula:

$$V_r = \frac{2 \cdot (f/2)}{70.2 \ (Hz/(m/s))} \tag{4.2}$$

In Figure 4.15 this velocity is plotted as a function of time for test #18. This plot shows clearly the detonation velocity in the donor section (0-1060 μsec) and when the detonation re-initiates in the acceptor section (approx.1970 μsec).
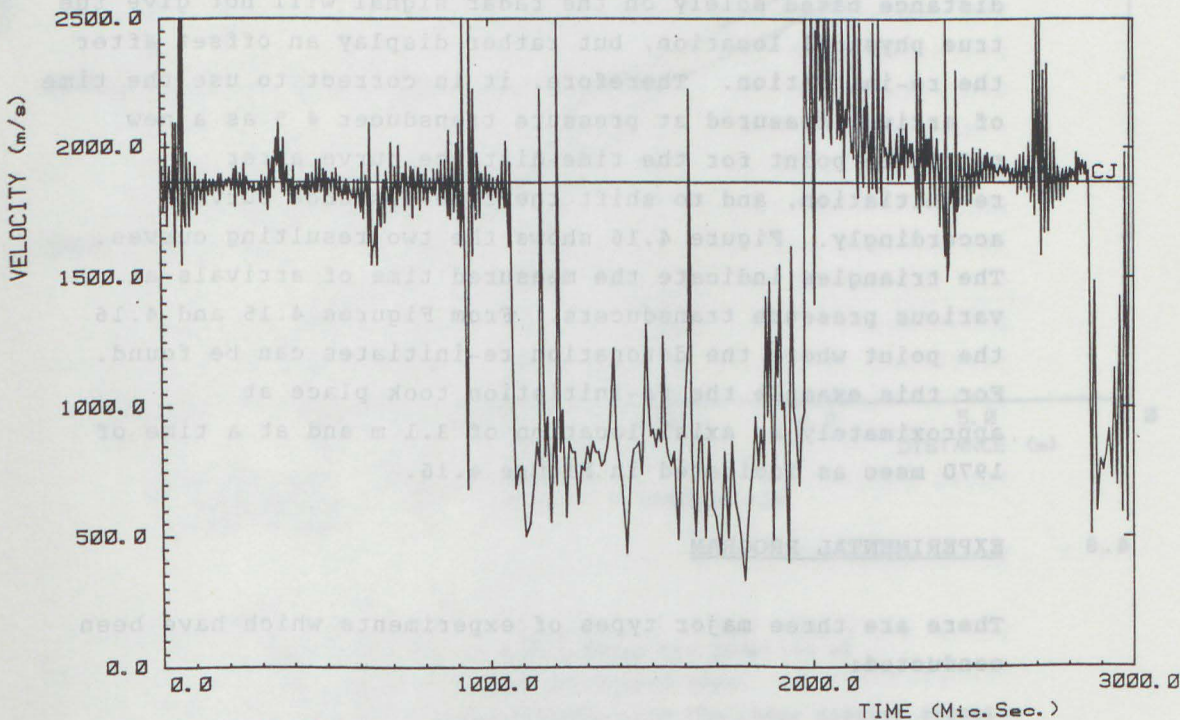
TEST NO.:018   DATE :01-MAR-84
7.75%C2H2-AIR / AIR (.10 m) / 7.75%C2H2-AIR
IDF-SINTEF 15

Figure 4.15

Velocity time diagram obtained from the radar doppler signal.

The axial position X_r of the reflecting target can also be estimated from the radar doppler signal. In principle, the velocity V_r can be integrated over time, and X_r is proportional to the number of times, n_r, that the radar signal crossed the zero line. This relationship can be written as:

$$X_r = \frac{2 \cdot (n_r - 1)}{70.2} \qquad (4.3)$$

The reflecting target seen by the radar is not a continous wave front during re-initiation period. The intergrated distance based solely on the radar signal will not give the true physical location, but rather display an offset after the re-initiation. Therefore, it is correct to use the time of arrival measured at pressure transducer # 5 as a new reference point for the time-distance curve after re-initiation, and to shift the time-distance curve accordingly. Figure 4.16 shows the two resulting curves. The triangles indicate the measured time of arrivals at various pressure transducers. From Figures 4.15 and 4.16 the point where the detonation re-initiates can be found. For this example the re-initiation took place at approximately an axial location of 3.1 m and at a time of 1970 msec as indicated in Figure 4.16.

4.8   EXPERIMENTAL PROGRAM

There are three major types of experiments which have been conducted:

- Detonations in homogeneous gas mixtures.
- Transmission of a shock wave from a detonation propagating into an inert mixture.
- Re-initiation of detonation across an inert region.

This section describes the experimental conditions and the purpose of the different tests. Some preliminary test will also be described briefly.

TEST NO.: 018   DATE : 01–MAR–84
7.75%C2H2–AIR /   AIR (.10 m) / 7.75%C2H2–AIR
IDF–SINTEF 15
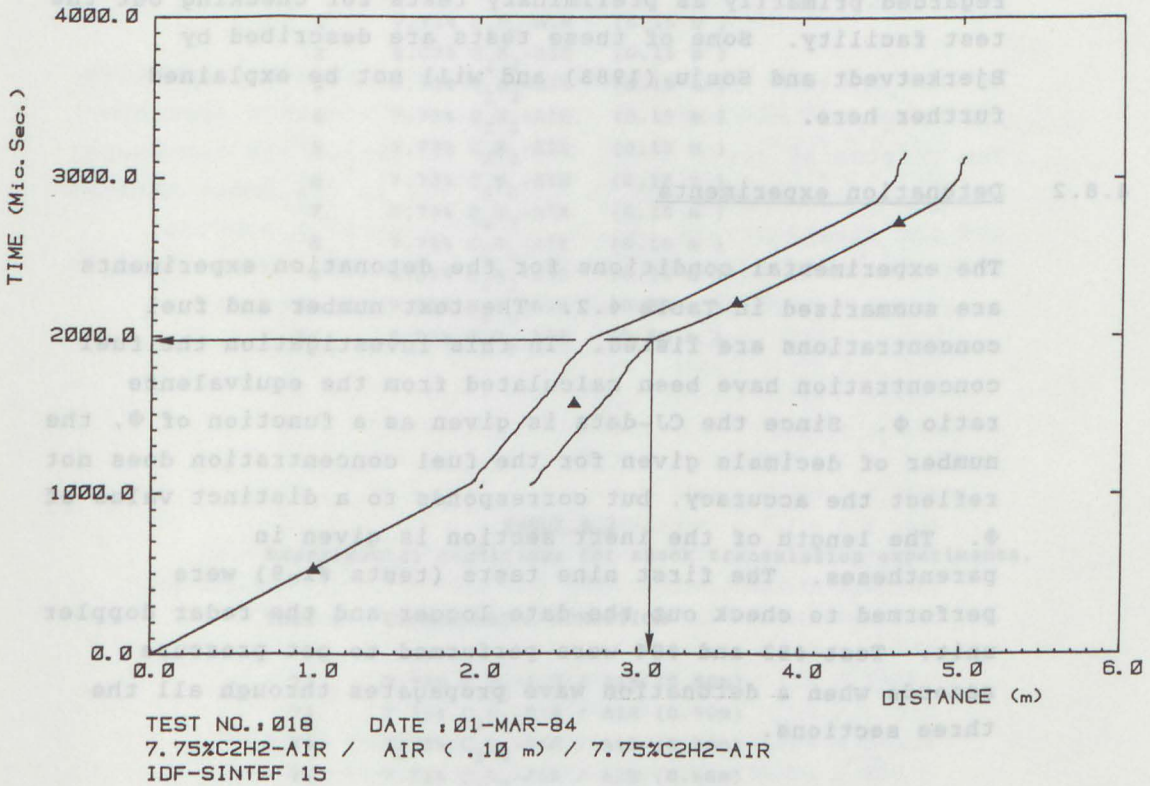
Figure 4.16
Time distance diagram showing the location of
re-initiation of the detonation wave.
——— Trajectories obtained from the radar doppler signal.
▲   Time of arrival at the pressure transducers.

4.8.1   Preliminary tests

Approximately 100 tests have been performed using the tape
recorder as data acquisition system.   These tests are
regarded primarily as preliminary tests for checking out the
test facility.   Some of these tests are described by
Bjerketvedt and Sonju (1983) and will not be explained
further here.

4.8.2   Detonation experiments

The experimental conditions for the detonation experiments
are summarized in Table 4.2.   The test number and fuel
concentrations are listed.   In this investigation the fuel
concentration have been calculated from the equivalence
ratio Φ.   Since the CJ-data is given as a function of Φ, the
number of decimals given for the fuel concentration does not
reflect the accuracy, but corresponds to a distinct value of
Φ.   The length of the inert section is given in
parentheses.   The first nine tests (tests #1-9) were
performed to check out the data logger and the radar doppler
unit.   Test #83 and #84 were performed to get pressure
records when a detonation wave propagates through all the
three sections.

4.8.3   Shock transmission experiments

Table 4.3 gives the experimental conditions for shock
transmission experiments.   In these tests both the inert and
acceptor section contain air.   A 500 mm inert section has
been used to obtain pressure records close to Interface I.
The tests were carried out with different concentrations of
acetylene-air and with stoichiometric ethylene-air.   The
acetylene concentration was varied to see the effect of
CJ-properties on the transmitted shock wave and to use the
results for comparison with numerical calculations.

TABLE 4.2 :

Experimental conditions for the detonation experiments

TEST #	EXPERIMENTAL CONDITION	
1	7.73% C_2H_2-AIR	(0.15 m)
2	5.07% C_2H_2-AIR	(0.15 m)
3	7.73% C_2H_2-AIR	(0.15 m)
4	7.73% C_2H_2-AIR	(0.15 m)
5	7.73% C_2H_2-AIR	(0.15 m)
6	7.73% C_2H_2-AIR	(0.15 m)
7	7.73% C_2H_2-AIR	(0.15 m)
8	7.73% C_2H_2-AIR	(0.15 m)
9	4.01% C_2H_2-AIR	(0.15 m)
83	7.73% C_2H_2-AIR	(0.50 m)
84	7.73% C_2H_2-AIR	(0.50 m)

TABLE 4.3

Experimental conditions for shock transmission experiments.

TEST #	EXPERIMENTAL CONDITION	
72	7.73% C_2H_2-AIR / AIR	(0.50m)
73	7.73% C_2H_2-AIR / AIR	(0.50m)
74	7.73% C_2H_2-AIR / AIR	(0.50m)
75	7.73% C_2H_2-AIR / AIR	(0.50m)
76	7.73% C_2H_2-AIR / AIR	(0.50m)
77	7.73% C_2H_2-AIR / AIR	(0.50m)
78	9.14% C_2H_2-AIR / AIR	(0.50m)
79	7.01% C_2H_2-AIR / AIR	(0.50m)
80	4.79% C_2H_2-AIR / AIR	(0.50m)
81	6.53% C_2H_4-AIR / AIR	(0.50m)
82	7.73% C_2H_2-AIR / AIR	(0.50m)
85	7.73% C_2H_2-AIR / AIR	(0.50m)
86	7.73% C_2H_2-AIR / AIR	(0.50m)
87	7.73% C_2H_2-AIR / AIR	(0.50m)

4.8.4   <u>Experiments with re-initiation of detonation across an inert</u>
         <u>region</u>

The experimental conditions for re-initiation of detonation
experiments are shown in Table 4.4 and 4.5.

Table 4.4 lists the experimental conditions for tests with
different gas mixtures in the donor and acceptor sections.
The purpose of these tests were to establish the influence
of the cell size and the CJ-properties in the donor section
and the reactivity of the gas in the acceptor section.
Stoichiometric ethylene-air and 7.01% acetylene-air ($\Phi=0.9$)
were used in the donor section. The characteristic
properties for these mixtures are listed in Table 4.6.

TABLE 4.4 :

Experimental conditions for re-initiation of detonation
across an inert region with different mixtures in donor and
acceptor section.

TEST #	EXPERIMENTAL CONDITION
34	7.01% C_2H_2-AIR / AIR(0.10m) / 9.14% C_2H_2-AIR
35	7.01% C_2H_2-AIR / AIR(0.10m) / 7.73% C_2H_2-AIR
36	6.53% C_2H_4-AIR / AIR(0.10m) / 9.14% C_2H_2-AIR
39	6.53% C_2H_4-AIR / AIR(0.10m) / 8.44% C_2H_2-AIR
38	6.53% C_2H_4-AIR / AIR(0.10m) / 7.73% C_2H_2-AIR
41	9.14% C_2H_2-AIR / AIR(0.10m) / 7.73% C_2H_2-AIR
40	9.14% C_2H_2-AIR / AIR(0.10m) / 7.01% C_2H_2-AIR
37	4.66% C_2H_4-AIR / AIR(0.10m) / 9.14% C_2H_2-AIR

TABLE 4.5 :
Experimental conditions for re-initiation of detonation across an inert region with same mixtures in donor and acceptor section.

TEST #	EXPERIMENTAL CONDITION
10	7.73% C_2H_2-AIR / AIR(0.15m) / 7.73% C_2H_2-AIR
11	7.73% C_2H_2-AIR / AIR(0.15m) / 7.73% C_2H_2-AIR
12	7.73% C_2H_2-AIR / AIR(0.15m) / 7.73% C_2H_2-AIR
13	7.73% C_2H_2-AIR / AIR(0.15m) / 7.73% C_2H_2-AIR
14	7.73% C_2H_2-AIR / AIR(0.10m) / 7.73% C_2H_2-AIR
15	7.73% C_2H_2-AIR / AIR(0.10m) / 7.73% C_2H_2-AIR
16	7.73% C_2H_2-AIR / AIR(0.10m) / 7.73% C_2H_2-AIR
17	7.73% C_2H_2-AIR / AIR(0.10m) / 7.73% C_2H_2-AIR
18	7.73% C_2H_2-AIR / AIR(0.10m) / 7.73% C_2H_2-AIR
19	7.73% C_2H_2-AIR / AIR(0.10m) / 7.73% C_2H_2-AIR
20	7.73% C_2H_2-AIR / AIR(0.10m) / 7.73% C_2H_2-AIR
21	7.73% C_2H_2-AIR / AIR(0.10m) / 7.73% C_2H_2-AIR
22	7.73% C_2H_2-AIR / AIR(0.10m) / 7.73% C_2H_2-AIR
23	7.73% C_2H_2-AIR / AIR(0.10m) / 7.73% C_2H_2-AIR
24	7.73% C_2H_2-AIR / AIR(0.10m) / 7.73% C_2H_2-AIR
29	9.14% C_2H_2-AIR / AIR(0.10m) / 9.14% C_2H_2-AIR
28	8.44% C_2H_2-AIR / AIR(0.10m) / 8.44% C_2H_2-AIR
33	8.44% C_2H_2-AIR / AIR(0.10m) / 8.44% C_2H_2-AIR
27	7.37% C_2H_2-AIR / AIR(0.10m) / 7.37% C_2H_2-AIR
25	7.01% C_2H_2-AIR / AIR(0.10m) / 7.01% C_2H_2-AIR
26	7.01% C_2H_2-AIR / AIR(0.10m) / 7.01% C_2H_2-AIR
30	6.53% C_2H_4-AIR / AIR(0.10m) / 6.53% C_2H_4-AIR
31	5.91% C_2H_4-AIR / AIR(0.10m) / 5.91% C_2H_4-AIR
32	5.29% C_2H_4-AIR / AIR(0.10m) / 5.29% C_2H_4-AIR
43	9.14% C_2H_2-AIR / AIR(0.15m) / 9.14% C_2H_2-AIR
44	8.44% C_2H_2-AIR / AIR(0.15m) / 8.44% C_2H_2-AIR
42	7.73% C_2H_2-AIR / AIR(0.15m) / 7.73% C_2H_2-AIR
45	7.37% C_2H_2-AIR / AIR(0.15m) / 7.37% C_2H_2-AIR

TABLE 4.5 (Continue):
Experimental conditions for re-initiation of detonation
across an inert region with same mixtures in donor and
acceptor section.   .

TEST #   EXPERIMENTAL CONDITION

46   9.14% C_2H_2-AIR / AIR(0.20m) / 9.14% C_2H_2-AIR
47   8.79% C_2H_2-AIR / AIR(0.20m) / 8.79% C_2H_2-AIR
48   8.44% C_2H_2-AIR / AIR(0.20m) / 8.44% C_2H_2-AIR
49   8.44% C_2H_2-AIR / AIR(0.20m) / 8.44% C_2H_2-AIR
50   8.44% C_2H_2-AIR / AIR(0.20m) / 8.44% C_2H_2-AIR
51   8.44% C_2H_2-AIR / AIR(0.20m) / 8.44% C_2H_2-AIR
52   8.44% C_2H_2-AIR / AIR(0.20m) / 8.44% C_2H_2-AIR
53   8.44% C_2H_2-AIR / AIR(0.20m) / 8.44% C_2H_2-AIR
54   8.44% C_2H_2-AIR / AIR(0.20m) / 8.44% C_2H_2-AIR
55   8.44% C_2H_2-AIR / AIR(0.20m) / 8.44% C_2H_2-AIR
56   8.44% C_2H_2-AIR / AIR(0.20m) / 8.44% C_2H_2-AIR
58   9.14% C_2H_2-AIR / AIR(0.20m) / 9.14% C_2H_2-AIR
59   7.73% C_2H_2-AIR / AIR(0.20m) / 7.73% C_2H_2-AIR
60   9.14% C_2H_2-AIR / AIR(0.20m) / 9.14% C_2H_2-AIR
61   8.44% C_2H_2-AIR / AIR(0.20m) / 8.44% C_2H_2-AIR
62   7.73% C_2H_2-AIR / AIR(0.20m) / 7.73% C_2H_2-AIR
63   8.44% C_2H_2-AIR / AIR(0.20m) / 8.44% C_2H_2-AIR
64   7.73% C_2H_2-AIR / AIR(0.20m) / 7.73% C_2H_2-AIR
65   7.73% C_2H_2-AIR / AIR(0.20m) / 7.73% C_2H_2-AIR
66   9.14% C_2H_2-AIR / AIR(0.20m) / 9.14% C_2H_2-AIR
67   9.14% C_2H_2-AIR / AIR(0.20m) / 9.14% C_2H_2-AIR
68   9.14% C_2H_2-AIR / AIR(0.20m) / 9.14% C_2H_2-AIR
69   9.14% C_2H_2-AIR / AIR(0.20m) / 9.14% C_2H_2-AIR
70   9.14% C_2H_2-AIR / AIR(0.20m) / 9.14% C_2H_2-AIR
71   9.14% C_2H_2-AIR / AIR(0.20m) / 9.14% C_2H_2-AIR

These mixtures have about the same CJ-properties. The cell size is about 4 times larger for the ethylene-air mixture than for the acetylene-air mixture. (Knystautas et al., 1984). These experiments were performed with acetylene-air in the acceptor section and with Φ varying from 0.9 to 1.2. To ascertain the effect of the CJ-properties of the detonation in the donor section, experiments with 9.14% acetylene-air ($\Phi=1.2$) were performed. In test #37 a relatively weak mixture with a large cell size was used in the donor section to see if the thickness of the detonation wave was of importance for the re-initiation process. In all of these tested, the inert region was 100 mm wide.

TABLE 4.6 :
Characteristical detonation properties for
7.01 % C_2H_2-AIR and
6.53 % C_2H_4-AIR .

Fuel	% Fuel	Φ	D_{CJ}(m/s)	P_{CJ}/P_0	S*(mm)	d_c**(m)
C_2H_2	7.01	0.9	1832	19.0	7	0.18
C_2H_4	6.53	1.0	1823	18.9	26	0.40

* : Knystautas et al. (1984)
**: Moen et al.(1984)

Table 4.5 lists the experimental conditions for the tests
when the gas mixtures in the donor and the acceptor section
were the same. These tests were performed to establish the
transmission width of the inert region and the gas mixture.

In some of the preliminary tests, tests #10 to #17, a small
overpressure in the donor and acceptor sections relative to
the pressure in the inert section occured because of a leak
in one of the valves. This can effect the interface
behaviour, and these results must be questioned since they
were not performed under well-controlled conditions.

A series of experiments with stoichiometric acetylene-air
and 100 mm inert section were performed to check the
reproducibility of the experiments. In test #22 a smoked
foil was mounted in the acceptor section.

For the 100 mm inert section various acetylene-air and
ethylene-air mixtures were used. For the 150 mm and the
200 mm only acetylene-air was used.

CHAPTER 5

DISCUSSION OF EXPERIMENTAL RESULTS AND COMPARISON WITH THEORY

5.1   INTRODUCTION

In this chapter results from the experimental investigations
described in Chapter 4 are discussed and compared with
numerical and analytical calculations.

In Section 5.2 the detonation wave and the expansion of the
combustion products are discussed with regards to wall
effects.

In Section 5.3 the magnitude of the wall effects are
ascertained from comparing experimental results with
numerical RCM-predictions of shock trajectories of a
transmitted shock wave. Other measurements, such as
pressure profiles and contact surface trajectories, are also
compared with numerical predictions.

Section 5.4 focuses on the influence of the experimental
conditions on the re-initiation process across an inert
region. The experimental results from changing the width of
the inert section and the gas mixture in the donor and
acceptor sections are explained. Other experimental
conditions, such as the sharpness of the inert region
boundaries and wall effects are also discussed. The
observations of the re-initiation process of the detonation
in the acceptor section are analyzed.

All the experimental results are summarized in table form in
Appendix F.

5.2   DETONATION PROPAGATION IN A HOMOGENEOUS GAS MIXTURE

In this section the observations of the detonation wave and
the expansion of the combustion products are described. The
detonation velocity, the structure of the front and the
pressure records are discussed and compared with analytical
results, numerical calculations and previous experimental
observations. The main purpose of this section is to
explain the conditions in the donor sections.

5.2.1   Detonation wave

A typical output signal from the radar doppler unit, when a
detonation wave is monitored, is shown in Figure 5.1. The
high frequency signal is the doppler signal, which is
proportional to the detonation velocity. The way the
microwaves are launched into the tube, give nodal points
where there are no or very small output signals such as seen
around 80 μsec and 380 μsec. Figure 5.2 shows the
velocity as calculated from the radar doppler signal. This
measured velocity is very close to the theoretical C-J value
which also is shown in the figure. Only at the positions
where the output signal is small is there any significant
difference from the theoretical value.

The velocities reduced from time of arrival of the wave
between the pressure transducer in test #84 are listed in
Table 5.1 . In test #84 all three sections were filled with
a stoichiometric mixture of acetylene-air. The C-J velocity
for this mixture is 1865 m/s. So, also, for this type of
measurement there is good agreement between the theoretical
value and measured values.

All the velocity measurements in the various tests measured between pressure transducers #1 and #2 are shown in Figures 5.3 and 5.4. The triangles give the velocity measurments from the pressure records. The errorbars indicate the scatter in the data. Velocities reduced from the radar doppler signal are shown as squares in these figures. Average velocity observed between the times of 150 μsec and 500 μsec are used. Except for the case of stoichiometric acetylene-air (7.73% C_2H_2), the squares represent measurements from individual tests. However, to establish error bars for stoichiometric acetylene-air the plotted value represent an average value for several representative tests. The theoretical C-J velocity is also plotted on these figures.

TABLE 5.1 :

Velocities obtained from time of arrival of the wave between the pressure transducer in a detonetion expriment

Velocities (m/s)	1-2 : 1881	1-2 : 1881
	2-3 : 1866	1-3 : 1873
	3-4 : 1894	1-4 : 1875
	4-5 : 1887	1-5 : 1877

Figure 5.1
Radar doppler signal.
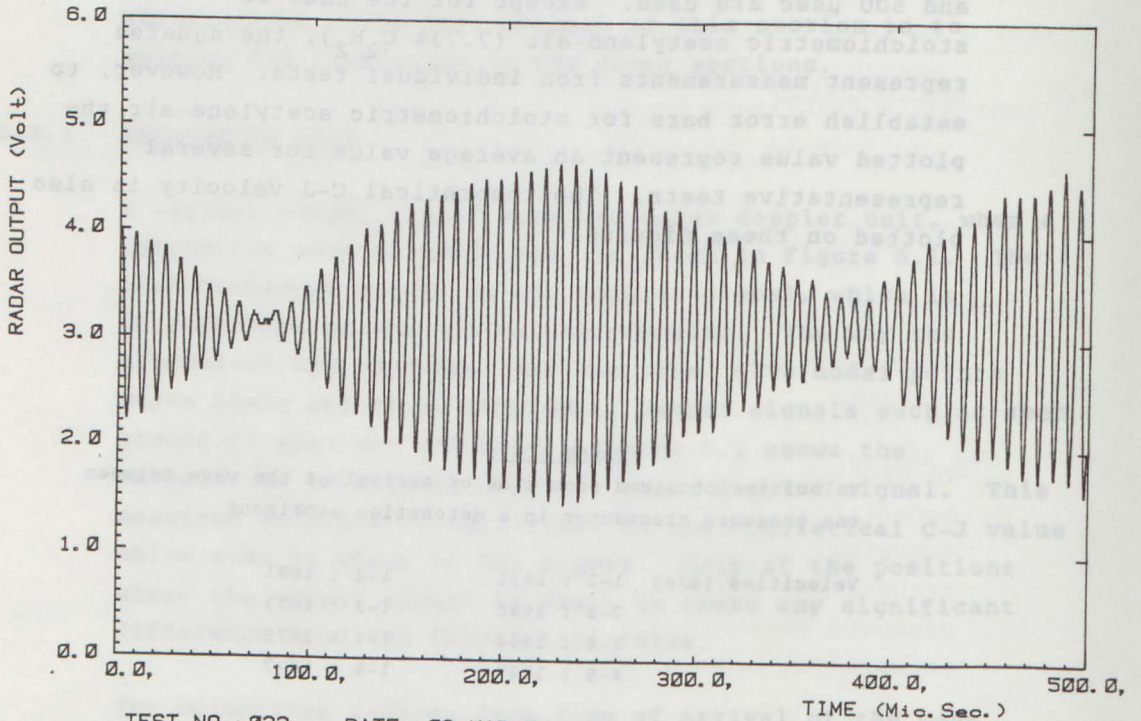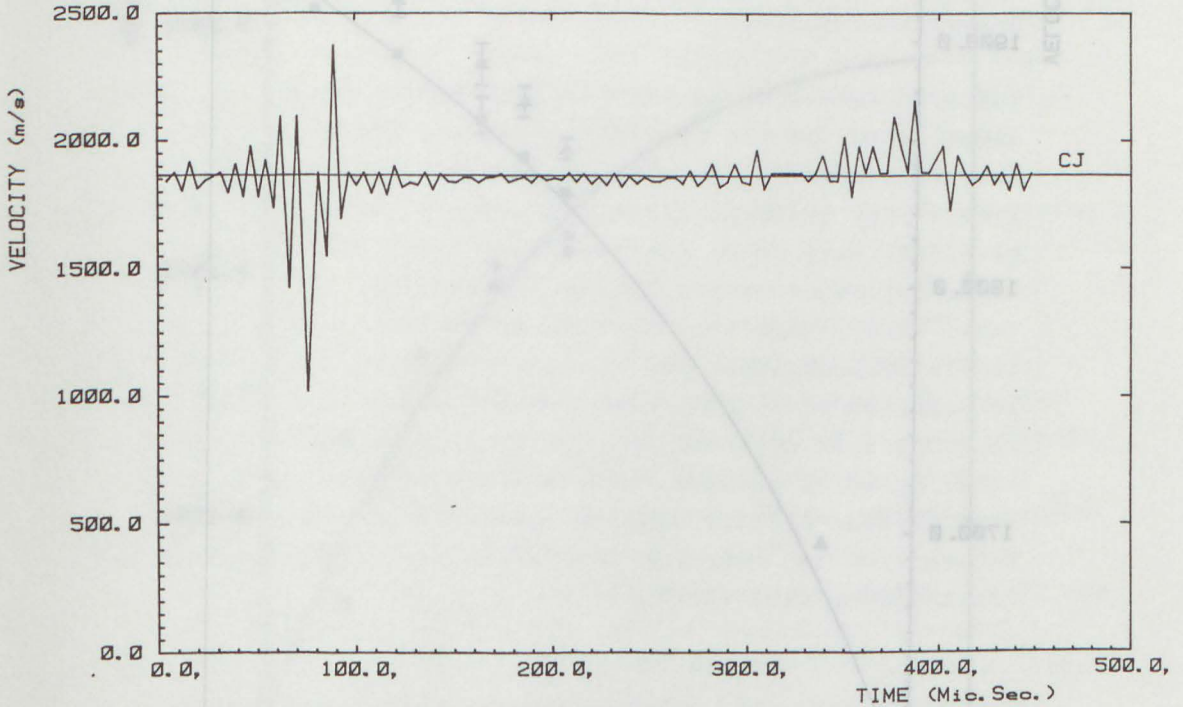
TEST NO.:022   DATE :02-MAR-84
7.75%C2H2-AIR /   AIR (.10 m) / 7.75%C2H2-AIR
IDF-SINTEF 15

Figure 5.2
    Detonation velocity obtained from radar doppler signal
    shown in Figure 5.1, compared with the theoretical C-J
    velocity.

DETONATION VELOCITY
C2H2-AIR
IDF-SINTEF 15
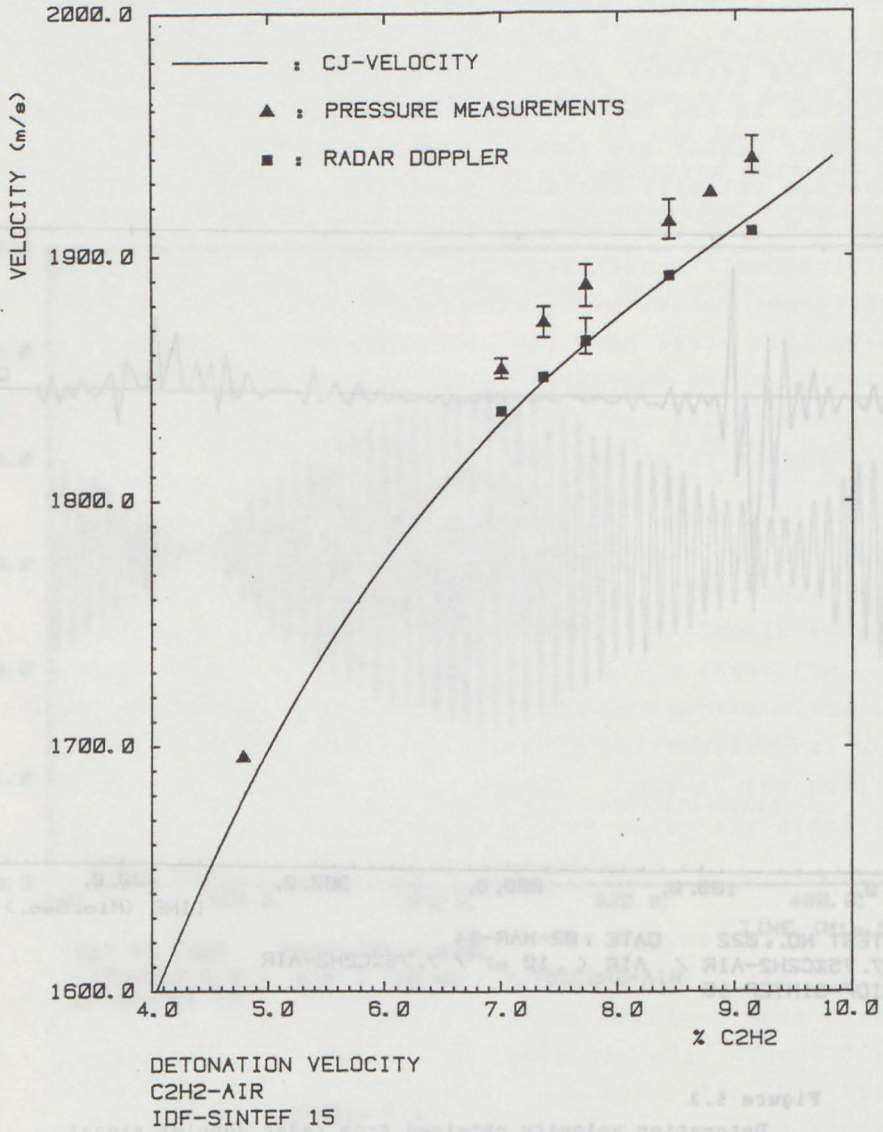
Figure 5.3

Detonation velocity versus the fuel concentration in
acetylene-air mixtures.

▲   Velocities obtained from time of arrival at
     pressure transducer #1 and #2.
■   Velocities obtained from radar doppler signal .
—   Theoretical C-J velocity.

DETONATION VELOCITY
C2H4-AIR
IDF-SINTEF 15
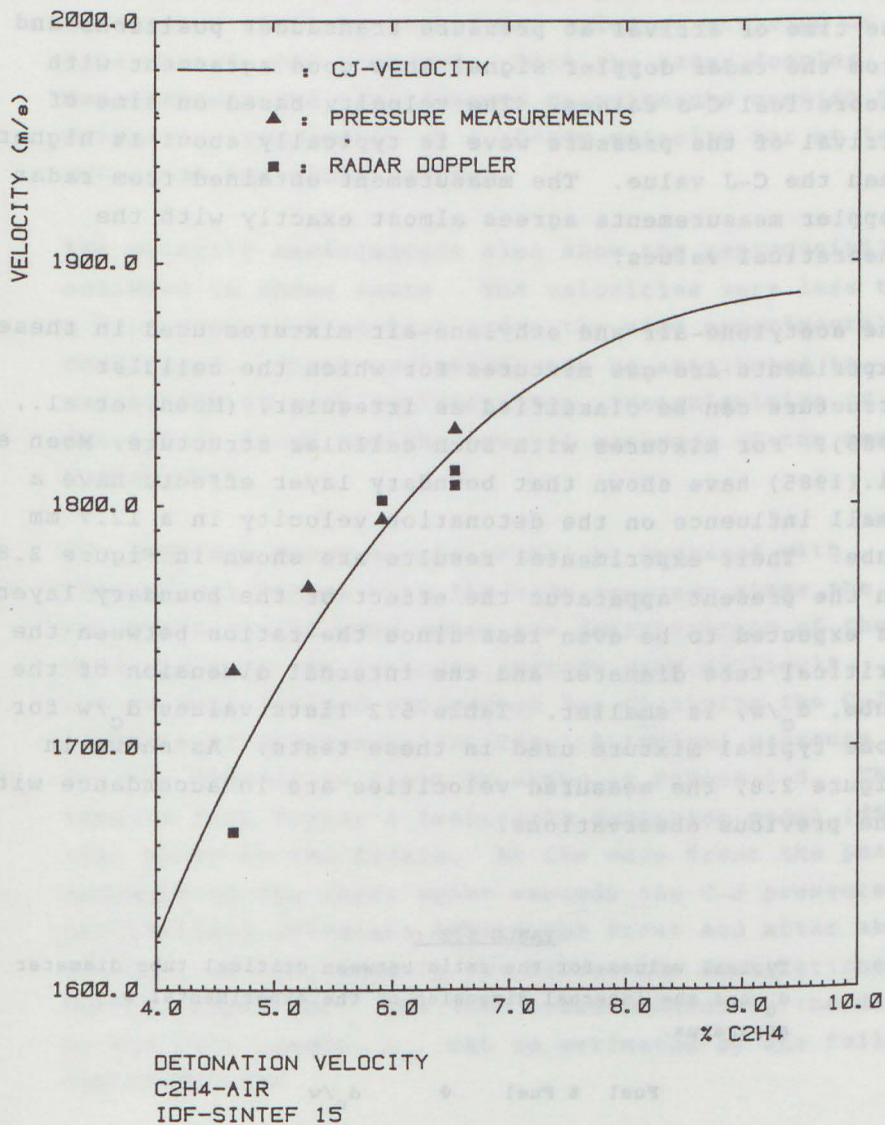
Figure 5.4
Detonation velocity versus the fuel concentration in
ethylene-air mixtures.
▲   Velocities reduced from time of arrival at pressure
      transducer #1 and #2.
■   Velocities reduced from radar doppler signal .
──   Theoretical C-J velocity.

One can conclude that detonation velocities measured from
the time of arrival at pressure transducer positions and
from the radar doppler signal show good agreement with
theoretical C-J values. The velocity based on time of
arrival of the pressure wave is typically about 1% higher
than the C-J value. The measurement obtained from radar
doppler measurements agrees almost exactly with the
theoretical values.

The acetylene-air and ethylene-air mixtures used in these
experiments are gas mixtures for which the cellular
structure can be classified as irregular, (Moen, et al.,
1985). For mixtures with such cellular structure, Moen et
al.(1985) have shown that boundary layer effects have a
small influence on the detonation velocity in a 12.7 mm
tube. Their experimental results are shown in Figure 2.8.
In the present apparatus the effect of the boundary layers
is expected to be even less since the ratios between the
critical tube diameter and the internal dimension of the
tube, d_c/w, is smaller. Table 5.2 lists values d_c/w for
some typical mixture used in these tests. As shown in
Figure 2.8, the measured velocities are in accordance with
the previous observations.

TABLE 5.2 :

Typical values for the ratio between critical tube diameter
d_c and the internal dimension of the experimental w
apparatus.

Fuel	% Fuel	Φ	d_c/w
C_2H_2	9.14	1.2	0.8
C_2H_2	7.73	1.0	1.1
C_2H_2	7.01	0.9	1.4
C_2H_2	4.78	0.6	5.8
C_2H_4	6.53	1.0	3.2
C_2H_4	4.66	0.7	10.0

The design criteria for the detonation tube that the
detonation shall be stabilized prior to arriving at
Interface I, has been met. Both the radar doppler
measurements and the pressure measurements confirm that the
detonation propagates at a steady velocity for at least 2
meters of the donor section.

The velocity measurements also show the reproducibility
achieved in these tests. The velocities vary less than
± 0.5% from test to test under the same experimental
conditions. These variations can be attributed to
variations in fuel concentration, irregularities of the
detonation front and the overall accuracy of the measuring
technique.

The pressure measurements cannot be compared with
theoretical values with the same accuracy since the
structure of the wave makes the determination of the C-J
pressure from the pressure records very difficult. There
are no well-defined procedures for obtaining the C-J
pressure from pressure records. A typical pressure record
for the detonation front is shown in Figure 5.5. The
results from Taylor's isentropic expansion model (dS=0) are
also shown in the figure. At the wave front the peak
pressure of the short spike exceeds the C-J pressure. The
oscillations attenuate behind the front and after about
40 μsec, as indicated by the arrow, the oscillations are
nearly damped out. The time corresponding to the distance
of the cell length, L_c, can be estimated by the following
approximation:

$$t_{L_C} \simeq \frac{L_C}{D} \simeq \frac{d_C}{13 \cdot 0.6 \cdot D} \tag{5.1}$$

By using such a value for the cell length, the oscillations
are damped out in a distance of about three cell lengths
downstream of the front for this case. In different
measurements, there was some variation of this distance,
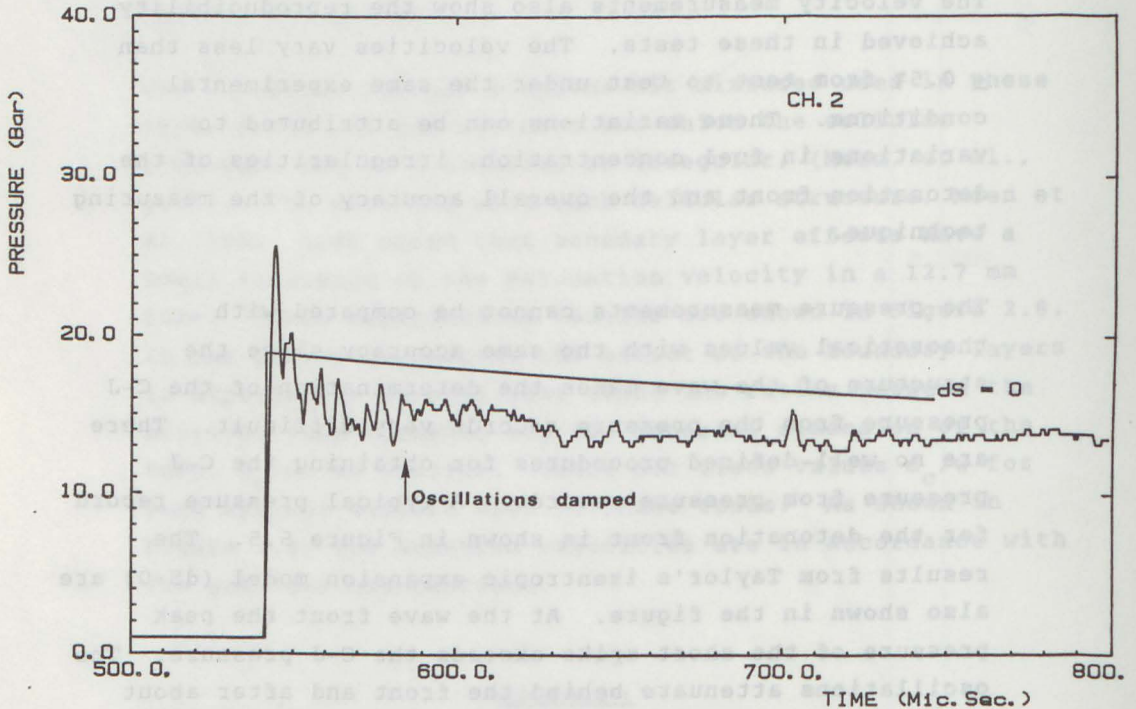
Figure 5.5

Pressure time diagram showing a typical measured
pressure profile for the detonation front and a profile
calculated by the isentropic expansion model (ds = 0).

however generally there was good agreement with the
observation reported by Edwards et al (1976). They observed
that the pressure oscillation dissipated after 2 to 4 cell
length. They relate this length to the thickness of the
detonation wave.

5.2.2   Expansion of the combustion products behind the detonation
        wave

The isentropic expansion model of Taylor (1950) and the
modified RCM-code are described in Chapter 3. These
one-dimensional models have been used to predict the
expansion of the combustion products behind a C-J detonation
wave. The assumption that the detonation wave propagates at
about C-J velocity was confirmed in the previous sub-section.

Generally, the measured pressure behind the detonation wave
is lower than the pressure predicted by Taylor's model.
This is illustrated in Figures 5.5 and 5.6 where the curve
marked ds=0 refers to Taylor's model. The discrepancy
between Taylor's model and the measurements is likely a
result of heat transfer loss and friction at the wall. As
shown in Figure 5.6 the measured pressure agrees better with
the RCM predictions, which takes these wall effects into
account. Due to the averaging of the pressure data in the
data-reduction process, the spike at the front has been
somewhat smoothened out. In the RCM calculation a friction
factor, C_f, equal to 0.008 has been used. This value
gives good agreement between the predicted shock trajectory
by RCM and the measured time of arrival in these
experiments. This will be shown later.

A significant deviation in pressure is observed when
comparing the pressure prediction from Taylor's model and
the RCM predictions. However, it is difficult to use
pressure measurements to accurately evaluate wall effects due
to the accuracy of the pressure measurements. In previous

PRESSURE (Bar)

20.0

dS=0

RCM - Cf=0.008

CH. 5

10.0

0.0

1000.0   2000.0   3000.0   4000.0   5000.0

TIME (Mio. Sec.)

TEST NO. : 084   DATE : 15-MAY-84
7.73%C2H2-AIR
IDF-SINTEF 15
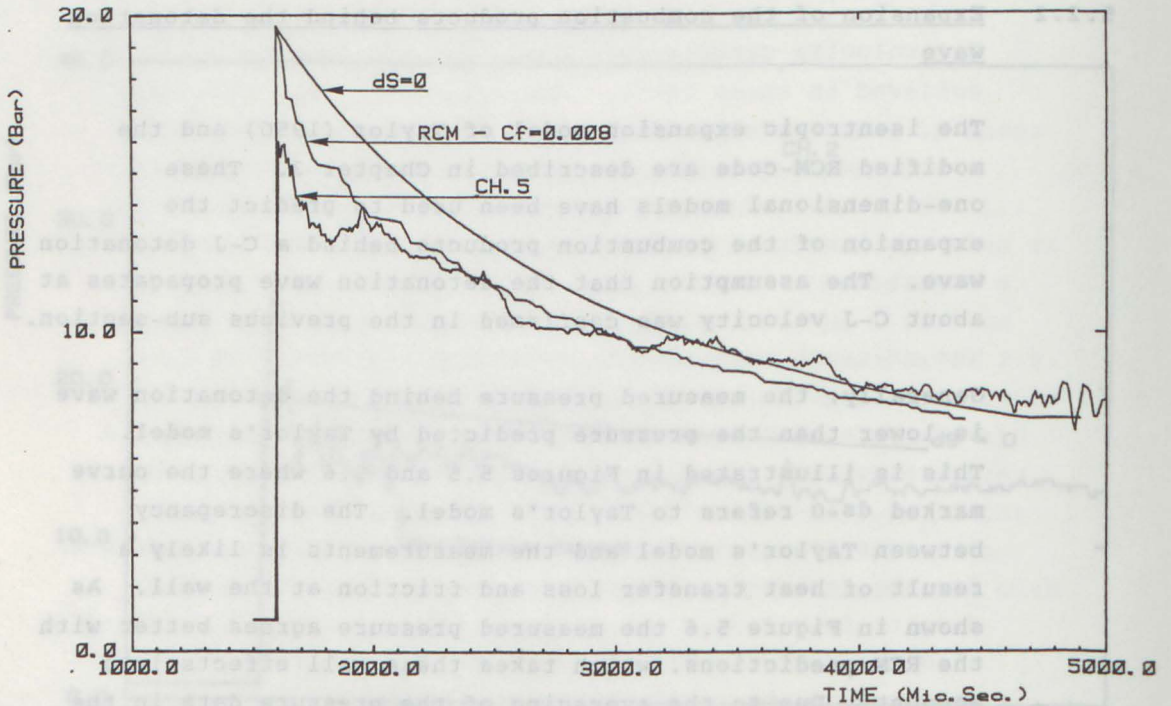
Figure 5.6

Pressure time diagram showing measured pressure profile
behind a detonation wave compared with calculated
profiles. The curves marked ds = 0 and C_f = 0.008
refers respectively to Taylor's isentropic model and RCM
calculation including heat transfer and friction.

reported experiments (Edward et al., 1970, Paillard et al., 1979 and 1981), such wall effects have been observed in narrow tubes. The present results shown that heat transfer and friction also have to be taken into account for larger tubes. This is an important finding which has to be taken into account when the strength of a shock wave caused by a detonation wave propagating into an inert region is to be predicted. The flow field behind a detonation is influenced by wall effects. This causes a reduction in the strength of the transmitted shock wave. Therefore, heat transfer and friction have to be accounted for in order to properly describe the experimental condition in the donor section.

5.2.3   Summary

The velocity measurements are in good agreement with the theoretical C-J velocites. The pressure measurements are generally lower than predicted by Taylor's model, which assumes an isentropic expansion of the combustion products. The measured pressure agrees better with the RCM predictions, which takes heat transfer and friction into account.

5.3   DETONATION PROPAGATION INTO AN INERT GAS

The aim of the investigation has been to characterize the experimental conditions in the acceptor section without combustion occuring. Experimental observations of shock and contact surface trajectories and pressure records are compared with calculations by the RCM-code. The calculations have been undertaken to ascertain the magnitude of the wall effects. Of particular importance is the influence of heat transfer and friction have on the decay of a transmitted shock wave and the flow field behind the shock wave.

5.3.1   <u>Transmitted shock wave</u>

Figure 5.7 illustrates the measurement of the trajectory of
the wave front when a detonation wave in stoichiometric
acetylene-air propagates into air. In this figure the time
and distance are measured from the arrival of the detonation
at the transducer #1 . For the same test, the average
velocities measured between the pressure transducer stations
are given in Table 5.3 . The velocity between transducer #2
and Interface I, 2-AIR, has been assumed to be equal to the
detonation velocity between transducer #1 and #2. When the
detonation wave reaches Interface I, the slope of the
trajector changes. Before Interface I the slope is constant
as a consequence of constant detonation velocity. After the
interface, the slope is steeper since the velocity of the
wave decreases. Table 5.3 shows that the shock wave
velocity decreases by about 100 m/s pr. meter as it
propagates down the acceptor section. In Figure 5.7 this
velocity decrease is represented by a steepening of the
slope of the curve.

<u>TABLE 5.3 :</u>

Velocities obtained from time of arrival of the wave between
the pressure transducer in a shock transmission expriment.

Velocities (m/s)   1-2   : 1884
                    2-AIR : 1884
                    AIR-3 : 1214
                    3-4   : 1104
                    4-5   : 1026
                    5-6   : 935
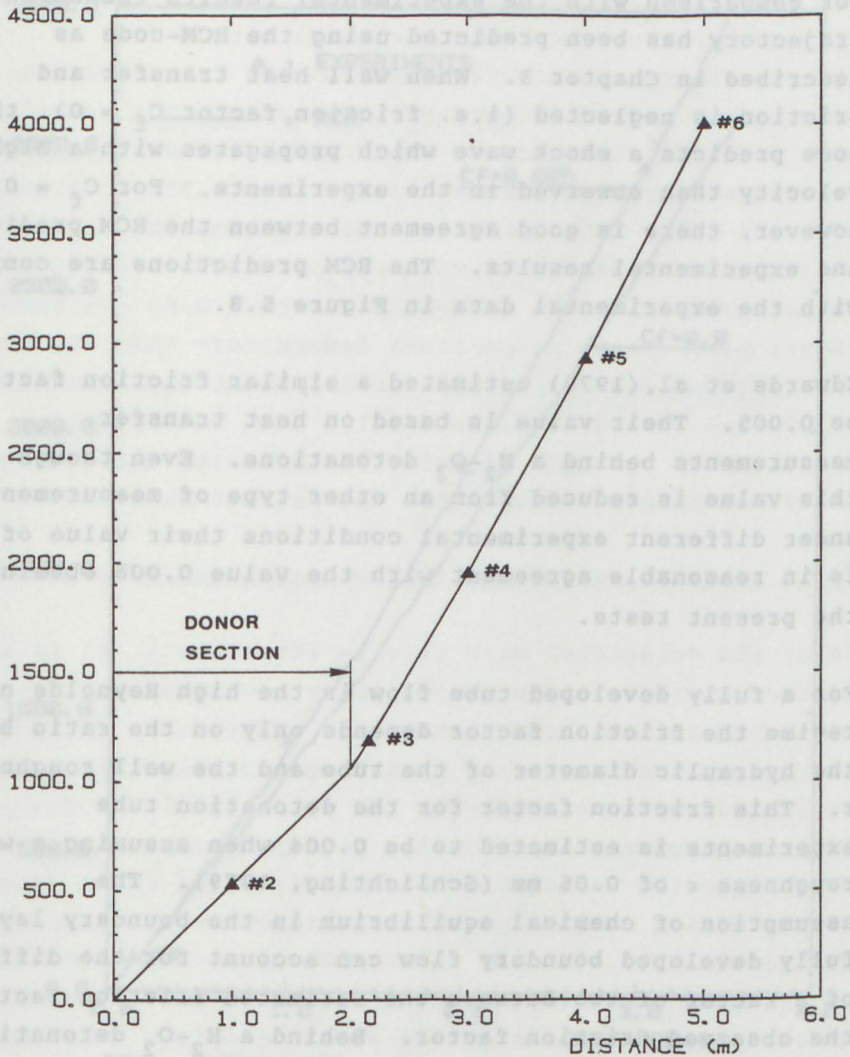
TIME OF ARRIVAL
7.73% C2H2-AIR / AIR
IDF-SINTEF 15

Figure 5.7
Time distance diagram showing the time of arrival for
wave front when a detonation wave in donor section
(0 - 2.0 meters) propagates into an inert gas in inert
and acceptor sections (2.0-5.3 meters).

For comparison with the experimental results the shock
trajectory has been predicted using the RCM-code as
described in Chapter 3. When wall heat transfer and
friction is neglected (i.e. friction factor C_f = 0), the
code predicts a shock wave which propagates with a higher
velocity than observed in the experiments. For C_f = 0.008,
however, there is good agreement between the RCM predictions
and experimental results. The RCM predictions are compared
with the experimental data in Figure 5.8.

Edwards et al.(1970) estimated a similar friction factor to
be 0.005. Their value is based on heat transfer
measurements behind a H_2-O_2 detonations. Even though
this value is reduced from an other type of measurement and
under different experimental conditions their value of C_f
is in reasonable agreement with the value 0.008 obtained in
the present tests.

For a fully developed tube flow in the high Reynolds number
regime the friction factor depends only on the ratio between
the hydraulic diameter of the tube and the wall roughness
ε. This friction factor for the detonation tube
experiments is estimated to be 0.004 when assuming a wall
roughness ε of 0.05 mm (Schlichting, 1979). The
assumption of chemical equilibrium in the boundary layer and
fully developed boundary flow can account for the difference
of a factor of two between the estimated friction factor and
the observed friction factor. Behind a H_2-O_2 detonation
wave Sichel and David (1966) have estimated the heat
transfer rate to be 60% higher for a chemical equilibrium
boundary layer than for a chemical frozen boundary layer.
The so called entrance effects due to developing boundary
layers can result in a significant increase in the friction
factor (Kays and Crawford, 1980). To compensate for these
various effects the value of C_f has to be increased.
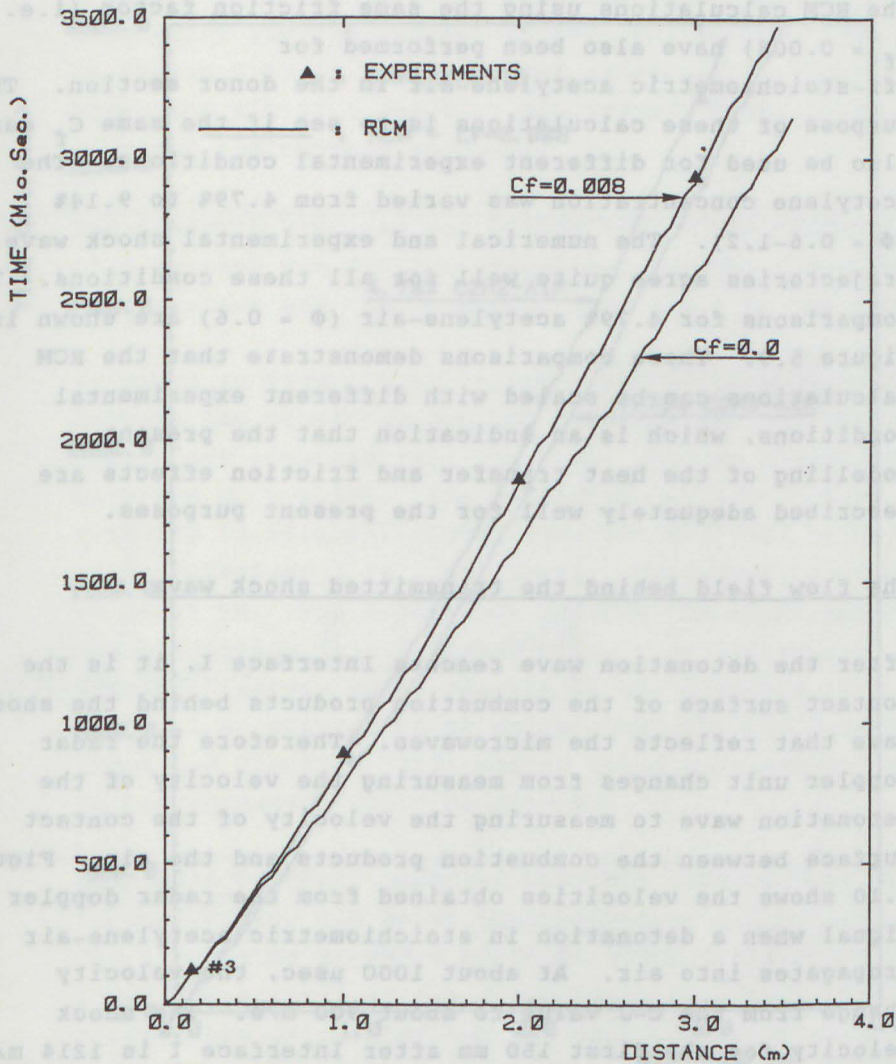
RCM – SHOCK WAVE
7.73% C2H2–AIR / AIR
IDF–SINTEF 15

Figure 5.8
Time distance diagram showing predicted shock
trajectories and measured time of arrival for a
transmitted shock wave propagating into the inert and
the acceptor sections.

$C_f = 0$ Heat transfer and friction not taken into
                         account.

$C_f = 0.008$ Heat transfer and friction taken into
                         account.

The RCM calculations using the same friction factor (i.e.
C_f = 0.008) have also been performed for
off-stoichiometric acetylene-air in the donor section. The
purpose of these calculations is to see if the same C_f can
also be used for different experimental conditions. The
acetylene concentration was varied from 4.79% to 9.14%
(Φ = 0.6-1.2). The numerical and experimental shock wave
trajectories agree quite well for all these conditions. The
comparisons for 4.79% acetylene-air (Φ = 0.6) are shown in
Figure 5.9. These comparisons demonstrate that the RCM
calculations can be scaled with different experimental
conditions, which is an indication that the present
modelling of the heat transfer and friction effects are
described adequately well for the present purposes.

5.3.2   The flow field behind the transmitted shock wave

After the detonation wave reaches Interface I, it is the
contact surface of the combustion products behind the shock
wave that reflects the microwaves. Therefore the radar
doppler unit changes from measuring the velocity of the
detonation wave to measuring the velocity of the contact
surface between the combustion products and the air. Figure
5.10 shows the velocities obtained from the radar doppler
signal when a detonation in stoichiometric acetylene-air
propagates into air. At about 1000 μsec, the velocity
change from the C-J value to about 900 m/s. The shock
velocity for the first 150 mm after Interface I is 1214 m/s,
as shown in Table 5.3. The gas velocity behind a shock wave
with this velocity is calculated to be 930 m/s, which agrees
quite well with the velocity of the combustion products
contact surface measured with the radar doppler unit. The
measured velocity of the contact surface decays as it
propagates into the acceptor section as seen in Figure
5.10. The trajectory of the contact surface can be
calculated from the radar doppler signal.
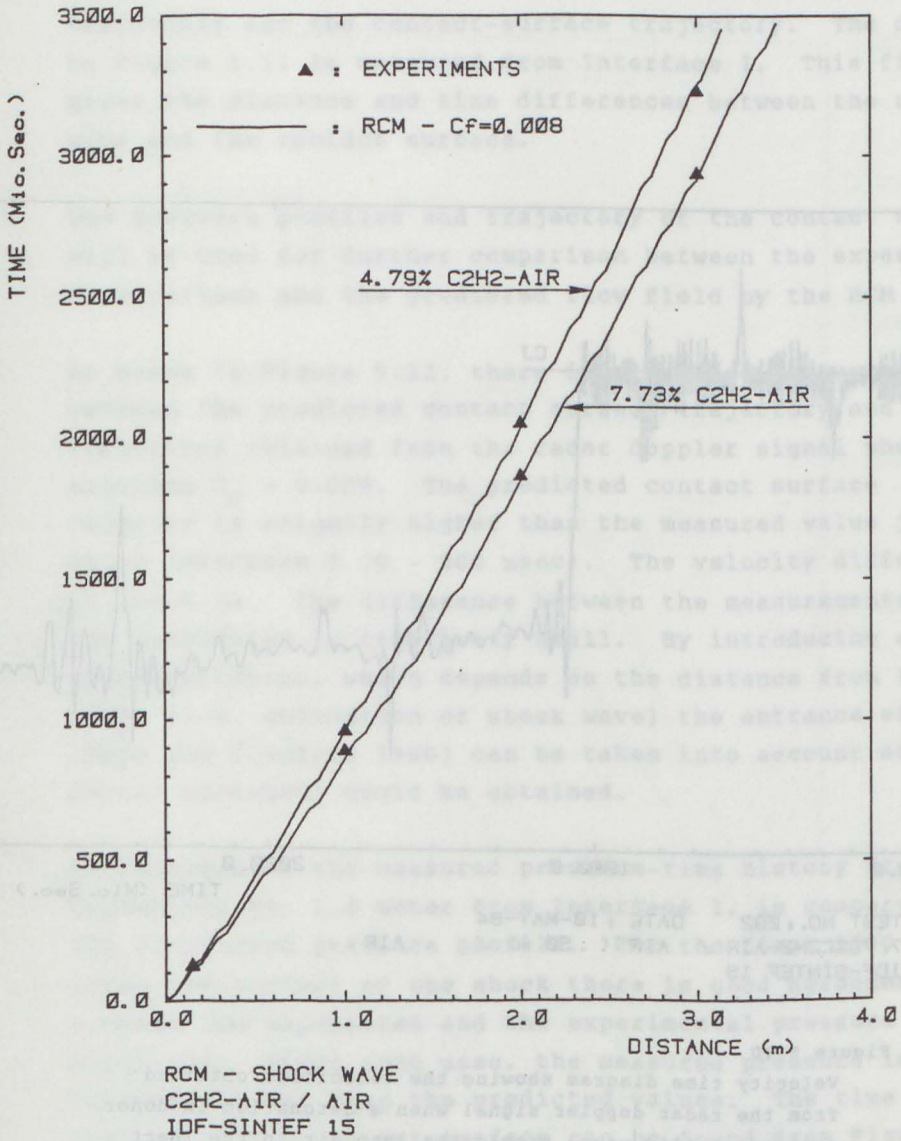
Figure 5.9

Time distance diagram showing predicted shock
trajectories and measured time of arrival for
transmitted shock waves propagating into the inert and
the acceptor sections for the two cases of 4.79% and
7.73% acetylene-air in donor section.

VELOCITY (m/s)

2500.0

2000.0   CJ

1500.0

1000.0

500.0

0.0
    0.0   1000.0   2000.0   3000.0
                                              TIME (Mic. Sec.)
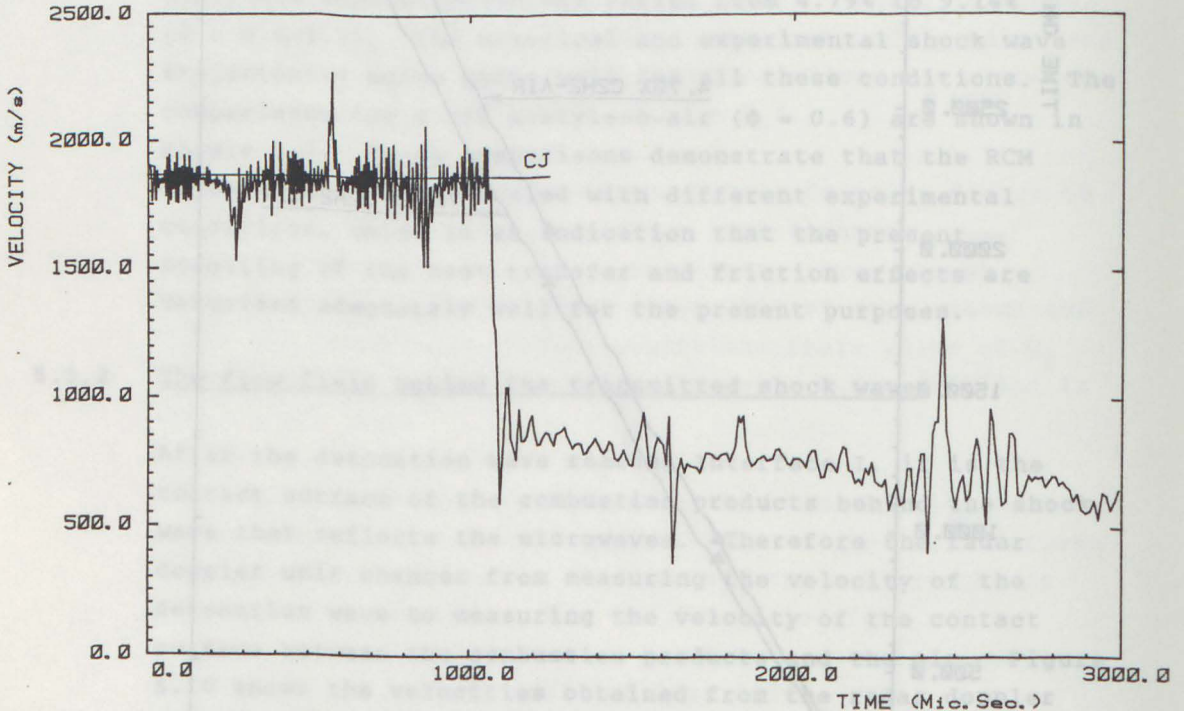
TEST NO.:082   DATE :10-MAY-84
7.73%C2H2-AIR / AIR (.50 m) /   AIR
IDF-SINTEF 15

Figure 5.10
    Velocity time diagram showing the velocities obtained
    from the radar doppler signal when a detonation in donor
    section (0-1060 μsec) propagates into air in the inert
    and the acceptor section. The measured velocity after
    1060 μsec corresponds to the velocity contact surface
    dividing the combustion products and the compressed air.

Figure 5.11 shows both the experimentally observed shockwave
trajectory and the contact-surface trajectory. The distance
in Figure 5.11 is measured from Interface I. This figure
gives the distance and time differences between the shock
wave and the contact surface.

The pressure profiles and trajectory of the contact surface
will be used for further comparison between the experimental
observations and the predicted flow field by the RCM code.

As shown in Figure 5.12, there is also good agreement
between the predicted contact surface trajectory and the
trajectory obtained from the radar doppler signal when
assuming C_f = 0.008. The predicted contact surface
velocity is slightly higher than the measured value just
after Interface I (0 - 500 μsec). The velocity difference
is about 5%. The difference between the measurements and
the prediction is relatively small. By introducing a
friction factor, which depends on the distance from the wave
front (i.e. detonation or shock wave) the entrance effect
(Kays and Crawford 1980) can be taken into account and even
better agreement would be obtained.

In Figure 5.13 the measured pressure-time history from
transducer #4, 1.0 meter from Interface I, is compared with
the calculated pressure profile. For the first 1000 μsec
after the arrival of the shock there is good agreement
between the calculated and the experimental pressure
histories. After 1000 μsec, the measured pressure is
somewhat higher than the predicted values. The time of
arrival of the contact surface can be found from Figure
5.11. It is approximatly 380 μsec later than the arrival
of the shock wave (i.e. 2340 μsec).
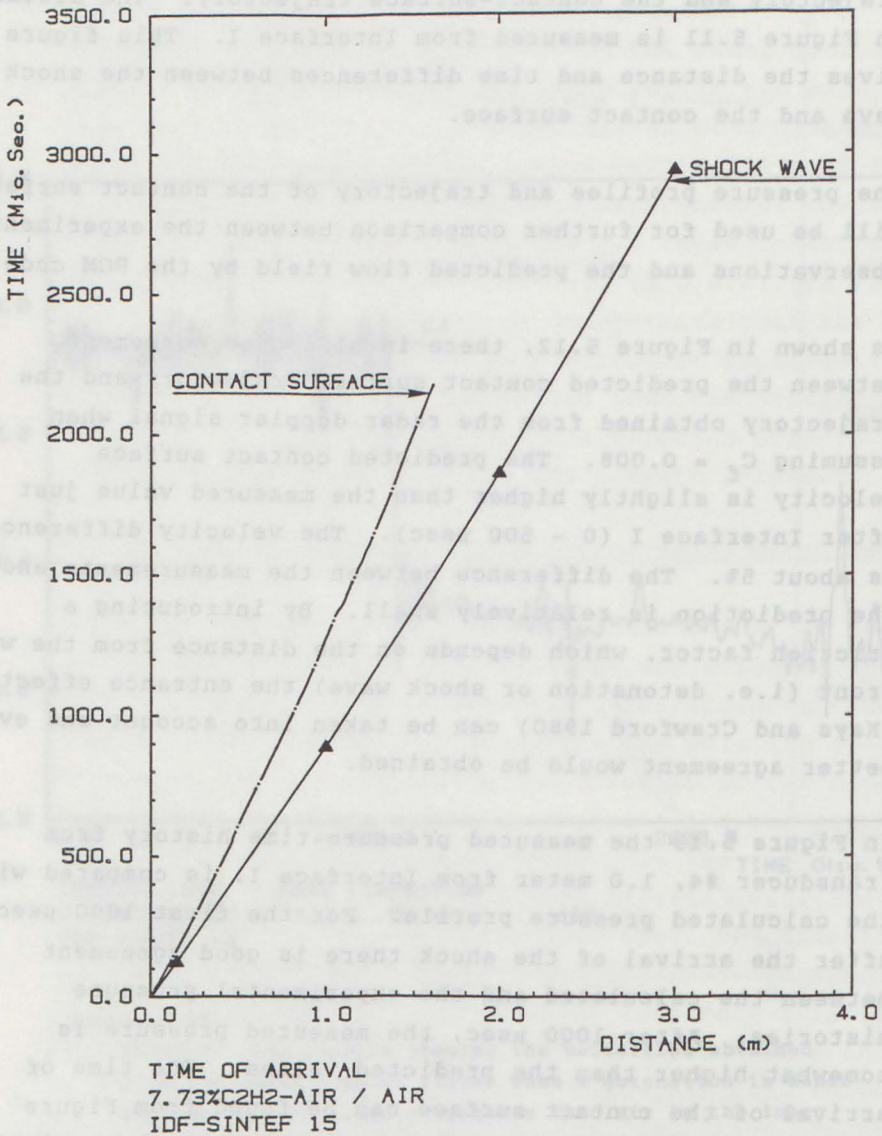
Figure 5.13

Pressure time diagram comparing measured pressure record
with calculated pressure history by using RCM-code when
a detonation wave propagates into an inert gas. The
position of the pressure transducer was 1 meter
downstream of interface I.
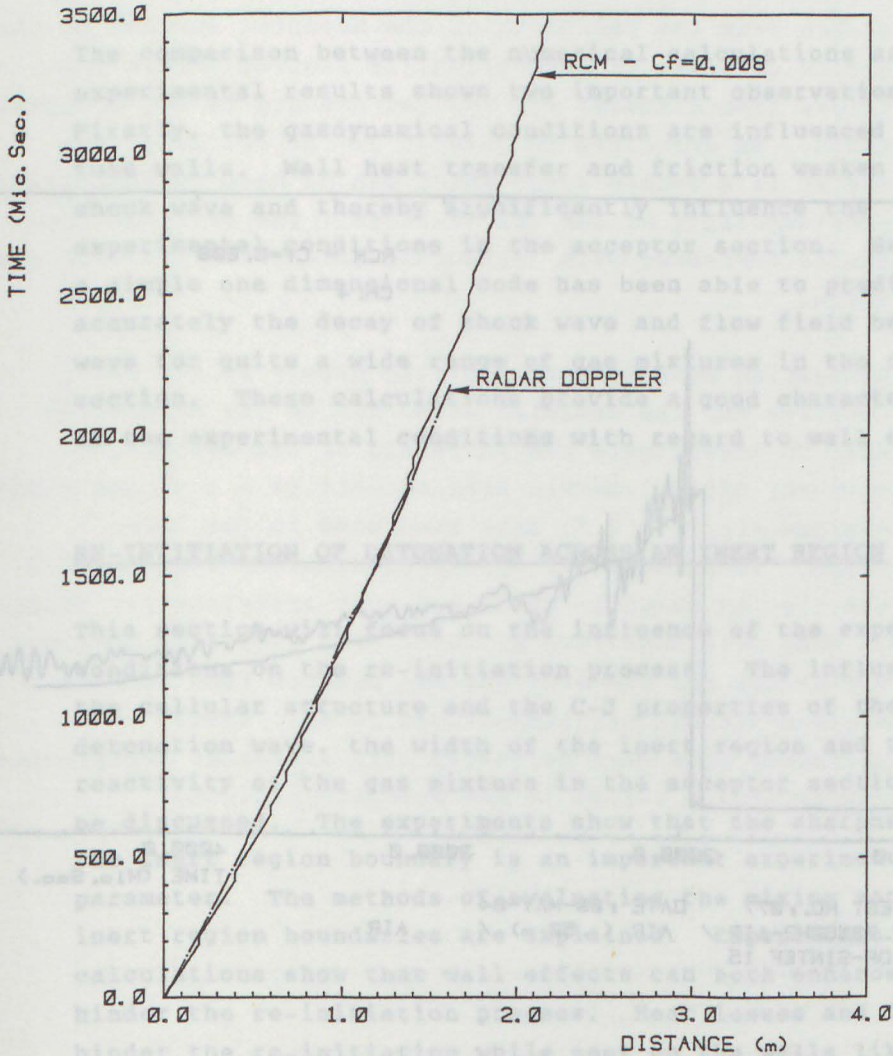
RCM — CONTACT SURFACE
7.73% C2H2-AIR / AIR
IDF-SINTEF 15

Figure 5.11
    Time distance diagram showing the contact surface
    trajectory obtained from radar doppler signal and the
    time of arrival for the shock wave at the pressure
    transducers in the inert and the acceptor section when a
    detonation wave propagates into an inert gas.
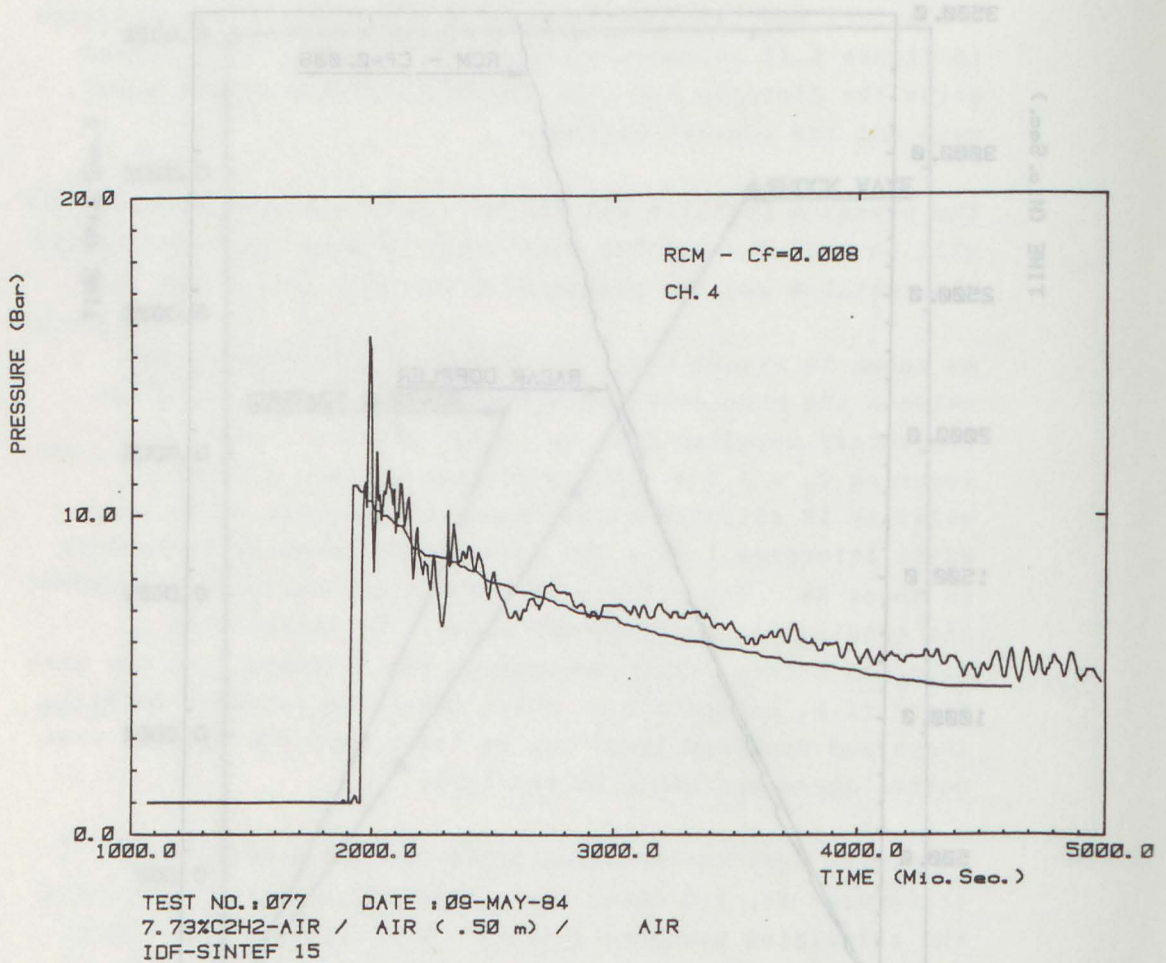
Figure 5.12
    Time distance diagram comparing measured contact surface
    trajectory obtained from radar doppler signal with
    predicted contact surface trajectory by using RCM-code
    when a detonation wave propagates into an inert gas.

5.3.3. Summary

The comparison between the numerical calculations and the
experimental results shows two important observations.
Firstly, the gasdynamical conditions are influenced by the
tube walls. Wall heat transfer and friction weaken the
shock wave and thereby significantly influence the
experimental conditions in the acceptor section. Secondly,
a simple one dimensional code has been able to predict quite
accurately the decay of shock wave and flow field behind the
wave for quite a wide range of gas mixtures in the donor
section. These calculations provide a good characterization
of the experimental conditions with regard to wall effects.

5.4   RE-INTITIATION OF DETONATION ACROSS AN INERT REGION

This section will focus on the influence of the experimental
conditions on the re-initiation process. The influence of
the cellular structure and the C-J properties of the
detonation wave, the width of the inert region and the
reactivity of the gas mixture in the acceptor section will
be discussed. The experiments show that the sharpness of
the inert region boundary is an important experimental
parameter. The methods of evaluating the mixing zone at the
inert region boundaries are explained. Experiments and
calculations show that wall effects can both enhance and
hinder the re-initiation process. Heat losses and friction
hinder the re-initiation while soot on the walls likely
accelerate the re-initiation process. The transition
process will also be discussed.

5.4.1   Variation of re-initiation with gas mixture

Experiments with a 100 mm inert region were undertaken to
investigate the influence of the gas mixtures in the donor
and acceptor sections on the re-initiation process. The
experimental results are shown in Figure 5.14.

In Figure 5.14 the transition distance, defined as the distance from the beginning of the acceptor section to the position of onset of detonation, is plotted versus the critical tube diameter for the gas mixture in the acceptor section. As described in Chapter 2, the critical tube diameter is a length scale which can be used to characterize the detonability of the gas mixtures. The critical tube diameter increases with decreasing detonability of the gas mixture.

A detonation wave is characterized mainly by the C-J properties and the cellular structure of the detonation wave. To investigate the influence of the cellular structure, stoichiometric ethylene-air ($\Phi = 1.0$) and 7.01% acetylene-air ($\Phi = 0.9$) have been used in the donor section. These mixtures have approximately the same C-J properties as shown in Table 4.6, but acetylene-air mixture is a much more sensitive mixture. The cell size is about 4 times larger for the ethylene-air mixture than for the acetylene-air mixture (Knystautas et al., 1984). Experiments have been performed with different acetylene-air mixtures ($\Phi = 0.9-1.2$) in the acceptor section.

3.0

2.5

2.0

1.5

TRANSITION DISTANCE (m)

1.0

0.5

0.0
   0.075   0.100   0.125   0.150   0.175   0.200
                  CRITICAL TUBE (m)
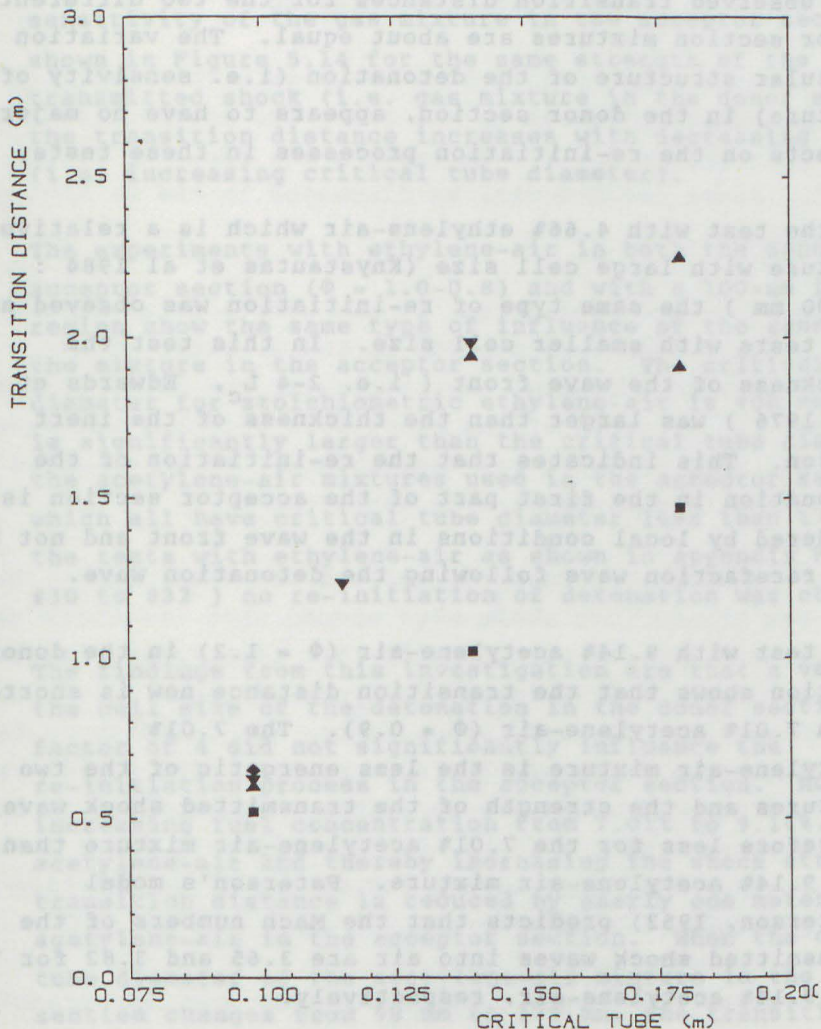
CnHm−AIR / AIR (.10m) / C2H2−AIR
IDF−SINTEF 15

Figure 5.14
Transition distance versus critical tube diameter for
gas mixture in acceptor section for various gas mixtures
in donor section.

▲   100 mm   7.01 % C_2H_2-AIR / AIR / C_2H_2-AIR
▼   100 mm   6.53 % C_2H_4-AIR / AIR / C_2H_2-AIR
■   100 mm   9.14 % C_2H_2-AIR / AIR / C_2H_2-AIR
◆   150 mm   4.66 % C_2H_4-AIR / AIR / C_2H_2-AIR

The observed transition distances for the two different
donor section mixtures are about equal. The variation of
cellular structure of the detonation (i.e. sensivity of the
mixture) in the donor section, appears to have no major
effects on the re-initiation processes in these tests.

In the test with 4.66% ethylene-air which is a relative weak
mixture with large cell size (Knystautas et al 1984 :
S=100 mm) the same type of re-initiation was obseved as for
the tests with smaller cell size. In this test the
thickness of the wave front (i.e. 2-4 L_c, Edwards et
al.,1976) was larger than the thickness of the inert
region. This indicates that the re-initiation of the
detonation in the first part of the acceptor section is
hindered by local conditions in the wave front and not by
the rarefaction wave following the detonation wave.

The test with 9.14% acetylene-air (Φ = 1.2) in the donor
section shows that the transition distance now is shorter
than 7.01% acetylene-air (Φ = 0.9). The 7.01%
acetylene-air mixture is the less energetic of the two
mixtures and the strength of the transmitted shock wave is
therefore less for the 7.01% acetylene-air mixture than for
the 9.14% acetylene-air mixture. Paterson's model
(Paterson, 1953) predicts that the Mach numbers of the
transmitted shock waves into air are 3.65 and 3.82 for 7.01%
and 9.14% acetylene-air, respectively.

These results shows that the strength of the transmitted
shock wave is important for the re-initiation process. The
strength of the transmitted shock wave depends on the C-J
properties and the length of the donor section. As shown in
the previous section it also is influenced by the magnitude
of the wall effects. One concludes that the C-J properties
of the detonation wave in the donor section are indeed one
of the controlling parameters for the re-initiation process.

The re-initiation process is also strongly dependent on the
sensitivity of the gas mixture in the acceptor section. As
shown in Figure 5.14 for the same strength of the
transmitted shock (i.e. gas mixture in the donor section)
the transition distance increases with decreasing sensivity
(i.e. increasing critical tube diameter).

The experiments with ethylene-air in both the donor and
acceptor section (Φ = 1.0-0.8) and with a 100-mm inert
region show the same type of influence of the sensitivity of
the mixture in the acceptor section. The critical tube
diameter for stoichiometric ethylene-air is 400 mm. 400 mm
is significantly larger than the critical tube diameters for
the acetylene-air mixtures used in the acceptor section
which all have critical tube diameter less than 175 mm. For
the tests with ethylene-air as shown in appendix F (test
#30 to #32) no re-initiation of detonation was observed.

The findings from this investigation are that a variation of
the cell size of the detonation in the donor section by a
factor of 4 did not significantly influence the
re-initiation process in the acceptor section. However, by
increasing fuel concentration from 7.01% to 9.14%,
acetylene-air and thereby increasing the shock strength, the
transition distance is reduced by nearly one meter for 7.01%
acetylene-air in the acceptor section. When the critical
tube diameter of the acetylene-air mixture in the acceptor
section changes from 98 mm to 175 mm, the transition
distance increases by nearly one meter when the donor
section is filled with 9.14% acetylene-air. A main
conclusion from these investigations is that the C-J
properties in the donor section and the sensivity of the gas
mixture in the acceptor section are the governing parameters
for the re-initiation of detonation.

5.4.2   Influence of width of the inert region

The experimental results from tests with the same
acetylene-air mixtures in the donor and acceptor sections
and with 100 mm and 150 mm regions are shown in Figure
5.15.   These results will be discussed in the following
paragraphs.

In the previous subsection, it has been concluded that the
re-initiation process depends on the strength of the
transmitted shock wave. By increasing the width of inert
region the strength of the shock wave entering the acceptor
section will decrease and consequently, it is expected that
the transition distance will increase.

Both the numerical calculations and the experimental results
for the transmitted shock wave showed that the shock wave is
decaying. However, to quantify this relatively slow decay
is not possible from the present measurements or
calculations. The resolution is too low relative to the
change in the width of the inert region. The re-initiation
process is very sensitive to rather small changes in the
width of the inert region. To quantify this decay process
in more details, experiments and numerical calculation with
higher resolutions are needed.

The results from these experiments show that the transition
distance increases by about 0.5 meter when the inert region
increases from 100 mm to 150 mm. As expected, the width of
the inert region has a strong influence on the re-initiation
process. It is believed that this influence is mainly due
to the effect of the width on the strength of the shock wave
entering the acceptor section.
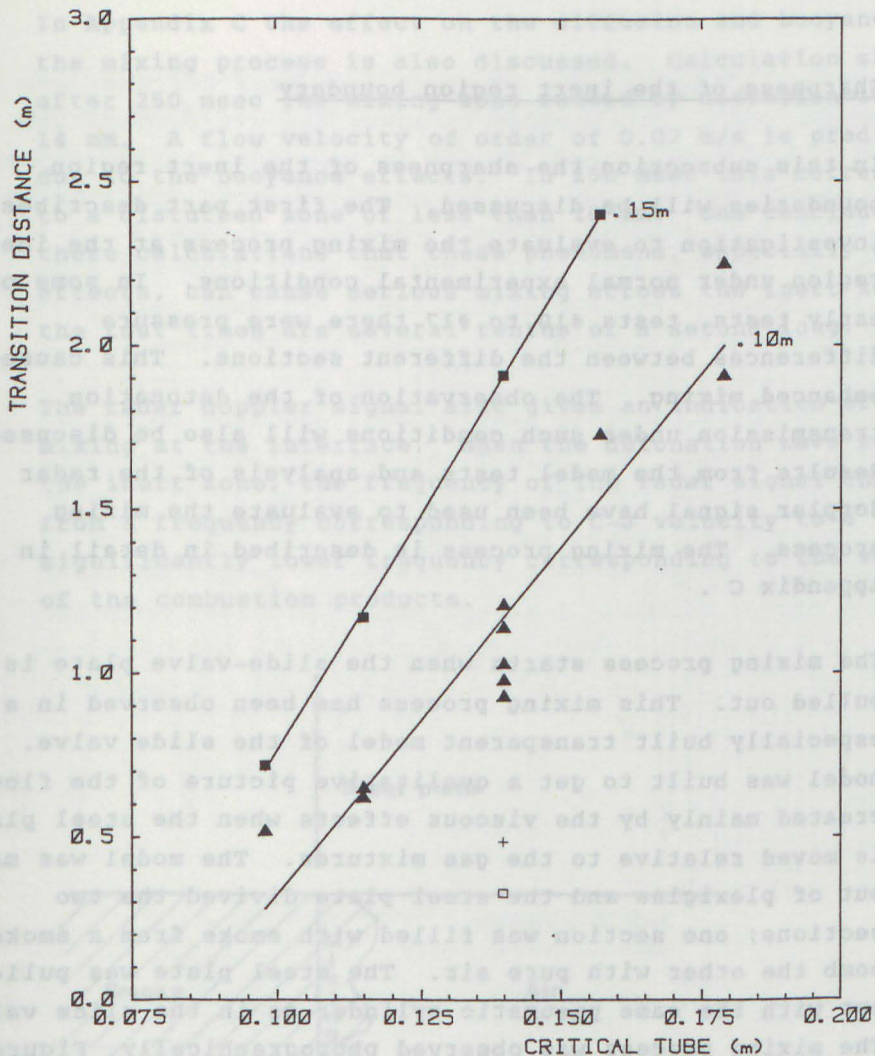
Figure 5.15
Transition distance versus critical tube diameter for
100 mm and 150 mm inert section and the same
acetylene-air mixture in the donor and the acceptor
sections.

▲   100 mm   Normal conditions.

+   100 mm   Smoked foil in acceptor section.

□   100 mm   Enhanced mixing at inert region boundary
               caused by pressure differences in the
               different sections.

■   150 mm   Normal conditions.

5.4.3   Sharpness of the inert region boundary

In this subsection the sharpness of the inert region
boundaries will be discussed. The first part describes the
investigation to evaluate the mixing process at the inert
region under normal experimental conditions. In some of the
early tests, tests #10 to #17, there were pressure
differences between the different sections. This caused
enhanced mixing. The observation of the detonation
transmission under such conditions will also be discussed.
Results from the model tests and analysis of the radar
doppler signal have been used to evaluate the mixing
process. The mixing process is described in detail in
Appendix C .

The mixing process starts when the slide-valve plate is
pulled out. This mixing process has been observed in a
especially built transparent model of the slide valve. The
model was built to get a qualitative picture of the flow
created mainly by the viscous effects when the steel plate
is moved relative to the gas mixtures. The model was made
out of plexiglas and the steel plate divived the two
sections; one section was filled with smoke from a smoke
bomb the other with pure air. The steel plate was pulled
out with the same pneumatic cylinder as in the slide valve.
The mixing process was observed photographically. Figure
5.16 shows a drawing of a photograph taken 271 msec after
the steel plate started to move, which is about the same
time it takes to carry out a detonation test. Apparently
the smoke is penetrating less than 30 mm into the air
region, so the total thickness of the mixing zone should be
less then 60 mm.

In Appendix C the effect on the diffusion and buoyancy on
the mixing process is also discussed. Calculation show that
after 250 msec the mixing zone caused by diffusion is
14 mm. A flow velocity of order of 0.07 m/s is predicted
due to the buoyance effects. In 250 msec this corresponds
to a disturbed zone of less than 20 mm. One concludes from
these calculations that these phenomena, especially buoyancy
effects, can cause serious mixing across the inert zone if
the test times are several tenths of a second long.

The radar doppler signal also gives an indication of the
mixing at the interface. When the detonation wave reaches
the inert zone, the frequency of the radar signal changes
from a frequency corresponding to C-J velocity to a
significantly lower frequency corresponding to the velocity
of the combustion products.
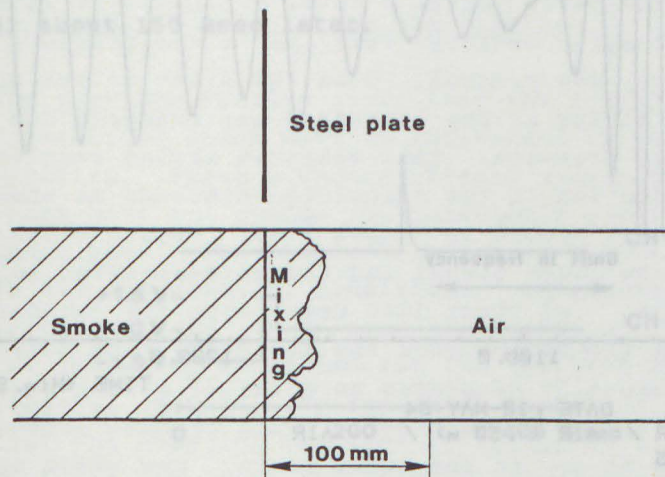
Figure 5.16
    Drawing of a photograph taken 271 msec after removal of
    slide plate showing the mixing process between smoke and
    air in the the slide wave model.

Figure 5.17 shows this shift in frequency for the case of a detonation in stoichiometric acetylene-air propagation into air. The change takes places in less than 2-3 wave lengths corresponding to about 30-45 mm, indicating that the extent of the mixing region is less than this length.
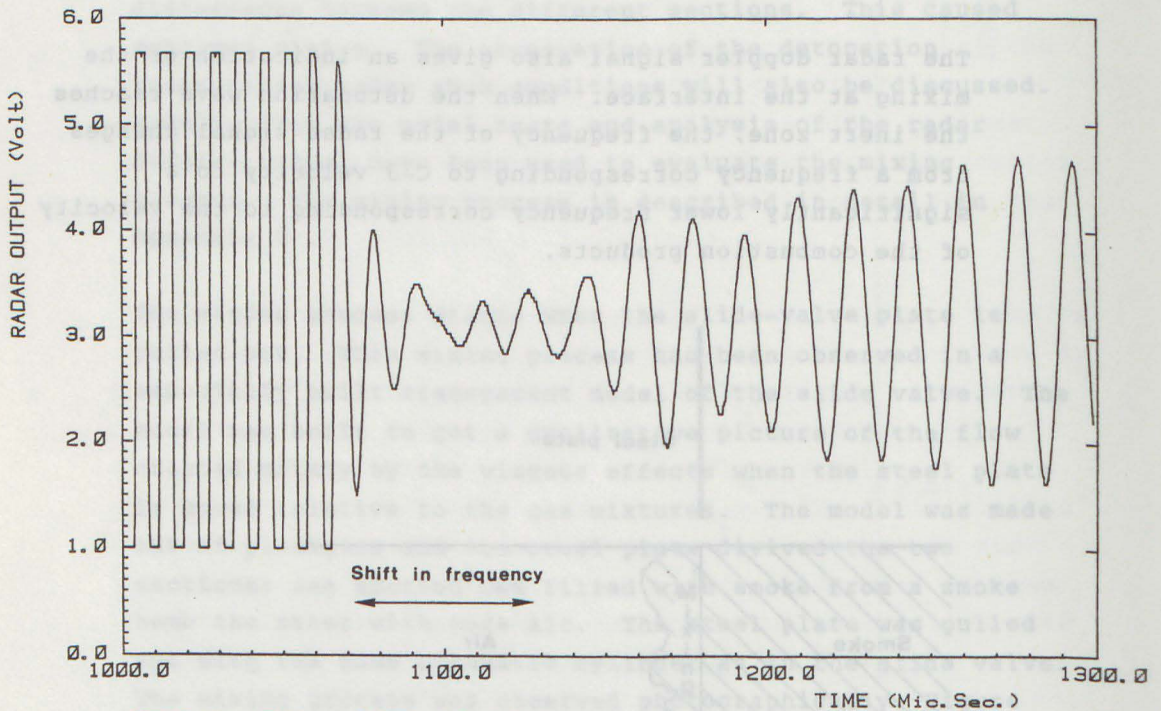
TEST NO.: 082   DATE : 10-MAY-84
7.73%C2H2-AIR / AIR (.50 m) /   AIR
IDF-SINTEF 15

Figure 5.17
    Radar doppler signal showing the zone for shift in frequency when the radar doppler unit change from observing the detonation wave to observing the contact surface.

Variations in the operation of the slide valve can also
cause variations of the sharpness of the inert region
boundary. Therefore it was decided to measure the motion of
the slide-valve plates. The set up is discussed in Section
4.2. Figure 5.18 shows a typical example of a scope trace
from the monitoring of the slide-valve motion. The scope was
triggered when the steel plates started to move. Channel 1
(CH 1) measured the signal from pressure transducer #1, and
CH 2 monitored the position of the steel plates. For the
first 100 msec the input signal of CH 2 is -1.5V which means
that both steel plates are moving. At about 100 msec slide
valve I is in an open position and the signal changes to
+1.5V . About 20 msec later the signal changes again, this
time the signal changes with -1.5V as slide valve II reaches
the open position. From the CH 1 pressure record one can
see that the detonation wave arrives at pressure transducer
#1 about 150 msec later.
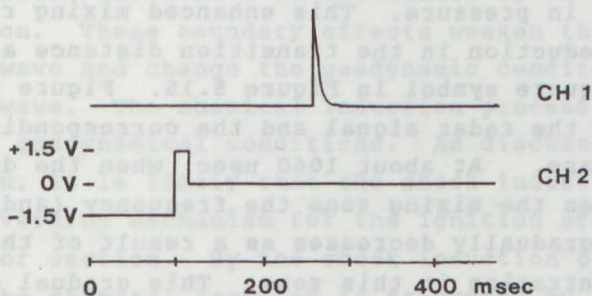
Figure 5.18
Scope trace for monitoring the slide valve motion.

Figure 5.18 was from test #55.   Test #54 and #55 had the
same gas mixture.   In test #54 the steel plates were removed
in 50 msec, which is the fastest opening observed.   The
experimental results are identical for the two tests.   This
indicates that the variation of the speed of the steel
plates from test to test is not changing the experimental
conditions significantly.

All these evaluations show that the total extent of the
mixing zones at the inert region boundaries is less than
60 mm and fairly similar from test to test.   Therefore,
under normal experimental conditions, a quite distinct inert
region is created.   For 100 mm inert section the region of
pure air is at least 40 mm.

In some of the early tests, a small overpressure in the
donor and acceptor sections relative to the pressure in the
inert section, was created.   When the slide valves were
opened, the mixing at the interface was enhanced due to the
difference in pressure.   This enhanced mixing resulted in
dramatic reduction in the transition distance as shown by
the open square symbol in Figure 5.15.   Figure 5.19a and
5.19b show the radar signal and the corresponding velocity
for this case.   At about 1060 μsec, when the detonation
wave reaches the mixing zone the frequency (and detonation
velocity) gradually decreases as a result of the reduced
fuel concentration in this zone.   This gradual decrease is
not observed in any of the other tests.   The shock wave
propagates through the inert section in about 85 μsec.
Just after the shock wave has entered the acceptor section
at about 1200 μsec, a low frequency signal with high
amplitude is observed.   The low frequency corresponds
approximately to the particle velocity behind the shock
wave.   The target that reflects the microwaves has only a
small velocity relative to the local particle velocity.   The
high amplitude is a result of a strongly reflecting target.

This indicates that a relatively large volume of burned gas
has suddenly been generated by a volumetric explosion behind
the shock wave. In the other experiments, such low
frequency and high amplitude signals were not observed.

One concludes that under normal conditions a distinct inert
region stops a detonation wave rather efficiently. However,
a change in the sharpness of the inert region boundary can
have dramatic effects on re-initiation. Since the
experimental results (i.e., the transition distance) depend
on this sharpness, the results depend critically on the
experimental procedure. It is therefore important and
necessary to characterize this dependancy in order to
compare results from investigations with different apparatus
and with different experimental procedures.

5.4.4. Influence of heat losses and friction

The previous section shows that the trajectory of the
transmitted shock wave is influenced by heat loss and
friction. These boundary effects weaken the transmitted
shock wave and change the gasdynamic conditions behind the
shock wave. The chemical induction process depends strongly
on the gasdynamical conditions. As discussed later in this
section, it is likely that the shock induction process is
the governing mechanism for the ignition of the gas in the
acceptor section. By the shock induction process one means
that the chemical reaction is triggered by the temperature
increase caused by the shock wave and that gas mixture
releases its chemical energy after going through the
chemical induction period. One-dimensional calculations of
the induction period has been performed in order to estimate
the influence of heat loss and friction on the ignition
process. As described in Section 3.7, the induction process
is calculated by following particle trajectories in the flow
field calculated by the RCM code and using the induction
time formula developed by Edwards et al.(1981).
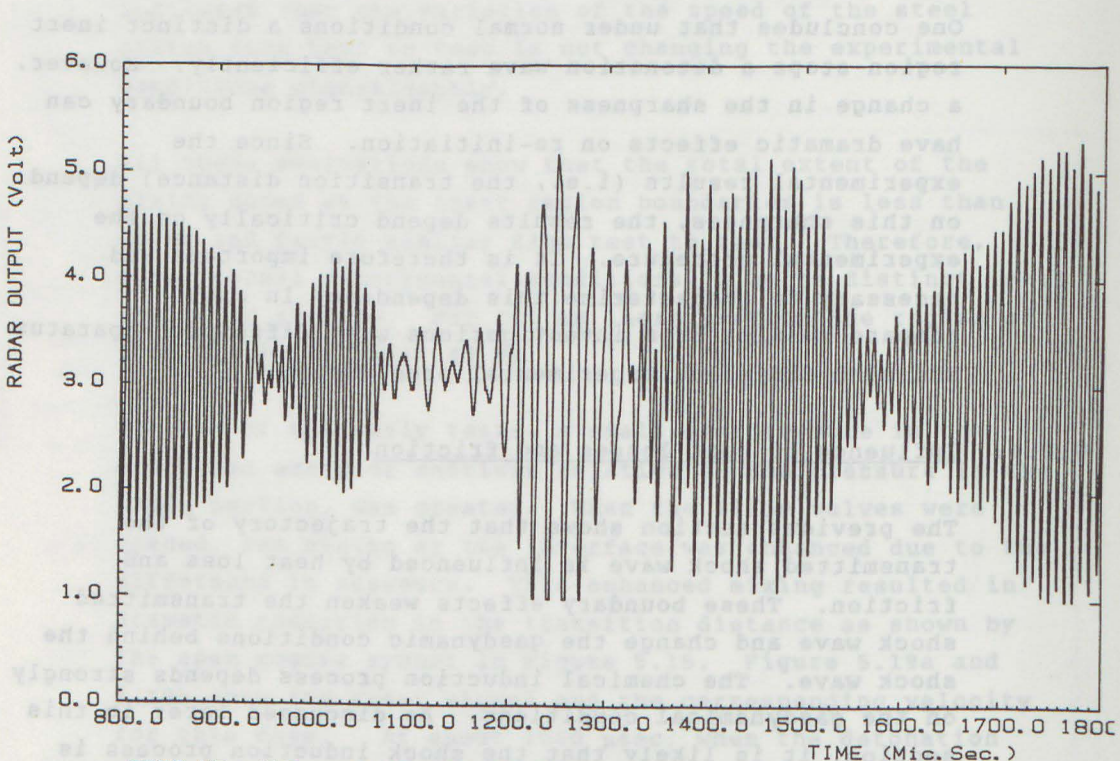
TEST NO.:016   DATE :25-FEB-84
7.75%C2H2-AIR / AIR (.10 m) / 7.75%C2H2-AIR
IDF-SINTEF 15

Figure 5.19a)
Radar doppler signal for acetylene-air (φ = 1.0) with
100 mm inert region for the case of different pressures
in the sections which caused mixing.

VELOCITY (m/s)

2500.0

2000.0

1500.0

1000.0

500.0

0.0

Velocity decay

800.0 900.0 1000.0 1100.0 1200.0 1300.0 1400.0 1500.0 1600.0 1700.0 1800.0

TIME (Mic. Sec.)

TEST NO. :016   DATE :25-FEB-84
7.75%C2H2-AIR / AIR (.10 m) / 7.75%C2H2-AIR
IDF-SINTEF 15

Figure 5.19b)

Velocity reduced from the radar doppler signal for
acetylene-air (ϕ = 1.0) with 100 mm inert region for
the case of different pressures in sections which caused
mixing.

Figure 5.20 shows the times for particles to go through
various fractions of the induction process as a function of
the initial particle position downstream of Interface I.
The induction time parameter ψ represents the fraction of
the induction process which the particles have gone
through. In these calculations heat loss and friction
(i.e. C_f = 0) are neglected. When heat transfer and
friction are taken into account, (i.e. C_f = 0.008), only
the particles in the two numerical cells closest to the
interface went through the whole induction process
(i.e. ψ = 1.0). For these particles the induction time
has been calculated to be 190 μsec. Particles whose
initial position is further downstream of Interface I, do
not go through the whole induction process within the
2500 μsec total time used in the calculations. These
calculations show that the induction time is very sensitive
to variations in the gasdynamic conditions behind the
transmitted shock. Wall effects, therefore, have a dramatic
effect on the induction process. This is illustrated in
Figure 5.21 where the times for particles to go through 5%
of the induction process (ψ = 0.05) with and without heat
transfer and friction, are shown.

Although the re-initation process in the acceptor section is
not completely one-dimensional, the calculations clearly
illustrate the strong influence of the tube boundaries on
the chemical induction time. This influence (i.e. an
increase in the chemical induction time), will cause a delay
in the onset of the detonation. From this evaluation of
boundary layer effects, it appears that the size of the
apparatus is a very important parameter for characterizing
the experimental conditions.

With the exception of Bull et al. (1981), other experiments
reported on detonation transmission across inert regions
have been performed in smaller apparatus than used in the
present investigation. The effect of the boundary layers
increases as the size of the apparatus decreases.
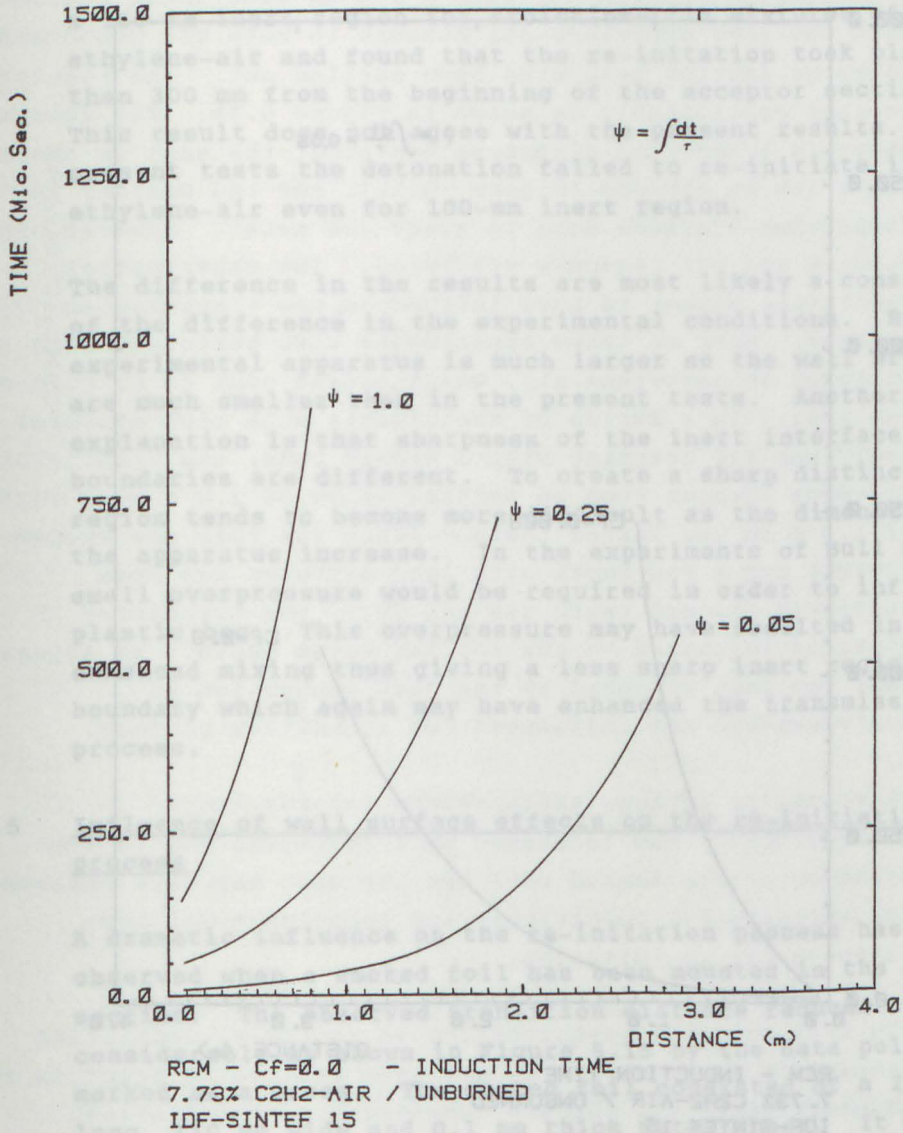
Figure 5.20
The fractional induction time versus the initial
particle position.
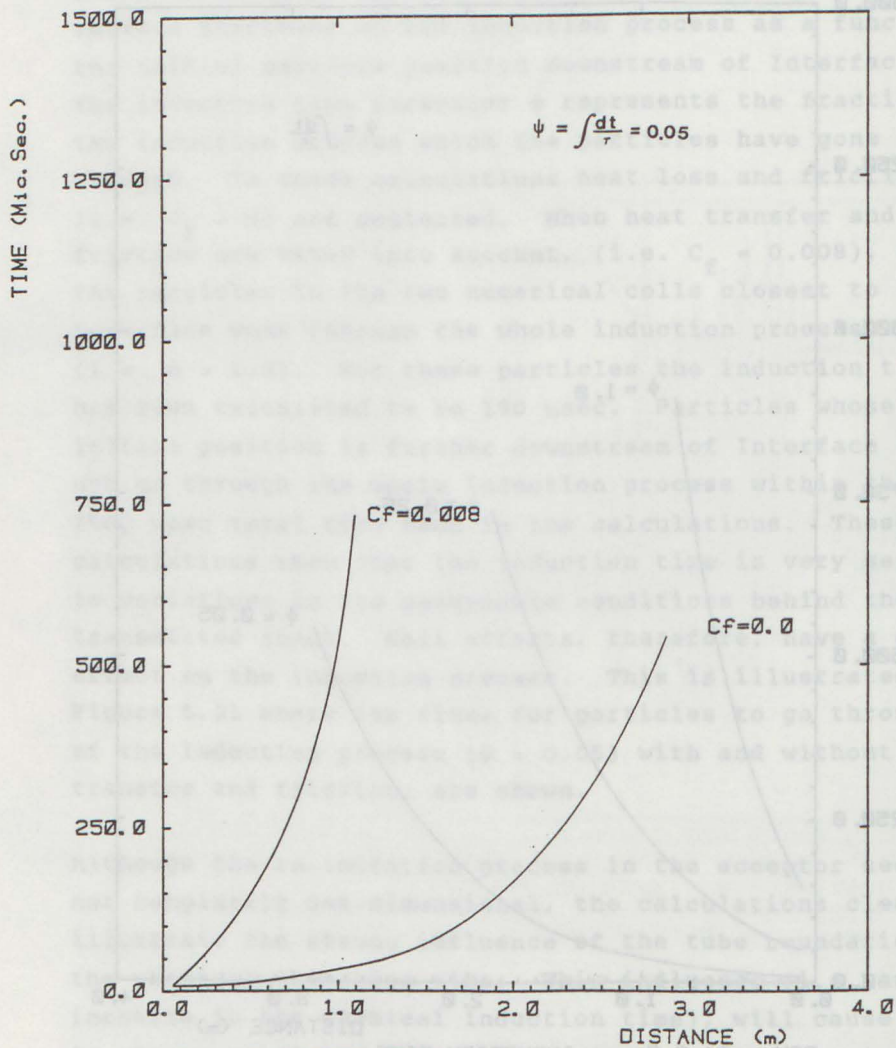
RCM – INDUCTION TIME
7.73% C2H2–AIR / UNBURNED
IDF–SINTEF 15

Figure 5.21
    The times for particles to go through 5% of the
    induction process ($\psi = 0.05$) versus initial particle
    position with ($C_f = 0.008$) and without ($C_f = 0$) heat
    transfer and friction.

Bull et al. have observed re-initiation of detonation across
a 150 mm inert region for stoichiometric mixtures of
ethylene-air and found that the re-initation took place less
than 300 mm from the beginning of the acceptor section.
This result does not agree with the present results. In the
present tests the detonation failed to re-initiate in
ethylene-air even for 100-mm inert region.

The difference in the results are most likely a consequence
of the difference in the experimental conditions. Bull's
experimental apparatus is much larger so the wall effects
are much smaller than in the present tests. Another
explanation is that sharpness of the inert interface
boundaries are different. To create a sharp distinct inert
region tends to become more difficult as the dimensions of
the apparatus increase. In the experiments of Bull et al. a
small overpressure would be required in order to inflate the
plastic bag. This overpressure may have resulted in
enhanced mixing thus giving a less sharp inert region
boundary which again may have enhanced the transmission
process.

5.4.5   Influence of wall surface effects on the re-initiation
        process

A dramatic influence on the re-initation process has been
observed when a smoked foil has been mounted in the acceptor
section. The observed transition distance reduced
considerably as shown in Figure 5.15 by the data point
marked as a cross. The smoked foil consisted of a 2.5 m
long, 110 mm wide and 0.1 mm thick metal sheet. It was
covered by soot from an acetylene torch. By mounting the
smoked foil in the acceptor section geometrical
irregularities may have been introduced which alter the
re-initiation process in a similar manner to that observed
by Gavrilenko et al.(1982 b). However, in the experiment
carried out just after the experiment with the smoked foil
(test #23), a shorter transition distance was also
observed. This indicates that the residual soot from the
smoked foil also has an influence.

Transmission experiments with a 200-mm wide inert region and with the same acetylene-air mixture in both the donor and acceptor section have also been carried out. The results scatter considerably as shown in Figure 5.22. The shortest observed transition distances are about the same as observed for a 150 mm air-gap (Figure 5.15), and the scatter in transition-distance data is about one meter. However, the results are not randomly scattered. The experimental conditions appear to have influenced the transmission process. Many of these experiments were performed with rich mixtures of acetylene-air, which caused soot to be formed in the tube. In a series of experiments with rich mixtures of acetylene-air starting with a closed tube, the transition distance changed from an initial value of 2.0 m to a value of 1.2 m in the latter tests. After the tube was vacuum cleaned and a few shots with lean mixtures had been performed (before tests #65 and #71), the transition distance increased to the initial value again. It appears that the soot produced by the rich combustion of acetylene-air has influenced the transition process.

There are no obvious explanations for the above observations. The increased wall roughness due to the presence of the smoked foil and the soot may have changed the experimental conditions, and turbulence may have enhanced the re-initation.

The soot can also have contributed to the re-initiation process in other ways. It may have started to react in the boundary layer and thereby enhanced the re-initation. Elsworth et al. (1969) observed that presence of particles in a rapid-compression machine resulted in non-uniform ignition and reduced chemical induction time. Radiative heating in dust clouds (i.e. particle ignition) has also been suggested as a flame acceleration mechanism (Wilson, 1980; Moore and Weinberg, 1981). The radiation heats the particles ahead of combustion zone and the hot particles ignites the gas. This mechanism may also have contributed
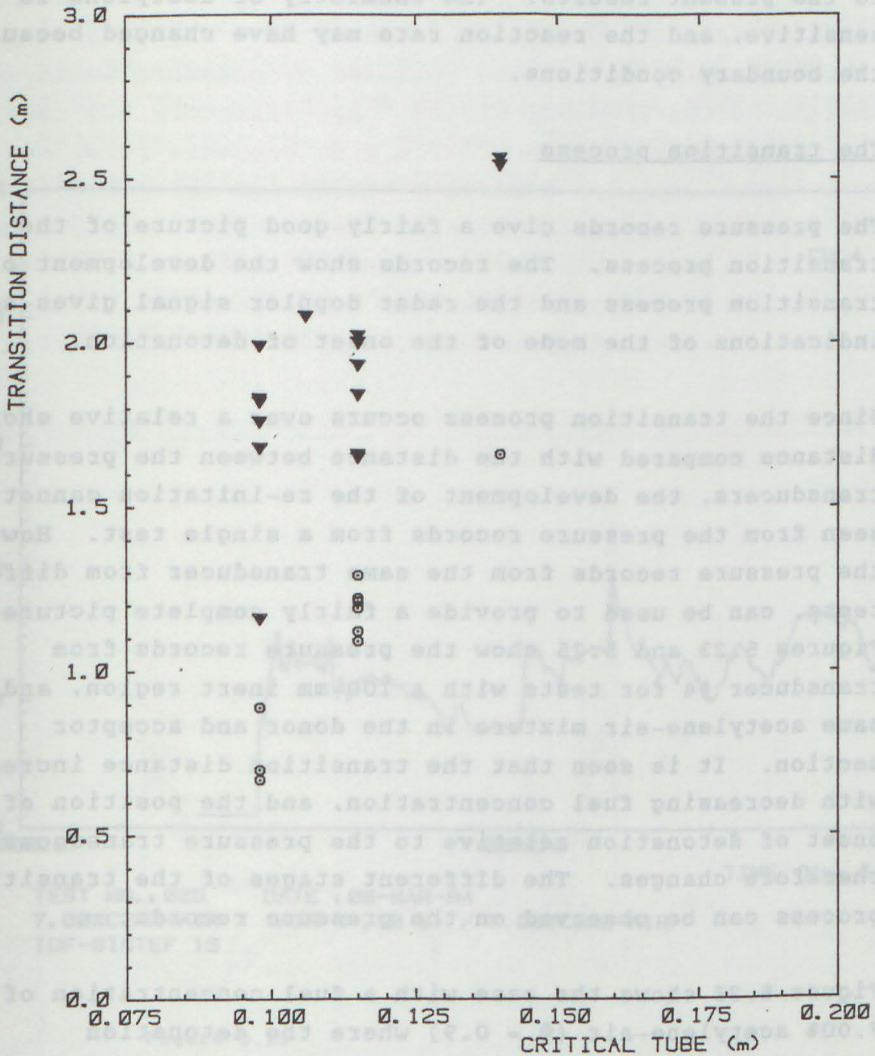
```
C2H2-AIR / AIR(.20m) / C2H2-AIR
IDF-SINTEF 15
```

Figure 5.22

Transition distance versus critical tube diameter for
200 mm inert section and the same acetylene-air mixture
in the donor and the acceptor section.

▼   Long transition distance.

⊙   Short transition distance.

to the present results. The chemistry of acetylene is very
sensitive, and the reaction rate may have changed because of
the boundary conditions.

5.4.6   The transition process

The pressure records give a fairly good picture of the
transition process. The records show the development of the
transition process and the radar doppler signal gives some
indications of the mode of the onset of detonation.

Since the transition process occurs over a relative short
distance compared with the distance between the pressure
transducers, the development of the re-initation cannot be
seen from the pressure records from a single test. However,
the pressure records from the same transducer from different
tests, can be used to provide a fairly complete picture.
Figures 5.23 and 5.25 show the pressure records from
transducer #4 for tests with a 100-mm inert region, and the
same acetylene-air mixture in the donor and acceptor
section. It is seen that the transition distance increases
with decreasing fuel concentration, and the position of
onset of detonation relative to the pressure transducer #4
therefore changes. The different stages of the transition
process can be observed on the pressure records.

Figure 5.23 shows the case with a fuel concentration of
7.00% acetylene-air ($\Phi = 0.9$) where the detonation
re-initates about 0.5 m behind the transducer. The leading
shock wave appears to be followed immediately by pressure
build up, indicating the combustion is occuring somewhere
between the shock front and the contact surface of Interface
II. At this stage in the transition process, the shock wave
is accelerated by the pressure waves from behind. The
induction time will decrease as the strength of the shock
wave increases. The shock wave observed at 3000 μsec. is
the retonation wave caused by the onset of detonation
downstream.

Figure 5.23

Pressure time history from transducer #4 when the detonation re-initiated 0.5 m after the tranducer.
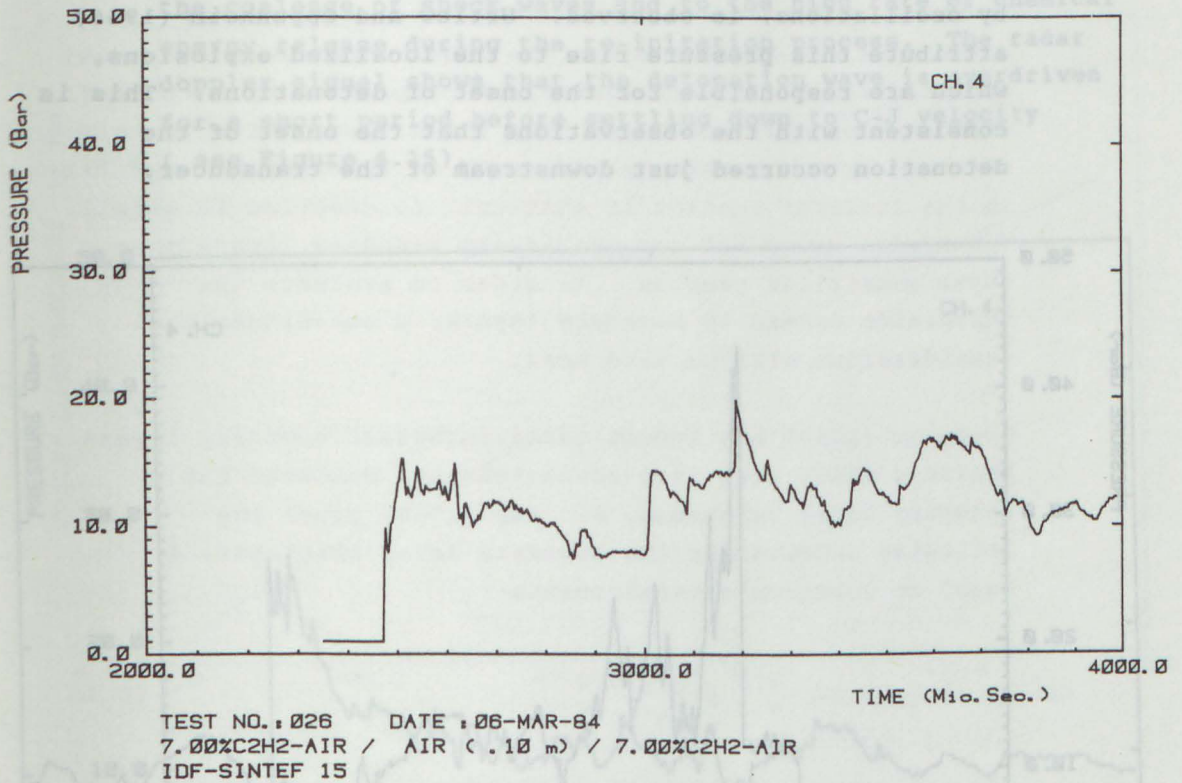
At 7.37% acetylene-air (Φ = 0.95), the detonation wave
re-initated 0.2 m behind the transducer. Figure 5.24 again
shows a leading shock wave followed by pressure build up
similar to the previous figure. Approximately 120 µsec
after the shock wave arrives, a high pressure rise, followed
by oscillations, is observed. Urtiew and Oppenheim (1966)
attribute this pressure rise to the localized explosions,
which are responsible for the onset of detonations. This is
consistent with the observations that the onset of the
detonation occurred just downstream of the transducer.
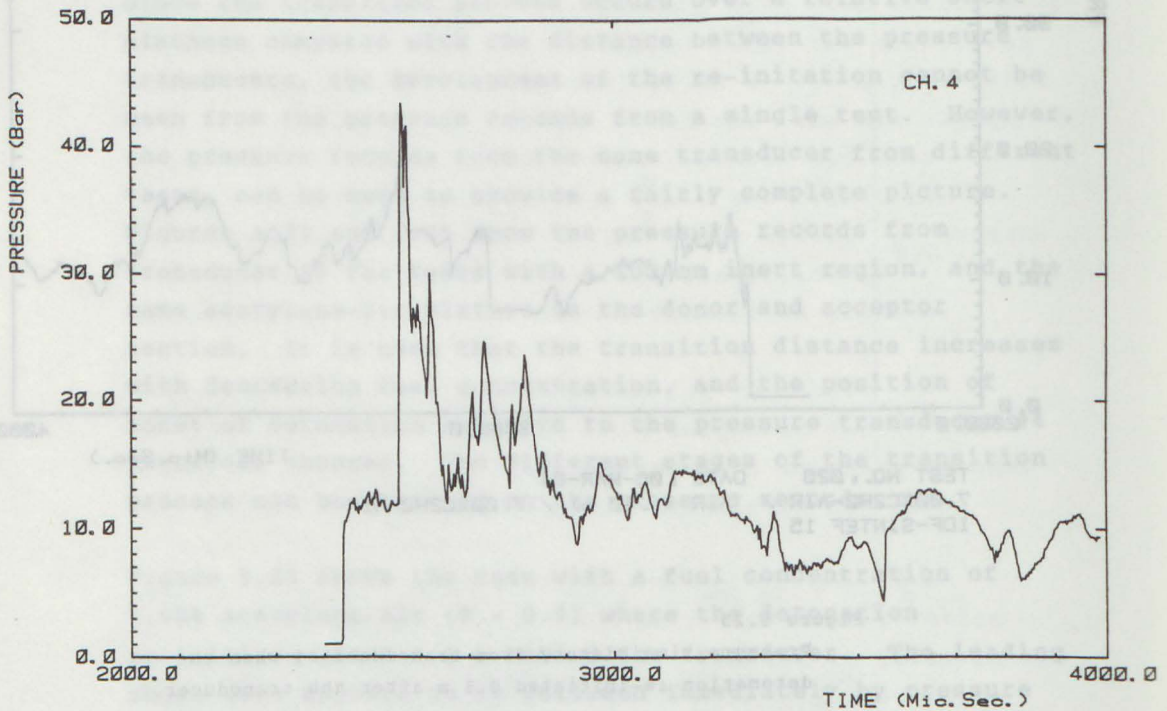
TEST NO.:027   DATE :06-MAR-84
7.37%C2H2-AIR /   AIR (.10 m) / 7.37%C2H2-AIR
IDF-SINTEF 15

Figure 5.24
Pressure time history from transducer #4 when the
detonation re-initiated 0.2 m after the pressure
transducer.

For stoichiometric acetylene in air(Φ = 1.0) the
detonation re-initiated before the pressure transducer. The
detonation re-initiated about 0.5 m before the transducer,
and an overdriven detonation is recorded as shown on Figure
5.25. This overdriven detonation has a higher pressure and
velocity than the C-J values. The wave is overdriven due
the coalesce of shock waves and to the high rate of chemical
energy release during the re-initation process. The radar
doppler signal shows that the detonation wave is overdriven
for a short period before settling down to C-J velocity
(see Figure 4.15).
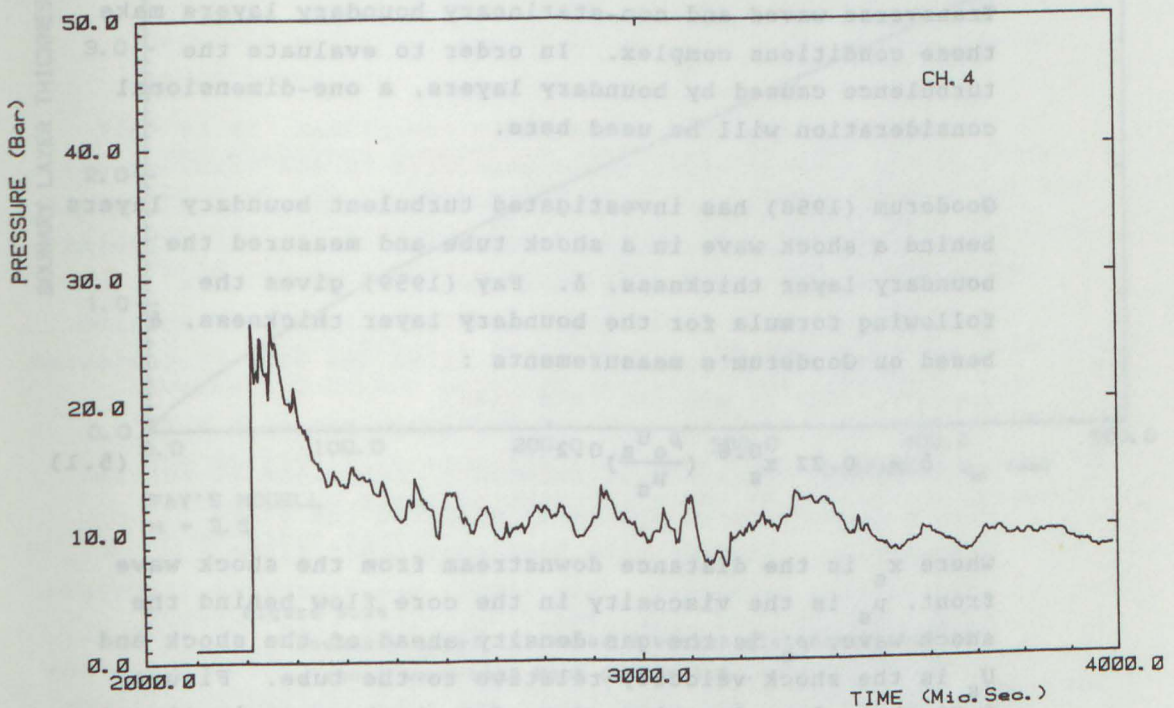
TEST NO. : 018   DATE : 01-MAR-84
7.75%C2H2-AIR /   AIR (.10 m) / 7.75%C2H2-AIR
IDF-SINTEF 15

Figure 5.25
Pressure time history from transducer #4 when the
detonation re-initiated 0.5 m before the pressure
transducer.

These pressure records are very similar to those reported by
Edwards et al.(1981) for detonation initiation by a planar
shock, thus, providing some evidence that the same
mechanism, i.e. shock induction process, is responsible for
the re-initiation process.

As shown by Urtiew and Oppenheimer (1966), turbulent
combustion can also generate the right conditions for onset
of detonations. A turbulent flame propagates by turbulent
diffusion of heat and mass. The flame propagation is mainly
governed by the intensity and scale of turbulence. The flow
in the acceptor section is difficult to describe in detail.
Transverse waves and non-stationary boundary layers make
these conditions complex. In order to evaluate the
turbulence caused by boundary layers, a one-dimensional
consideration will be used here.

Gooderum (1958) has investigated turbulent boundary layers
behind a shock wave in a shock tube and measured the
boundary layer thickness, δ. Fay (1959) gives the
following formula for the boundary layer thickness, δ
based on Gooderum's measurements :

$$\delta = 0.22 \; x_s^{0.8} \; (\frac{\rho_o U_s}{\mu_s})^{0.2} \qquad\qquad (5.1)$$

where x_s is the distance downstream from the shock wave
front, μ_s is the viscosity in the core flow behind the
shock wave, ρ_o is the gas density ahead of the shock and
U_s is the shock velocity relative to the tube. Figure
5.26 shows δ as function of x_s for shock waves in air at
Mach-number 3.5. The shock wave propagating into the
acceptor section has an initial Mach-number of about 3.5 for
the mixtures used in this test. The thickness of the
boundary layer in the acceptor section should not differ
significantly from the boundary layer thickness predicted by
Fay's relation, although the initial shock wave is not
one-dimensional, and it is not followed by at constant
pressure region like in a shock tube.

$$\delta = 0.22 \, x_s^{0.8} \, \left(\frac{\rho_o U_s}{\mu_s}\right)^{0.2}$$

FAY'S MODELL
M = 3.5

Figure 5.26

Boundary layer thickness δ versus distance x_s behind
a shock wave with Mach number 3.5 .

This value will therefore be used to approximate the boundary layer thickness in the acceptor section. It can be seen in Figure 5.11 that when the shock wave has travelled 1.5 m from Interface I the distance between the shock wave and the contact surface is about 400 mm. At this point the boundary layer thickness at the contact surface should be in order of 3 mm as shown in Figure 5.26. Compared with the tube dimension (w = 125 mm), the boundary layer thickness δ is small. From these one-dimensional considerations it appears that the turbulent boundary layer in the acceptor section consists of a very thin zone. Even if this thin zone burns, it will have small effect on the average conditions.

Although the transmitted shock is non-planar, it is felt that the type of disturbance generated by the transverse waves are not likely to create turbulence with proper scale and intensity for turbulent combustion in core flow behind the shock wave. The fact that the tests with 7.01% acetylene-air and 6.53% ethylene-air in the donor section, which gives different cell sizes, give the same transmission results tends to support this view.

From this it appears that turbulent combustion is not the main mechanism which initially supports the flame propagation. It must have been some other flame acceleration mechanism. Lee (1981) has discussed different flame acceleration mechanisms. He calls them positive feedback mechanisms since the flame in interaction with the confinement and the flow field are creating the conditions for increased reaction rate.

One of these positive feedback mechanisms is the type of phenomena that Edwards et al. (1981) have observed. The reaction zone generates pressure waves. This pressure waves catch up with the shock front and increase the strength of the shock and thereby decreases the induction time. This mechanism is likely to contribute in the present experiments.

Moen et al.(1981) have indentified another mechanism
characterized by amplification of acoustic oscillations at
the reaction front. They were observing the acceleration
phase of a so called galloping detonation. The acceleration
of the reaction zone is controlled by amplification of
transverse waves in the reaction zone behind the leading
shock wave. The frequency of the pressure oscillation at
the reaction zone is approximately equal to the lowest
acoustic frequency of the tube. Moen et al.(1981) claim
that this acoustic mode is more dependent of the tube
diameter channel than on the chemical kinetics of the gas
mixture. The acoustic flame acceleration mode is also a
possible mechanism in the acceptor section of the present
experiments.

Even turbulent combustion cannot be excluded in the later
phase of the re-initiation process, since instabilities and
pertubartions caused by the flame interaction with the flow
field can also create turbulence and flame acceleration.

It is very difficult to point out the mechanism which is
dominating in the acceptor section. The problem is that
more than one mechanism can be important and their effects
are difficult to separate from each other. Therefore, it is
difficult to describe accurately the re-initiation process
in acceptor section.

However, it is felt that the fact that the transition
distance increases with the critical tube diameter (i.e.
decreasing sensitivity of the gas mixture), is an indication
that the re-initiation process mainly is controlled by the
gasdynamic and chemical-kinetic conditions.

The different modes for the onset of detonation as observed
by Urtiew and Oppenheim (1966) cannot be identified from the
present pressure records. One of the difficulties in
monitoring the onset of detonation is that this phenomena is
usually not planar. The pressure signal therefore depends

on the position of the localized explosions relative to the
pressure transducer position. The pressure records are
difficult to interpret in such detail because the pressure
records do not show the direction of motion of the pressure
waves.

The radar doppler signal does not give a complete picture of
the onset of detonation either. With regards to the details
of the onset mechanisms there are large uncertainties in
what the radar signal represents. This is mainly because
the reflecting reaction zone is three-dimensional, with a
spectrum of velocities along the tube direction. The
discussion of various modes must, therefore, be viewed as a
tentative interpretation of the onset of detonation.

The experiments with a 200-mm wide inert region and the same
acetylene-air mixture in the donor and acceptor sections
gave scatter in transition distance as shown in Figure
5.22. In the following the radar doppler recordings for
long and short transition distance will be discussed with
regard to the mode of onset of detonation.

Typical radar records for short transition distances are
shown in Figures 5.27 a) and 5.27 b), and for long
transition distances in Figures 5.28 a) and 5.28 b). For a
short transition distance, the transition appears to occur
due to an acceleration process. A shown in Figure
5.27 b)the velocity increases gradually up to about C-J
velocity in the period between 1900 and 2100 μsec. For
the long transition distance, the velocity from the radar
doppler measurements (Figure 5.28 b)) has a plateau at
about 1500 m/s before the velocity increases higher than the
C-J velocity. There is also a difference in amplitude of
the frequency signal for the two cases as shown in Figures
5.27 a) and 5.28 b). For the short transition distance,
when the velocity increases gradually, the amplitude is
relatively small. This indicates a local phenomena.

The signal from the re-initiated wave is irregular in
amplitude likely caused by an unstable wave. For the long
transition distance, the amplitude changes suddenly a the
same point as the velocity increases to 1500 m/s. This
strong amplitude signal suggests a more uniform planar
combustion zone.

Urtiew and Oppenheim (1966) showed that onset of detonation
can take place in different modes. This work is used as a
guide to explain the radar doppler signals. One of the
modes Urtiew and Oppenheim observed was onset of detonation
at contact discontinuity. Two shock waves coalesce and form
a contact discontinuity. The gas at the contact
dicontinuity goes through the induction process and forms a
planar reaction zone. The onset of detonation occurs in
this reaction zone. This mode has similarities with the
records from the case of long transition distance. The
velocity plateau at 1500 m/s is likely a planar reaction
zone caused by gasdynamical conditions. The other modes
Urtiew and Oppenheim observed, involves localized phenomena
in boundary layers. The same as seems to appear in the case
of short transition distance. This also indicates that wall
effects may be responsible for the reduced transition
distance.

5.4.7   Summary

These experiments have shown that detonation waves in
acetylene-air are able to re-initiate across inert regions
with widths of 100 to 200 mm. However, under similar
conditions ethylene-air failed to re-initiate. The C-J
properties in the donor section and the reactivity of the
gas in the acceptor section are the governing parameters for
the transition distance. The re-initiation process is very
sensitive to sharpness of the inert region. The evaluation
of the sharpness of the inert region under normal conditions
confirms that the experiments were carried out with a rather
well defined inert region. Enhanced mixing at the interface
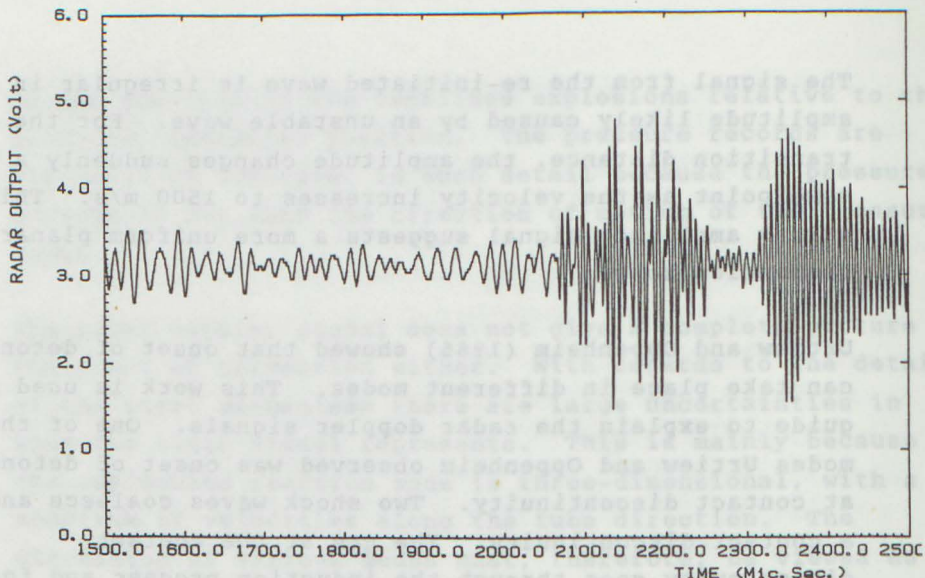
TEST NO. : 053 . DATE : 23-MAR-84
8.44%C2H2-AIR / AIR (.20 m) / 8.44%C2H2-AIR
IDF-SINTEF 15
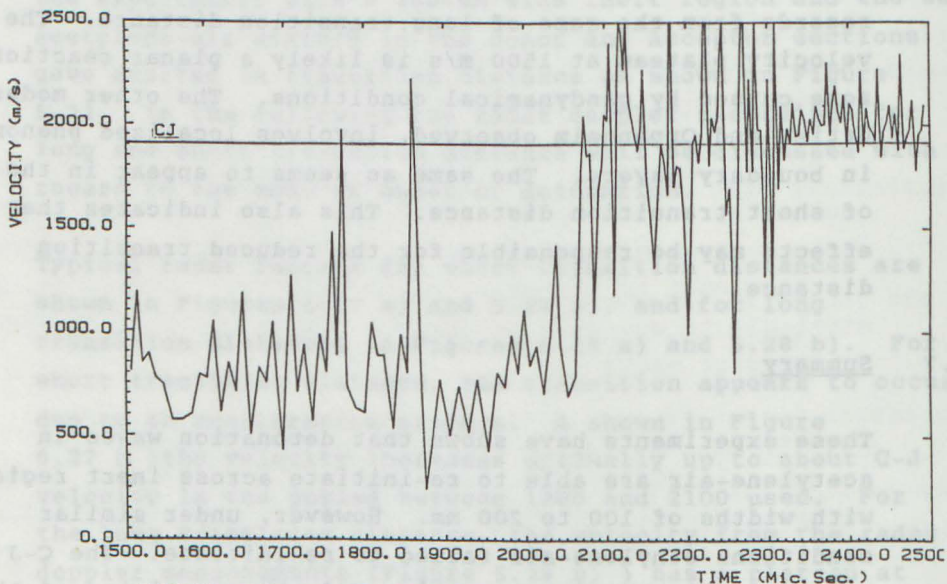
TEST NO. : 053 . DATE : 23-MAR-84
8.44%C2H2-AIR / AIR (.20 m) / 8.44%C2H2-AIR
IDF-SINTEF 15

Figure 5.29
Radar doppler measurement from a test classified as
short transition distance.
a) Radar doppler signal.
b) Velocity obtained from radar doppler signal.

TEST NO.:063   DATE :28-MAR-84
8.44%C2H2-AIR / AIR (.20 m) / 8.44%C2H2-AIR
IDF-SINTEF 15

TEST NO.:063   DATE :28-MAR-84
8.44%C2H2-AIR / AIR (.20 m) / 8.44%C2H2-AIR
IDF-SINTEF 15
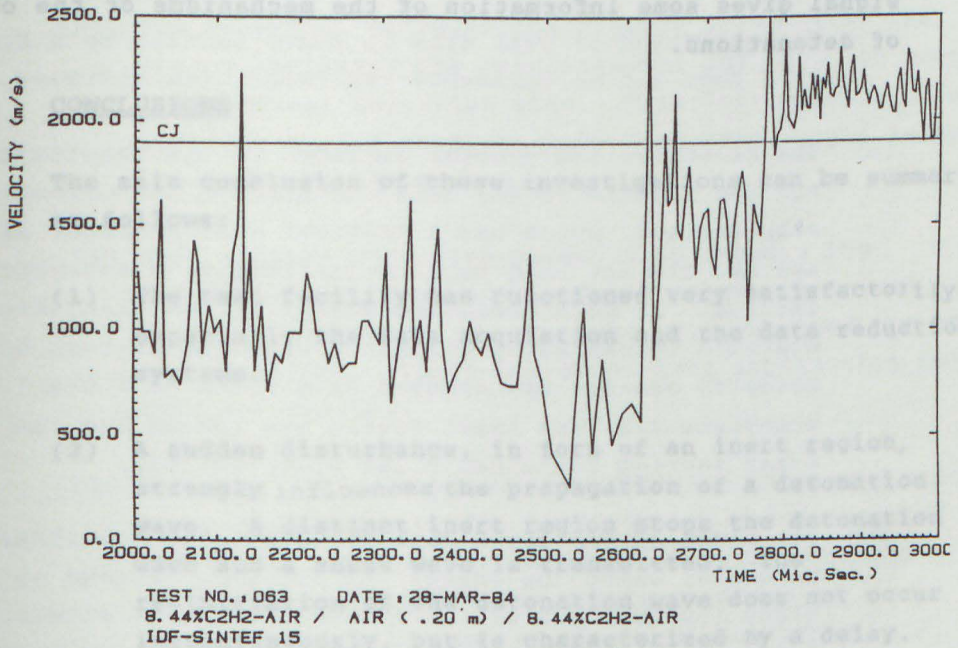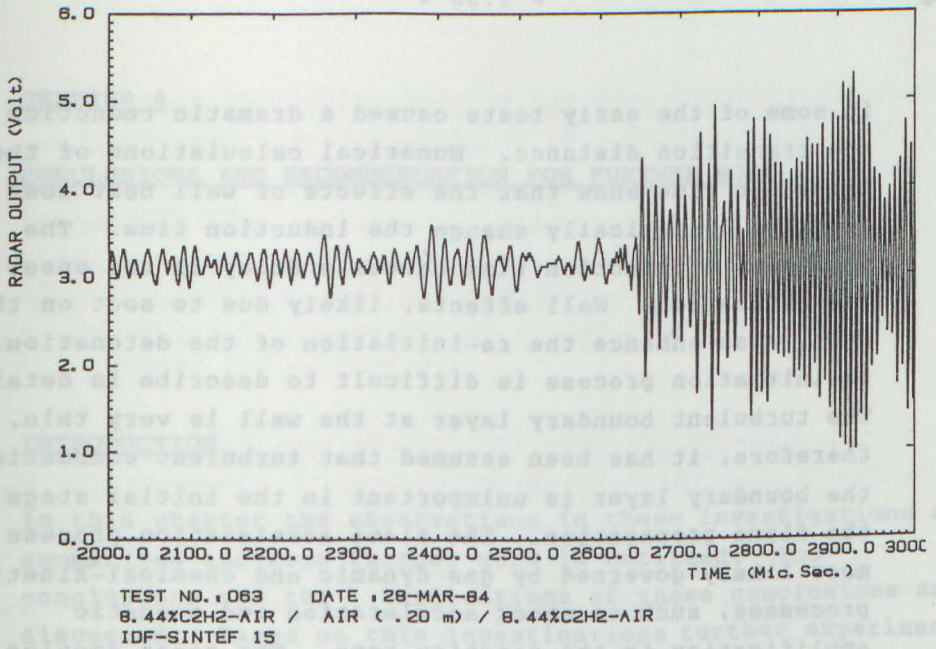
Figure 5.27
    Radar doppler records from a test classified as long
    transition distance.
    a) Radar doppler signal.
    b) Velocity obtained from the radar doppler signal.

in some of the early tests caused a dramatic reduction of the transition distance. Numerical calculations of the induction time show that the effects of wall heat loss and friction dramatically change the induction time. The increase in induction time causes a delay in the onset of the detonation. Wall effects, likely due to soot on the wall, also enhance the re-initiation of the detonation. The re-initiation process is difficult to describe in detail. The turbulent boundary layer at the wall is very thin, and therefore, it has been assumed that turbulent combustion in the boundary layer is unimportant in the initial stage of the flame propagation. The flame acceleration process is most likely governed by gas dynamic and chemical-kinetic processes, such as shock acceleration and acoustic amplification in the reaction zone. The radar doppler signal gives some information of the mechanisms of the onset of detonations.

CHAPTER 6

CONCLUSIONS AND RECOMMENDATION FOR FURTHER WORK

6.1 INTRODUCTION

In this chapter the observations in these investigations are summarized and some further work is outlined. The conclusions and the implications of these conclusions are discussed. Based on this investigations further experiments are proposed.

6.2 CONCLUSIONS

The main conclusion of these investigations can be summarized as follows:

(1) The test facility has functioned very satisfactorily, especially the data acquistion and the data reduction systems.

(2) A sudden disturbance, in form of an inert region, strongly influences the propagation of a detonation wave. A distinct inert region stops the detonation wave and a shock wave is transmitted. The re-initiation of the detonation wave does not occur instantaneously, but is characterized by a delay.

(3)   The re-initiation of detonations depends strongly on
       the experimental conditions. The conditions for
       re-initiation of detonation in the present apparatus
       have been established. With an inert air gap
       (0.1-0.2 m) re-initiation occured in acetylene-air
       (Φ = 0.9-1.2). Under similar conditions with
       ethylene-air (Φ = 0.8-1.0) the detonation wave failed
       to re-initiat.

(4)   The re-initiation process depends strongly on the C-J
       properties of the detonation in the donor section.
       When the acetylene concentration was increased from
       7.01% to 9.14% the transition distance decreased by
       about 1.0 meter when the inert section was 100 mm and
       the acceptor section contained 7.01% acetylene-air.

(5)   The variation of cell size in donor section by a factor
       of 4 does not to influence the transition distance.

(6)   The re-initiation process depended on the reactivity of
       the gas mixture in the acceptor section. Stoichiometric
       ethylene-air, which has a critical tube diameter of
       400 mm, did not lead to a re-initiation in acceptor
       section. In more sensitive mixtures, the transition
       distance increased by one meter when the mixture of the
       acceptor section was changed from 9.14% to 7.01%
       acetylene-air; the inert region was 100 mm and the
       donor section contained 9.14% acetylene-air.

(7)   The width of the inert section is also an experimental
       parameter which the transition distance depends on
       since the strength of the transmitted shock entering
       the acceptor section decreases with increasing width.
       For the same acetylene-air mixture (Φ = 0.9-1.2) in
       donor and acceptor sections, the transition distance
       increased by about 0.5 meter when the width of the inert
       region was increased from 100 mm to 150 mm.

(8)   The re-initiation process was very sensitive to the
      sharpness of the inert region. Enhanced mixing at the
      inert region boundary reduced the transition distance
      drastically.

(9)   The RCM-code have successfully been used to predict the
      non-isentropic expansion of the combustion products
      behind C-J detonations.

(10) The shock wave transmitted into the acceptor section is
      influenced by heat transfer and friction. Numerical
      calculations including heat transfer and friction to
      the wall are in good agreement with experimental
      observation of the trajectory and the flow field behind
      the transmitted shock wave.

(11) The numerical calculations clearly illustrated the
      strong influence the heat transfer and friction have on
      the chemical induction time. This influence, i.e. an
      increase in the chemical induction time, would delay
      the onset of detonation.

(12) Wall effects were also observed to enhance the
      re-initiation of detonations. Presence of smoked foils
      or presumably soot on the tube wall enhanced the onset
      of detonation. There are no obvious explanation for
      this observation.

(13) The fact that the transition distance increases with
      increasing width of the inert region and decreasing
      reactivity in acceptor section indicates that the
      re-initiation process was mainly governed by
      gasdynamical and chemical-kinetical processes.

6.3   IMPLICATIONS OF THE CONCLUSIONS

The experiments show that a distinct inert region is
effective in stopping a detonation wave in fuel-air
mixtures. The suggested method to stop a detonation in a
confined situation by using an artificial inert plug is in
principle an effective way of stopping a detonation wave.
However, there are obviously some practical difficulties of
creating a distinct inert region, specially in a ventilation
system where the gas is flowing. The reliability of such a
quenching device for detonation waves will depend on how
well a distinct inert region can be created since the
re-initiation process depends on sharpness of the inert
region.

It is very difficult to scale the present results to other
degrees of confinement and other gas mixtures since the
re-initiation process was influenced by the tube walls. The
different mechanisms that were involved in the re-initiation
process can either be enhanced or damped by wall effects.
The different mechanisms were not identified so it is
difficult to scale the results from the present test. To
obtain quantitative information of re-initiation of
detonation across an inert region for an unconfined
situation, larger scale experiments are needed.   By going
to a large scale the relative influence of wall effects will
be reduced.

The results indicate that even in an unconfined situation a
distinct inert region will rather efficiently stop the
propagation of a detonation wave. However, it is
unreasonable to use this as an argument for ruling out
detonation propagation through a real gas cloud. In a real
gas cloud a distinct inert zone as created in the present
experiments will likely not exist. The enhanced
re-initiation which was observed with a less distinct air
gap is probably more relevant for detonation propagation in
inhomogeneous clouds. To simulate such conditions,
experiments with detonation transmission across weak
fuel-air mixtures should be performed.

It is known that wall effects caused by geometrical
rregularities can enhance onset of detonation. The
observation in these tests that wall effects likely caused by
soot on the wall, can also influence the re-initiation of the
detonation wave, is of importance. In order to compare and
to scale experimental results from initiation of detonation
in various situations such effects have to be understood.

The observation is also of practical importance, especially
if the mechanism is related to non-reactive dust particles
such as the flame acceleration mechanism due to radiative
heating of dust clouds. In real gas explosions dust will be
present. The question is: Can the dust enhance the
initiation of detonation? If this is true, this is a very
important aspect of safety. Therefore it is important to
further ivestigate the enhanced re-initiation mechanism
caused by wall effects.

6.4   RECOMMENDATIONS FOR FURTHER WORK

This investigation has shown that the experimental
conditions were influenced by wall effects,and therefore,it
is difficult to scale to other conditions. In the further
work on re-initiation of detonation across an inert region
the effects of the walls should be minimized to simulate
unconfined situations. Therefore,experiments should be
performed on a larger scale than in the present
investigation. For a tube with a 600 mm diameter the
one-dimensional induction time calculations show only a
small effect of heat transfer and friction. The mixing
process at the interface have to be studied and
characterized as a part of the investigation. A 600 mm
diameter tube is a scale which practicaly can be handled.
Therefore,an experiment in a 600 mm tube seems to be a
reasonable scale for further experiments. Tests with both
shock transmission and detonation re-initiation should be
performed. The shock transmission results could be used to
test out the RCM-code

when the wall effects are small. Re-initiation of detonation
experiments in a larger scale will give more quantitative
information of the capability of detonation waves to
transfer across an inert region. Comparison with the
present results will give some indications of what influence
the wall effects can have on the re-initiation process.

To improve operation of the present test facility a
graphical terminal for displaying the records should be
incooperated. With the present system plotting of the
results is time consuming. Use of a graphical system could
reduce this time drastically.

To get a more detailed picture of the re-initiation process
other diagnostics should be used. A photographical
investigation is probably the only way to get detailed
information of the re-initiation process such that the dominant
mechanisms involved in the acceleration process, can be
identified. With high speed film of 40 000 frames pr. sec.
the propagation of the reaction zone can be observed. The
combination of such photographic observation with pressure
and radar doppler signals will give more information on the
re-initiation process.

The tests with enhanced mixing at the inert region boundary
showed that the re-initiation process depended on the fuel
gradient at or in the inert region. Tests where the inert
region is replaced by a region containing weak fuel-air
mixtures are of interest to establish what concentration
level will support re-initiation of detonation. The effects
of variation of the fuel concentration are important in a
real gas cloud.

The observation that wall effects enhanced the re-initiation
process, should be investigated further. Tests where
non-reactive dust is placed in the acceptor section, should be
performed to see if radiative heating of the dust can
enhance the re-initiation.

The resolution of the RCM calculations should be increased. The experimental results show that small variations in the shock strength entering the acceptor section result in large variations in the transition distance. An increase of the resolution of the calculations would give more quantitative information of the change in gas-dynamical conditions.

6.5   END STATEMENT

This investigation has demonstrated the complexity of re-initiation of detonation across an inert region. The re-initiation process was strongly influenced by the experimental conditions. A complete understanding of the re-initiation process has not yet been established and further work is needed. The success of further experimental work will depend critically on how well the experimental conditions can be characterized and varied independently.

LIST OF REFERENCES

Bazhenova, T.V., Fokeev, V.P., Lobastov, Yu., Brossard, J.,
Bonnet, T., Brion, B. and Charpentier, N.: "Influence of
the Nature of Confinement on Gaseous Detonation". AIAA
Progress in Astronautics and Aeronatics (edited by
Bowen, Manson, Oppenheim and Soloukhin), Vol. 75, pp.
87-107, AIAA, New York.

Bjerketvedt, D. and Sonju, O.K. (1983): "Detonation
Transmission Across an Inert Region". SINTEF Report:
STF 15 A83043, Trondheim, Norway.

Bjerketvedt, D. (1985): "Programmer for high speed data-
logger - Detonasjonsforsøk" SINTEF notat, Trondheim,
Norway. (In preparation)

Bollinger, L.E., Fong, M.C. and Edse, R. (1961):
"Experimental Measurements and Theoretical Analysis of
Detonation Induction Distances". ARS Journal 31, No. 5,
p. 588.

Bone, W.A., Fraser, R.P. and Wheeler, W.H. (1935):
"A photographic Investigation of Flame Movements in
Gaseous Explosions - Part VII - The Phenomen of Spin in
Detonation". Phil. Trans., A, 235, 29-68.

Boris, J.P. (1976): "Flux-corrected transport modules for
solving generalized continuity equations". Naval
Research Laboratory Memorandum Report No. 3237.

Borisov, A.A. (1980), Private communication, Institute of
Chemical Physics, USSR Academy of Sciences, Moscow

Bull, D.C., Elsworth, J.E., and Hooper, G. (1979)
Combustion and Flame 35, 27-40.

Bull, D.C., Elsworth, J.E. and McLeod, M.A. (1981):
"Initiation of Unconfined Gas Detonation in
Hydrocarbon-Air Mixture by a Sympathetic Mechanism".
Gasdynamics of Detonation and Explosions: AIAA Progress
in Astronautics and Aeronatics (edited by Bowen, Manson,
Oppenheim and Soloukhin), Vol. 75, pp. 61-72, AIAA, New
York.

Bull, D.C., Elsworth, J.E., Shuff, P.J. and Metcalfe, E
(1982) "Detonation Cell Structures in Fuel/Air
Mixtures", Combustion and Flame 45, 7-22.

Bull, D.C., (1982) "Gas Phase Detonation"
Proceedings of the International Conference on Fuel-Air
Explosions held at McGill University, Montreal, Canada
Editors: J.H.S.Lee and C.M.Guirao. University of
Waterloo Press.

Chorin, A.J. (1976): "Random choice solution of hyperbolic
system". J. Comp. Phys., Vol. 22, p. 517.

Courant, R. and Friedrichs, K.O. (1948): "Supersonic Flow and
Shock Waves, pp. 103 and 181, Intersience Publishers,
Inc., New York.

Desbordes, D., Manson, N. and Brossard, J. (1981): "Pressure
Evolution behind spherical and Hemispherical Detonations
in Gases". Gasdynamics of Detonations and Explosions:
AIAA Progress in Astronautics and Aeronatics (edited by
Bowen, Manson, Oppenheim and Soloukhin), Vol. 75, pp.
150-165, AIAA, New York.

Eckert, E.R.G. and Drake, R.M. (1972): "Analysis of Heat and
Mass Transfer". McGraw-Hill, Kogakusha, Tokyo.

Edwards, D.H., Williams,.G.T. and Breeze, J.C.(1959)
"Pressure and velocity measurements on detonation waves
in hydrogen-oxygen mixtures." J. fluid Mech. 6 p 497.

Edwards, D.H., Brown, D.R., Hooper, G. and Jones, A.T.
(1970): "The Influence of Wall Heat Transfer on the
Expansion Following a C-J Detonation". J. Phys. Fluids 2
(3), 283-289.

Edwards, D.H., Jones, A.T. and Phillips, D.E. (1976):
"The location of the Chapman-Jouguet Surface in a
Multiheaded Detonation Wave". Journal of Physics D:
Applied Physics 9, 1331.

Edwards, D.H., Thomas, G.O. and Williams (1981): "Initiation
of Detonation by Steady, Planar Incident Shock Wave".
Combustion and Flame 43, 187-198.

Edwards, D.H. (1982): "The Behaviour of Detonation Waves in
Single Phase Heterogenious Systems". Abstracts from 1982
AFOSF Contractors meeting on air breathing Combstion
Dynamics Reseach at University of Southern California.

Edwards, D.H., Thomas, G.O. and Sutton, G. (1983):
"The Behavior of Detonation Waves at Concentration
Gradients". Presented at the 9th ICODERS, Poitier,
France, July 1983.

Elsworth, J.E., Haskell, W.W., and Read, I.A. (1969)
Combustion and Flame 13, 477.

Fay, J.A. (1959): "Two-dimensional detonations: Velocity
deficits". Phys. Fluids 2, 283-289.

Fickett, W. and Davis, W.C. (1978): "Detonation", pp. 21 and
59, University of California Press, Berkeley, California.

Fujiwara, J. and Hasegawa, T. (1981): "Oxyhydrogen Detonations under Surface Catalysts". Gasdynamics of Detonation and Explosions: AIAA Progress in Astronautics and Aeronatics (edited by Bowen, Manson, Oppenheim and Soloukhin), Vol. 75, pp. 61-72, AIAA, New York.

Gavrilenko, T.P., Grigorev V.V., Zndan, S.A., Nikolaev,Yu.A., and Fedenok, V.I.(1982):"Exitation by a gas detonation of shock waves in tubes." Fizika Goreniya i Vzryva, 18, No. 1, 89-94.

Gavrilenko, T.P., Krasnov, A.N. and Nikolaev, Yu.A. (1982b): "Transfer of a Gas Detonation Through an Inert Gas Plug". Fizika Goreniya i Vzryva, 18, No. 2, 127-131.

Greatrix, D.R. and Gottlieb, J.J. (1983):, "An Analytical and Numerical Study of a Shock Wave Ineraction With an Area Change". UTIAS Report No.268. University of Toronto, Canada.

Geiger, W. (1983):, private communication ,Battelle Institue e.v., Frankfurt,West Germany,.

Glimm, J. (1965): "Solution in the large for nonlinear hyperbolic systems for equations". Comm. Pure Appl. Math., Vol. 18, p. 697.

Gooderum, P.B. (1958): "An experimental study of the turbulent boundary layer on a shock-tube wall." NACA tech. Note 4243.

Gordon, S. and McBride, B. (1976): Computer program for calculation of complex chemical equililbrium compositions, rocket performance, incident and reflected shocks and Chapman-Jouguet detonations, NASA SP-273.

Gottlieb, J.J. (1983), private communication, UTIAS, University of Toronto, Canada.

Hiramatsu, K. Fujiwara, T. and Taki, S. (1984):
"A Computational Study of Transmission of Gaseous
Detonation to Unconfined Space", presented at 20th
International Symposium on Combustion, Ann Arbor,
Michigan, Aug. 12-17, 1984.

Jenssen, A. (1985), private communication. Norwegian Defence
Construction Service (FBT), Oslo, Norway.

Kays, W.M. and Crawford, M.E. (1980): "Convective Heat and
Mass Transfer. McGraw-Hill, New York.

Knystautas, R., Lee, J.H. and Guirao, C.M. (1982):
"The critical tube diameter for detonation failure in
hydrocarbon-air mixtures". Combustion and Flame 48,
63-83.

Knystautas, R., Guirao, C., Lee, J.H. and Sulmistras, A.
(1984): "Measurements of Cell Size in Hydrocarbon-Air
Mixtures and Predictions of Critical Tube Diameter,
Critical Initiation Energry and Detonability Limits".
Dynamics of Shock Waves, Explosions and Detonations:
AIAA Progress in Astronautics and Aeronatics (edited by
Bowen, Manson, Oppenheim and Soloukhin), Vol. 94, pp.
23-37, AIAA, New York.

Langseth, J.H. (1980): "Har vi lært noe av Flixborough 1974?
Gasseksplosjoner forsatt den store fare". Teknisk
Ukeblad/Teknikk nr. 11.

Libouton, J.C., Dormal, M. and Van Tiggelen, P.J. (1981):
"Reinitiation process at the end of the detonation
cell". Gasdynamcs of Detonations and Explosions: AIAA
Progress Astronautics and Aeronautics (edited by Bowen,
Manson, Oppenhiem and Soloukhin), Vol. 75, pp. 358-369,
AIAA, New York.

Lean, B. and Dixon, H.B. (1892): "Experiments on the Transmission of Explosions Across Air Gaps". Manchester Memoirs, 16. Mem. Manch. Let. Phil. Soc., 4, 4th Series, 16-22.

Lee, J.H., Guiaro, C.M., Chiu, K.W. and Bach, G.G. (1977): "Blast Effects from Vapor Cloud Explosions", 1977 AIChE, Loss Prevention Symposium, Houston, Texas.

Lee, J.H.S., Knystautas, R. and Yoshikawa (1978): "Photochemical initiation of gaseous detonations", Acta Astronautica, 5 : (971-982)

Lee, J.H.S. and Moen, I.O. (1980): "The Mechanism of Transition from Deflagration to Detonation on Vapour Cloud Explosions". Progress in Energy and Combustion Science, 6, 4, 349-389.

Lee, J.H.S. (1982): "Phenomenology of Gas Exploisions". Norwegian Defence Construction Service (FBT) Course Norsjø Norway.

Lee, J.H.S. (1984): "Dynamic Parameters of Gaseous Detonations". Ann. Rev. Fluid Mech., 16, pp. 311-336.

Mathisen, G (1983), private communication. Micro-Mathisen Trondheim, Norway.

Matsui, H.and Lee, J.H (1978) "On the Measure of Relative Detonation Hazards of Gaseous Fuel-Oxygen and Air Mixtures", 17th Symposium (International) on Combustions, pp. 1269-1279, The Combustion Institute, Pittsburgh, Pa.

Meyer, J.W., Urtiew, P.A. and Oppenheim, A.K. (1970): "On the inadequacy of gasdynamic process for triggering the transition to detonation". Combustion and Flame, 14, pp. 13-20.

Mirels, H. (1957): "The wall boundary layer behind a moving shock wave". Boundary Layer Research, edited by H. Görtler, Freiburd/Br. Symposium, Aug. 26-29, 1957, pp. 283-293.

Mitrofanov, V.V. and Soloukhin, R.I. (1965): "The Diffraction of Multifront Detonation Waves". Soviet Physics-Doklady 9, 1055.

Moen, I.O., Donato, M., Knystautas, R. and Lee, J.H. (1981): "The Influence of Confinement on the Propagation of Detonations Near the Detonability Limits". 18th Symposium (International) on Combustion, pp. 1616-1622, The Combustion Institute, Pittsburgh, Pa.

Moen, I.O., Murray, S.B., Bjerketvedt, D., Rinnan, A., Knystautas, R. and Lee, J.H. (1982): "Diffraction of detonation from tubes into a large fuel-air explosive cloud". 19th Symposium (International) on Combustion, pp. 635-644, The Combustion Institute, Pittsburgh, Pa.

Moen, I.O. (1985), private communication. Defence Research Establishment Suffield, Ralston, Alberta, Canada.

Moen, I.O., Funk, J.W., Ward, S.A., Rude, G.M. and Thibault, P.A. (1984): "Detonation length scales for fuel-air explosives". Dynamics of Shock Waves, Explosions and Detonations: AIAA Progress in Astronautics and Aeronatics (edited by Bowen, Manson, Oppenheim and Soloukhin), Vol. 94, pp. 55-79, AIAA, New York.

Moen, I.O., Sulmistras, A., Thomas, G.O., Bjerketvedt, D. and Thibault, P.A. (1985): "The Influence of Cellular Regularity on the Behavior of Gaseous Detonations", for presentation at the 10th International Colloquium on Dynamics of Explosions and Reactive Systems, Berkeley, California, Aug. 4-9.

Moen, I.O., Bjerketvedt, D., Jenssen, A. and Thibault, P.A.: "(1985b) Transition to Detonation in a Large Fuel-Air Cloud". Submitted to Combustion and Flame as a Short Communication.

Murray, S.B. (1985): "The Influence of Initial and Boundary Conditions on Gaseous Detonation Waves". Ph.D. Thesis, Mechanical Engineering Department, McGill University, Montreal, Canada.

Paillard, C., Dupré, G., Lisbet, R., Combourieu, J., Fokeev, V.P. and Gvozdeva, L.G. (1979): "Study of hydrogen azide detonation and heat transfer behind the wave in narrow tubes". Acta Astronautica 6 (3-4), 227-242.

Paillard, C., Dupre, G., Lisbet, R., Combuoriew, J., Fokeev, V.P., Gvozdeva, L.G. and Bazhenova, T.V. (1981): "Pressure and Wall Heat Transfer behind a Hydrogen/Azide Detonation Wave in Narrow Tubes". Gasdynamics of Detonations and Explosions: AIAA Progress in Astronautics and Aeronautics (edited by Bowen, Manson, Oppenheim and Soloukhin), Vol. 75, pp. 134-149, AIAA, New York.

Paterson, S. (1953): "Contact Transmission of Detonation". Proceedings of the Fourth Symposium (International) on Combustion, p. 468, The Williams and Wilkings Company, Baltimore.

Pförtner, H., Schneider, H., Drenchan, W. and Koch, C.: "Flame Acceleration and Pressure Built-up in Free and Partial Confined Hydrogen-Air Clouds". Dynamics of shock Waves, Explosions and Detonations: AIAA Progress in Astronautics and Aeronautics (edited by Bowen, Manson, Oppenheim and Soloukhim), Vol. 94, pp. 55-79, AIAA, New York.

Raufoss (1982, 1983 and 1984) see Jenssen (1985)

Saito, T. and Glass, I.I. (1979): "Application of Random-Choice Method to Problems in Shock and Detonation Wave Dynamics". UTIAS Report No. 240, University of Toronto.

Schlichting, H. (1978): "Boundary Layer Theory", 7th Ed. McGraw-Hill, New York.

Shapiro, A.H. (1954): "The Dynamics and Thermodynamics of Compressible Fluid Flow". Vol. II, The Ronald Press Company, New York.

Sichel, M. and David, T.S. (1966): "Heat Transfer behind Detonations in H_2-O_2 mixtures". AIAA, J. 4 (6), 1089-1090.

Smith, G.D. (1978): "Numerical solution of Partial Differential Equations: Finite Difference Methods". Clarendon Press, Oxford.

Sod, G.A. (1977): "A survey of several finite difference methods for systems of non linear hyperbolic conservation laws". J. Comp. Phys., Vol. 83, p. 232.

Strehlow, R.A. (1969): "The nature of transverse waves in detonations". Astronaut. Acta 14, 539-548.

Strehlow, R.A., Adamczyk, A.A. and Stiles, R.J. (1972): "Transient Studies of Detonation Waves". Astro. Acta. 17, 509-527.

Strehlow, R.A. (1980), University of Illinois, Urbana, USA, private communication.

Strehlow, R.A. (1984), Combustion Fundamentals, McGraw - Hill Book Company, New York.

Taylor, G.I. (1950): "The dynamics of the combustion products
    behind plane and spherical detonation fronts in
    explosives". Proc. R. Soc. A, 200, 235-247.

Taylor, G.I. (1950b): "The Formation of a Blast Wave by a
    Very Intense Explosion, I. Theoretical Discussion".
    Proc. Roy. Soc., London, (A), 201, 159.

Thibault, P.A. (1983), private communication.
    Combustion Dynamics Limited, Ralston, Alberta, Canada.

Ungut, A., Shuff, P.J. and Eyre, J.A. (1984): "Initiation of
    unconfined gaseous detonation by diffraction of a
    detonation front emerging from a pipe". Dynamics of
    Shock Waves, Explosions and Detonations: AIAA Progress
    in Astronautics and Aeronautics (edited by Bowen,
    Manson, Oppenheim and Soloukhin), Vol. 94, pp. 523-545,
    AIAA, New York.

Urtiew, P.A. and Oppenheim, A.K. (1966): "Experimental
    Observations of the Transition to Detonation in an
    Explosive Gas". Proc. Roy. Soc. A 295, 13-28.

Urtiew, P. and Oppenheim, A.K. (1967): "Detonation ignition
    induced by shock merging". Eleventh Syposium
    (International) on Combustion, The Combustion Institute,
    Pittsburgh.

Vasiliev, A.A., Gavrilenko, T.P. and Topchian, M.E. (1972):
    "On the Chapman-Jouguet Surface in Multi-headed Gaseous
    Detonations". Astronautica Acta 17, 499.

Westbrook, C.K. and Urtiew, P.A. (1984): "Use of Chemical
    Kinetics to Predical Parameters of Gaseous Detonation".
    Fizika Goreniya i Vzryva 19 (6).

Wilson, W. (1980), private communication, Science
    Applications, Inc., La Jolla, Ca.

Zeldovich, Ya.B. (1940): "On the Theory of the Propagation of
Detonation in Gaseous Systems". Translation: NACA TM
1261, Nov. 1950.

Zeldovich, Ya.B. and Kompaneets, A.S. (1960): "Theory of
Detonation". New York and London: Academic Press.

APPENDICIES

A : Nomenclature
B : Riemann Problem.
C : Mixing at the Inert Region Boundary.
D : Wave Interaction with the Interfaces.
E : Use of Data Reduction Programes
F : List of Experimental Results.

- A.1 -

APPENDIX A

NOMENCLATURE

Letters

A_x [m^2]   Flow area.

C_+ [m/s]   Right running characteristics, $C_+ = u + c$

C_- [m/s]   Left running characteristics, $C_- = u - c$

C_f [-]   Friction factor

$$C_f = \frac{\tau_w}{\frac{1}{2}\rho u^2}$$

C_p [J/kg K]   The specific heat at constant pressure

c_{tail} Speed of sound at the end of rarefaction wave

c_v [J/kgK]   The specific heat at constant volume

c [m/s]   Speed of sound

c_{CJ} [m/s]   C-J speed of sound

D_{CJ} [m/s]   Chapman-Jouguet detonation velocity

D [m/s]   Detonation velocity

dA [m^2]   Surface area.

d_c [m]   Critical tube diameter

e [J/m^3]   Energy per unit volum

F Matrix

$$F = F(G) = \begin{bmatrix} \rho u \\ \rho u^2 + p \\ (e+p)u \end{bmatrix}$$

[F/A]   Fuel-air ratio

f [sec^{-1}]   Frequency of radar doppler signal

G		Matrix

$$G = \begin{bmatrix} \rho \\ \rho u \\ e \end{bmatrix}$$

g_i^n	Defined by Eqs. 3.14 and 3.15
h [J/m²K]	The heat transfer coefficient
i [-]	Integer
j [-]	Integer
L_c [m]	Cell length
L [m/s]	Invariant, $L = 2r$
n_r [-]	The number of times the radar doppler signal crosses the zero line
n [-]	Integer
$[O_2]$ [moles/liter]	Molar concentration of oxygen
Pr [-]	Prandtl number
p_{CJ} [bar] or [Pa]	C-J pressure
p_{tail}	Pressure at the end of rarefaction wave
p [bar] or [Pa]	Pressure
Q [kJ/kg]	Heat of reaction
$\dot{q}''$ [W/m²]	The heat transfer rate to the wall
Re [-]	Reynolds number
r [m/s]	Riemann invariant
	$r = \dfrac{u}{2} - \dfrac{c}{\gamma - 1}$
s [J/kg K]	Entropi
S [m]	Cell size
T [K]	Gas temperature
T_r [K]	Recovery temperature

T_w [K]   Wall temperature

t [s]   Time from origin of detonation

t_s [s]   Shock passage time

U_p [m/s]   Piston velocity

U_s [m/s]   Shock wave velocity

u [m/s]   Gas velocity relative to laboratory frame

u_{CJ} [m/s]   C-J gas velocity

V   Solution of the Riemann problem

V_r [m/s]   Velocity reduced from the radar doppler signal

$$V_r = \frac{2 (f/2)}{70.2(Hz/m/s)}$$

W   Matrix

$$W = \frac{dA}{A_x dx} \begin{bmatrix} 0 \\ \tau_w \\ \dot{q} \end{bmatrix}$$

w [m]   Internal dimension of square channel in experimental apparatous, w = 125 mm

X_r [m]   Distance reduces from the radar doppler signal

$$X_r = \frac{2(n_r-1)}{70.2}$$

$\bar{x}$ [-]   Dimensionless distance

$$\bar{x} = x/x_D$$

x [m]   Distance

x_D [m]   Position of detonation wave

x_s [m]   Distance downstream from the shock front

$\bar{y}$ Average value of sampling values

$$\bar{y} = \frac{\sum\limits_{i=j}^{j+n-1} y_i}{n}$$

y_i Sampling value at sampling point i

Greek letters

ε [mm]	Wall roughness
γ [-]	The ratio of the specific heats
Δ [m]	Induction length
Δx [m]	Length increment
Δt [s]	Time increment
δ [mm]	Boundary layer thickness
μ_s [kgm^2/s]	Viscosity behind shock front
ξ [-]	Random number on the interval [0,1]
ρ [kg/m^3]	Density
ρ_{CJ} [kg/m^3]	C-J density
ρ_o [kg/m^3]	Initial dencity
τ [s]	Induction time
τ_w [N/m^2]	Friction at the wall
ϕ [-]	Equivalence ratio

$$\phi = \frac{[F/A]_\phi}{[F/A]_{\phi=1}}$$

Where [F/A] is the fuel-air ratio.

ψ [-]   Induction time parameter

$$\psi = \int_{t_S}^{t} \frac{dt}{\tau}$$

Ref.: Strehlow, 1984.

Subscripts

CJ	Chapman-Jouguet condition
o	Intial condition
w	Condition at wall
$-$	Average value
*	Solution of Riemann problem
tail	End of rarefaction wave

APPENDIX B

RIEMANN PROBLEM

The purpose of this appendix is to give a description of Riemann problem and its solution. The solution of the Riemann problem is used both in the model by Paterson (1959) for refraction of detonation waves on an inert gas interface, and in the numerical calculations in the RCM code.

The Riemann problem is discussed in detail in the book by Courant and Friedrics (1948).

The Riemann problem is to solve the gasdynamics equation for the following boundary conditions at time t = 0.

$$\left.\begin{array}{c} u_1 \\ p_1 \\ \rho_1 \end{array}\right\} \quad x < 0$$

$$\left.\begin{array}{c} u_0 \\ p_0 \\ \rho_0 \end{array}\right\} \quad x > 0$$

$$\begin{array}{c|c} u_1 & u_0 \\ p_1 & p_0 \\ \rho_1 & \rho_0 \end{array}$$

$$x = 0$$

Figure B 1 :
   Initial condition for a Riemann Problem.

The two states are independent.

To ananlyze this problem it is convenient to use a
p-u diagram. Possible states which can be reached from
state u_0, p_0 and ρ_0, when the gas either is
compressed by a shock wave or expanded by a rarefraction
wave is shown in figure B.2. The arrow gives the direction
of the wave. S stands for shock wave and R for rarefaction
wave. A shock wave S will increase the pressure. A
rarefaction wave R will decrease the pressure. The change
in gas velocity depends on wave direction. A shock wave
will increase the gas velocity in the same direction as wave
propagates. For the rarefaction wave the increase velocity
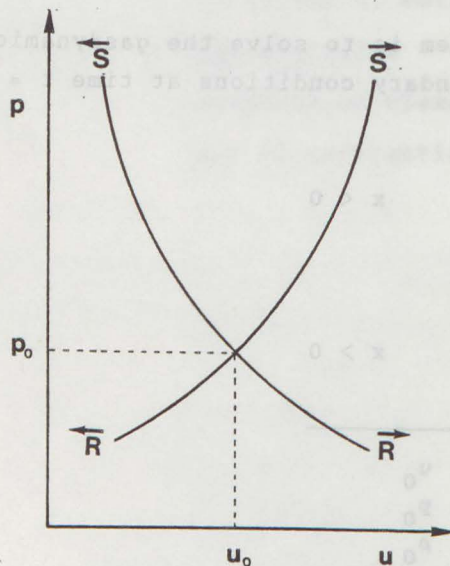will be in the opposit direction of wave propagation.

Figure B 2 :
    p-u diagram showing the possible states which can be
    reached from state 0 when the gas is compressed by a
    shock S or a rarefaction wave R. The arrows indicates
    the wave direction.

The possible solutions is divided into four regions depending on type and direction of the wave. The analytical solution is for right running wave:

$$\vec{S} : u = u_0 + \Phi_0 (p) \qquad\qquad p > p_0 \qquad\qquad \text{(shock wave)}$$

$$\vec{R} : u = u_0 + \psi_0 (p) \qquad\qquad p < p_0 \qquad\qquad \text{(rarefaction wave)}$$

Left running wave:

$$\overleftarrow{S} : u = u_0 - \Phi_0 (p) \qquad\qquad p > p_0 \qquad\qquad \text{(shock wave)}$$

$$\overleftarrow{R} : u = u_0 - \psi_0 (p) \qquad\qquad p < p_0 \qquad\qquad \text{(rarefaction wave)}$$

where

$$\Phi_0(p) = (p-p_0) \sqrt{\frac{1-\gamma^2}{(p+\gamma^2 p_0)\rho}}$$

$$\psi_0(p) = \frac{1-\gamma^4}{\gamma^2} \cdot \rho_0^{-\frac{1}{2}} \cdot p_0^{\gamma/2} \left(p^{(\gamma-1)/2\gamma} - p_0^{(\gamma-1)/2\gamma}\right)$$

The Riemann problem in figure B.1 have state (0) right of the interface and state (1) left of the interface. From the interface a right running wave will propagate into state (1) and a left running wave will propagate into state (0). The type of wave depends on the intial conditions and the properties of the gases.

To satisfy continuity the pressure and the gas velocity have to be equal for both states after being crossed by their respective waves. Here the solution for this pressure and this velocity are marked p* and u*. In a p-u diagram the solutions for p* and u* are found at the interception of curves for right and left running waves.

When the value for p* and u* is known the velocities of the shock waves, heads and tails of rarefaction waves and the contact surface (i.e. gas velocities) can be predicted, which means that the total flow field can be predicted.

To illustrate such a solution the shock tube problem will be discussed. The shock tube is a very common experimental arrangement for studying shock waves. Initially a shock tube is a long tube which is divided into two sections, a high pressure section with pressure p_1, and a low pressure section with pressure p_0. The two sections are divided by a diaphragm. The gas in both sections are at rest (i.e. $u_1 = u_0 = 0$). At time equal zero (t = 0) the diaphragm rupture and a right running shock wave propagates into the low pressure section, and a left running rarefaction wave propagates into the high pressure section. The solution of this flow field can be solved as a Riemann problem. The solutions for p* and u* are shown on Figure B.3.

Figure B 3 :
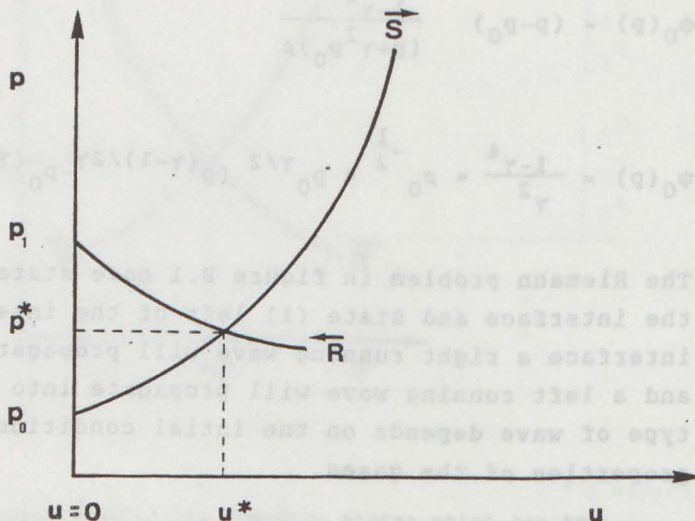   p-u diagram showing the solution of a shock tube
    problem.

The solution for shock wave rarefaction wave and contact surface trajectories are illustrated in a time-distance diagram in Figure B.4. The pressure profile at time t, is shown in Figure B.5.
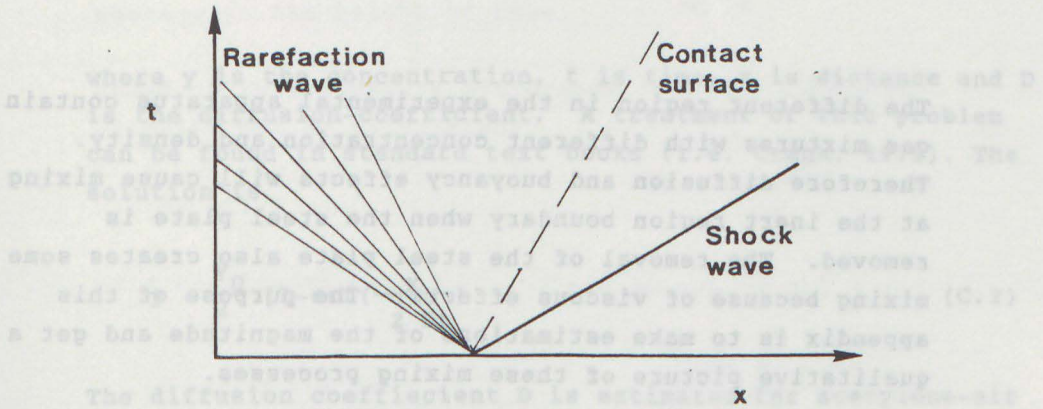
Figure B 4 :
Time-distance diagram showing the wave trajectory for a shock tube problem.
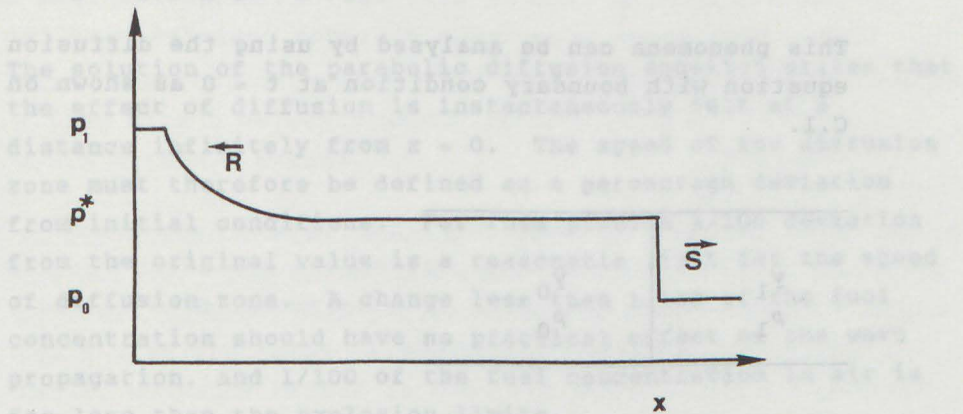
Figure B 5 :
Pressure profile for a shock tube problem.

APPENDIX C

MIXING AT THE INERT REGION BOUNDARY.

The different region in the experimental apparatus contain gas mixtures with different concentration and density. Therefore diffusion and buoyancy effects will cause mixing at the inert region boundary when the steel plate is removed. The removal of the steel plate also creates some mixing because of viscous effects. The purpose of this appendix is to make estimations of the magnitude and get a qualitative picture of these mixing processes.

Different pressure level in the sections will also destroy a one-dimensional interface.

Diffusion

This phenomena can be analysed by using the diffusion equation with boundary condition at t = 0 as shown on Figure C.1.

Y_1
ρ_1 Y_0
                            ρ_0

− ∞   0   + ∞
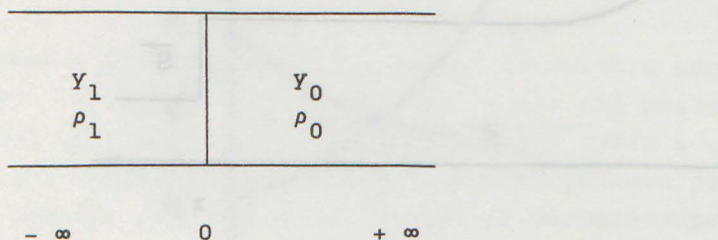
Figure C 1 :
    Initial condition at an idealized inert region boundary.

Diffusion equation:

$$\frac{\delta y}{\delta t} = D \frac{\delta^2 y}{\delta x^2} \qquad\qquad (C.1)$$

where y is the concentration, t is time, x is distance and D is the diffusion-coefficient. A treatment of this problem can be found in standard text books (i.e. Crank, 1975). The solution is

$$y = \frac{y_0}{2} \left[1 - erf\left(\frac{x}{2\ Dt}\right) \right] \qquad\qquad (C.2)$$

The diffusion coeffiecient D is estimated for acetylene-air by using the method described by Treybal (1980). For $p = 1$ bar and $t = 18$ °C the diffusion coefficient, D, is estimated to

$$D = 1.8 \times 10^5 \ m^2/s$$

The solution of the parabolic diffusion equation states that the effect of diffusion is instantaneously felt at a distance infinitely from $x = 0$. The speed of the diffusion zone must therefore be defined as a percentage deviation from initial conditions. For this problem 1/100 deviation from the original value is a reasonable limit for the speed of diffusion zone. A change less then 1/100 of the fuel concentration should have no practical effect on the wave propagation, and 1/100 of the fuel concentration in air is far less than the explosion limits.

Thickness of diffusion wave:

$$x = x_1 + |x_2| = 2\ |x_2|$$
$$y(x_1,t) = 0.01\ y_0 \qquad x > 0$$
$$y(x_2,t) = 0.99\ y_0 \qquad x < 0$$

Using the solution of the diffusion equation:

$$- erf \left(\frac{x_2}{2 \sqrt{Dt}} \right) = 0.98 \qquad (C.3)$$

From erf-table:

$$- \frac{x_2}{2 \sqrt{Dt}} = 1.65 \qquad (C.4)$$

For t = 0.25 sec we get

$$\Delta x = 14 \text{ mm}$$

For ethylene-air/air system the spread of the diffusion zone will be less because the diffusion coefficient for ethylene is smaller than for acetylene.

For a diffusion time of 0.25 sec the diffusion zone is 14 mm. This is an acceptable distance compared with the thickness of the inert region.

Buoyancy

Even though there are only small density differences across the interface, buoyancy will create a flow in the two gas mixtures. The following is a rough estimate of the flow velocity caused by buoyancy.

Assume the situation is as shown on figure C.1. Different fuel concentration gives different densities for x < 0 and x > 0 close to time t = 0 there is no flow in system, but the density difference implies a pressure difference across the interface. If one assume that there are no pressure difference at the center line, the average pressure

difference between the center line and the walls are:

$$\Delta p = g(w/4) \cdot (\rho_1 - \rho_0)$$

where w is the height of tube.

Based on this pressure difference Δp a corresponding velocity can be calculated:

$$\Delta p = 1/2 \; \rho \; u^2$$

As a result one gets:

$$u = \sqrt{g \cdot w \left(1 - \frac{\rho_0}{\rho_1}\right)}$$

For stoichiometric acetylene-air and air the density ratio is 1.008 and this gives an estimate flow velocity of:

$$u = 0.07 \; m/s$$

This rough estimate show that the density difference creates a flow with a velocity which destroy an inert region of 0.1 m within a second.

In the actual system inertia and viscous effects will resist the motion. The velocity caused by buoyancy will therefore be small in the first period of the mixing process. In the tests with the model of the valves, which will be decribed later, bouyancy effect is observed after about 1.0 sec but not at 0.25 sec.

For a time of 0.25 sec the movement, caused by bouyancy, of the interface should be less than 15 mm.

Viscous effects

The friction between gas and the moving steel plate will set
the gas in motion and create mixing between the different
regions. To obtain a qualitative picture of the mixing
process caused by viscous effects a model of the valve was
built. The model consisted of a transparent channel made of
plexiglas and one of steel plates with the phneumatical
cylinder from a slide valve. The model is sketched in
figure C 2.
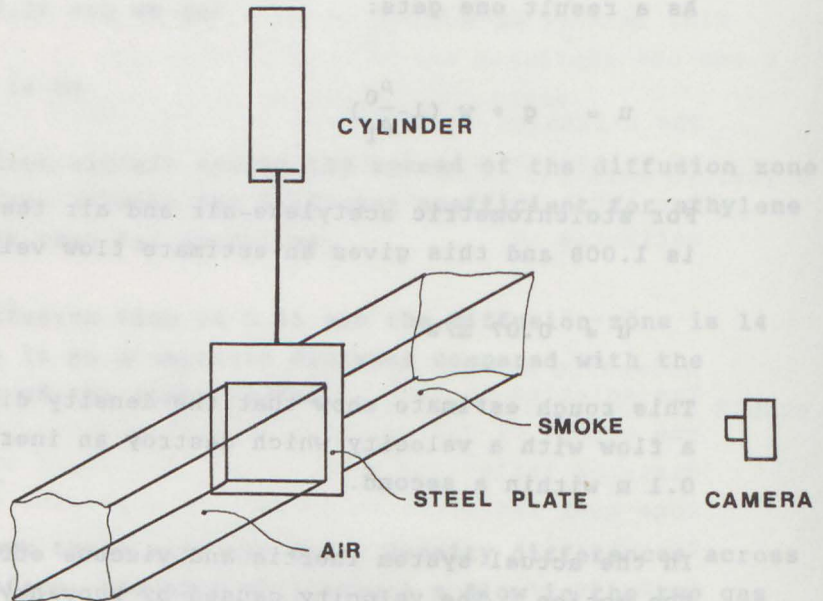
Figure C 2 :
Slide valve model for mixing tests.

The steel plate could divide the channel into two sections.
In a test one of these sections was filled with smoke from a
smoke bomb. The other section was filled with air. When
the steel plate was removed the mixing process was observed
photographically.

Figure C.3 shows a photograph taken 271 msec after the steel
plate started to move, which is about the same time is takes
to carry out a detonation test. The observed mixing zone is
less than 60 mm in width. (See also Figure 5.16)
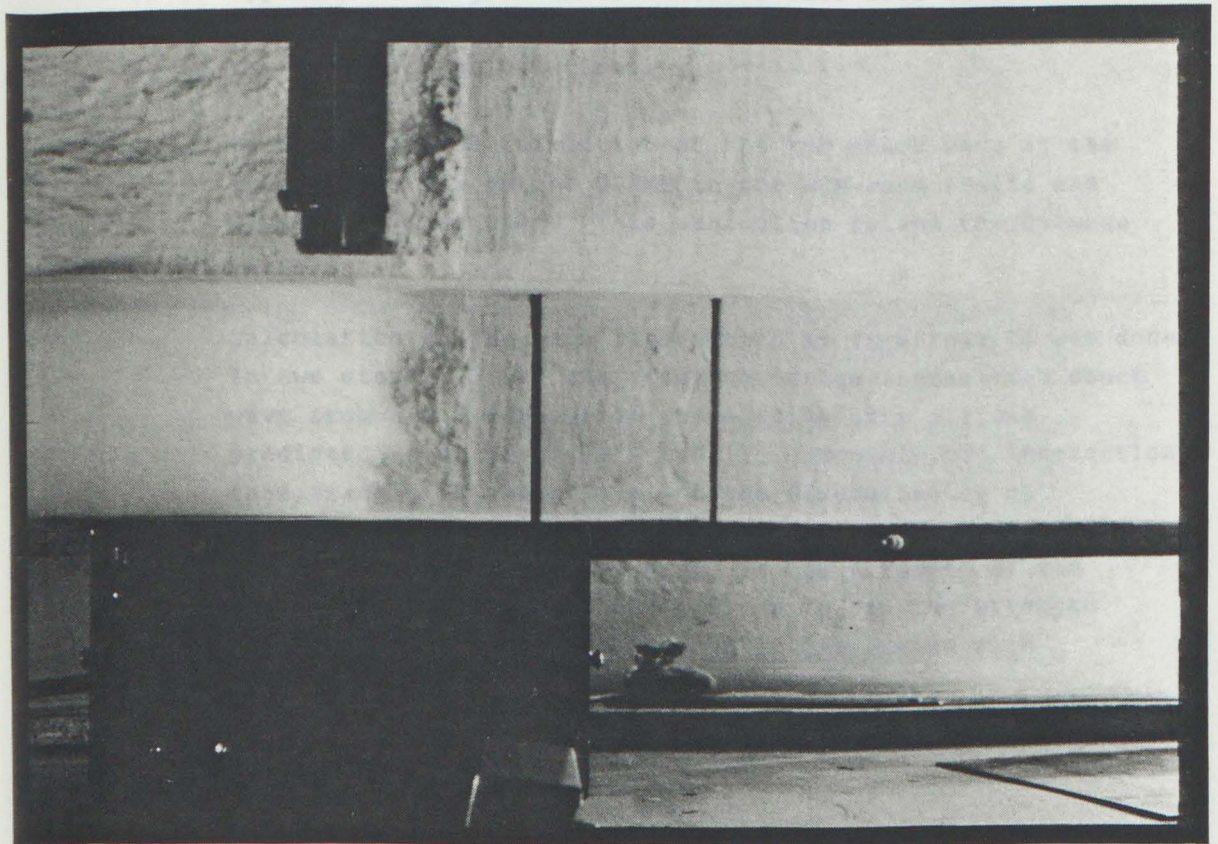
Figure C 3 :
   Photograph taken 271 msec after removal of slide plate
   showing the mixing process betwween smoke and air in the
   slide wave model.

One concludes from these calculations and the model tests
that especially the buoyancy effect will cause serious
mixing across the inert zone if the test times are several
tenths of a second or longer. Therefore it is necessary to
have fast-acting slide valves and to carry out the
detonation test within 300 msec as in this experiment.

Figure C.3.1

Photograph taken 171 msec after removal of slide plate
showing the mixing process between gases and air in the
slide wave model.

APPENDIX D

WAVE INTERACTION WITH THE INTERFACES

In a re-initiation of detonation experiments the transmitted shock wave will interact with the discontinuity at interface II. The reflected wave will be weak since the properties of air and fuel-air are about the same. The purpose of this appendix is to give an estimate of this wave interaction and to discuss the simplification by neglecting Interface II in the numerical calculations.

To calculate the refraction of the the shock wave at the interfaces, subroutine GLIMM in the RCM-code (Saito and Glass,1979) was used. This subroutine solves the Riemann problem.

Calculation of the wave interaction at Interface II was done in two steps. First the strength of the transmitted shock wave from a C-J detonation propagating into air was predicted (i.e. Paterson's model). Secondly the interaction this trasmitted shock wave and the discontinuity at Interface II was predicted. The results of the predictions are shown in Table D 1 . p_1/p_0 is the strength of the transmitted shock wave into air. p_2/p_0 is the strength of the transmitted shock wave after ineraction with Interface II.

Table D 1 :Predicted shock strength

p_1/p_0 : detonation refacting into air.

p_2/p_0 : after interaction with Interface II

Φ	p_{CJ}/p_0	p_1/p_0	p_2/p_0
0.6	15.37	12.83	12.77
0.8	17.63	14.79	14.69
1.0	19.13	15.99	15.87
1.2	20.14	16.82	16.73

C_2H_2-AIR
t = 25 C

It is only a small difference in shock strength between the incoming wave and the transmitted wave at Interface II.

To check the approximation of neglecting Interface II in the numerical calculations the strength of the transmitted shock wave from a C-J detonation propagating directly into fuel-air was predicted. The results are shown in Table D 2 .

Table D 2 :Predicted shock strength

p_3/p_0 : detionation refacting into fuel-air

Φ	p_{CJ}/p_0	p_3/p_0
0.6	15.37	12.79
0.8	17.63	14.72
1.0	19.13	15.90
1.2	20.14	16.75

C_2H_2-AIR
t = 25 C

There are only a small deviation in shock strength between
p_3/p_0 and p_2/p_0 in table D 1 . The approximation of
neglecting Interface II in the numerical calculations should
therefore not result in major errors.

APPENDIX E

USE OF DATA REDUCTION PROGRAMMES

This appendix shows the terminal display when the data
reduction programmes are used.

All the underlined words are the answers the user must type
in.

Two programmes were used to create one plot. The first
programme named HSDET# read the raw data and created
plotting file(s). Secondly a program named DETPL# was used
to plot this file. HSDET0 created in addition to plotting
files also a data file showing the experimental conditions.

The resulting plots from running the programmes follows the
printouts of the terminal display.

```
.RUN HSDET0

    TEST NUMBER ? : 18

    NUMBER OF CHANNELS ? (1-9) :5

    1    4.7940
    2    8.1360
    3    5.8561
    4    8.5077
    5    9.4620

    CHANGE SCALING FACTOR ? Y/N : Y

    1    4.7940

    CHANGE SCALING FACTOR ? Y/N : N

    2    8.1360

    CHANGE SCALING FACTOR ? Y/N : N

    3    5.8561

    CHANGE SCALING FACTOR ? Y/N : Y

    SCALING FACTOR ? (Bar/V):7.643

    4    8.5077

    CHANGE SCALING FACTOR ? Y/N : N

    5    9.4620

    CHANGE SCALING FACTOR ? Y/N : N

    1    4.7940
    2    8.1360
    3    7.6430
    4    8.5077
    5    9.4620

    CHANGE SCALING FACTOR ? Y/N : N

    SAMPLE NUMBER FOR THE MEAN VALUES ? :100

    1    0.0000
    2    1.0000
    3    2.6000
    4    3.6000
    5    4.6000

    CHANGE TRANSDUCER POSITION ? Y/N : N

    INERT REGION ? Y/N : Y

    2.0000

    CHANGE THE INERT REGION POSITION ? Y/N : N
```

DATO : 01-MAR-84

KL.SLETT : 09:45:39C

KANAL NR. : 1
SAMPLE RATE : 1
DELAY TIME : 1
STARTADR. : 0
ANTALL MÅLEPUNKTER : 16383

DATO : 01-MAR-84

KL.SLETT : 09:45:39C

KANAL NR. : 2
SAMPLE RATE : 1
DELAY TIME : 1
STARTADR. : 0
ANTALL MÅLEPUNKTER : 16383

DATO : 01-MAR-84

KL.SLETT : 09:45:39C

KANAL NR. : 3
SAMPLE RATE : 1
DELAY TIME : 1
STARTADR. : 0
ANTALL MÅLEPUNKTER : 16383

DATO : 01-MAR-84

KL.SLETT : 09:45:39C

KANAL NR. : 4
SAMPLE RATE : 1
DELAY TIME : 1
STARTADR. : 0
ANTALL MÅLEPUNKTER : 16383

DATO : 01-MAR-84

KL.SLETT : 09:45:39C

KANAL NR. : 5
SAMPLE RATE : 1
DELAY TIME : 1
STARTADR. : 0
ANTALL MÅLEPUNKTER : 16383

                       1 - 2   :1888.2
                       2 -AIR :1888.2
                      AIR- 3   :1174.6
                       3 - 4   :1555.7
                       4 - 5   :1939.5

STOP --

.TYPE D83018.DAT

```
              DETONATION TRANSMISSION ACROSS AN INERT REGION
                            IDF-SINTEF 15
```

```
        TEST NO.:018     DATE :01-MAR-84     TIME :09:45:39

           TEMPERATURE :    18.0 C          PRESSURE : 737 Torr

                        LENGTH (M)                GAS COMP.
DONOR SECTION      :        5.0              7.75%C2H2-AIR
INERT SECTION      :         .10                  AIR
ACCEPTOR SECTION   :        3.0              7.75%C2H2-AIR
BOOSTER SECTION    :        1.75             C2H2+1.5 O2
```

```
     FLOWMETERS :              FUEL                  OXIDIZER

                    RANGE (%)   PRES.(Ato)   RANGE (%)   PRES.(Ato)

DONOR SECTION    :    18.9         1.5         37.0         3.0
INERT SECTION    :                             20.0
ACCEPTOR SECTION :    18.9         1.5         37.0         3.0
BOOSTER SECTION  :    14.0         1.5         20.0         1.5
```

MEASURING POINT	1	2	3	4	5	6
TRANSDUCER	603B	603B	603B	603B	603B	RADAR
TRANSDUCER NO	50188	100590	100589	50187	123488	
TRANS. CALL. (pC/bar)	6.50	4.89	4.49	5.94	4.68	
AMPLIFIER MODEL	504A5	5001	568	568	5001	
AMPLIFIER NO	SN0554	SN17841	SN2164	SN2156	SN14948	
SENSITIVITY	5.0	8.00	3.5	5.0	8.0	
RANGE (bar/V)	5	5	10	10	5	
FILTER (kHz)	150	180	--	—	15	

CHANNEL NO:	1	2	3	4	5
CHANNEL CALL (Vout/Vin)	0.9133	1.0116	1.0199	0.9894	.9033
TRANSDUCER POS. (M)	0.000	1.000	2.600	3.600	4.600
SAMPLE RATE	1	1	1	1	1
DELAY TIME	1	1	1	1	1
SCALING FACTOR (Bar/V)	4.794	8.136	7.643	8.508	9.462
TIME OF ARRIVAL (Mic.Sec.)	0.6	530.2	1570.6	2213.4	2729.0

```
VELOCITIES (M/S) :                          CJ-INERT INTERFACE (M) :  2.000

                        1 - 2  :1888.2
                        2 -AIR :1888.2
                        AIR- 3 :1174.6
                        3 - 4  :1555.7
                        4 - 5  :1939.5
```

TIME DELAY : .24 SEK   COUNT DOWN : 2.10

COMMENTS : ADAPTER TRANSDECER # 4 WAS DESTROIED. NEW GREEN CABLE ON #4 BEFORE
          SHOT
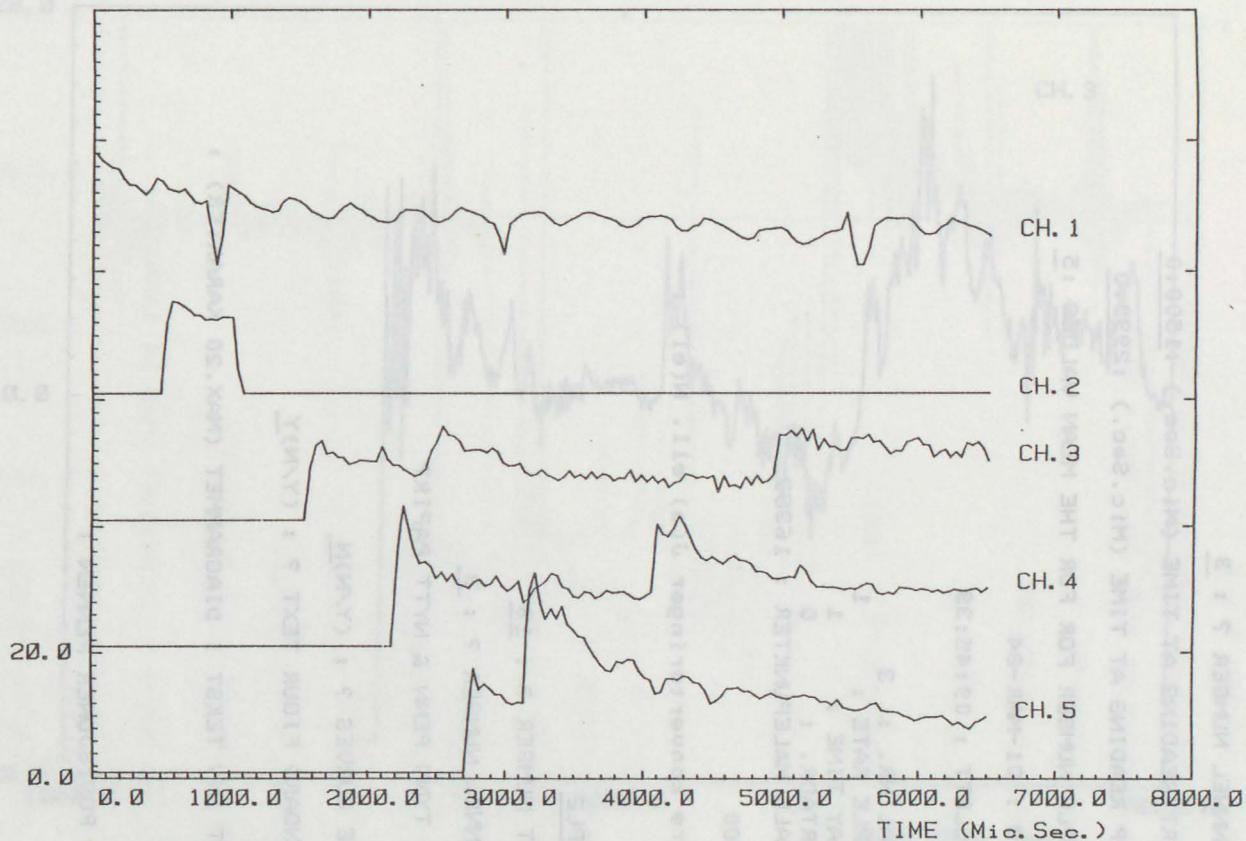
RUN DETPLO

TEST NUMBER ? : 18

PAUSE -- TYNN PENN & NYTT PAPIR?

PAUSE -- POSISJONER PENNEN !

PAUSE -- POSISJONER PENNEN !

PAUSE -- POSISJONER PENNEN !

PAUSE -- POSISJONER PENNEN !

PAUSE -- POSISJONER PENNEN !

STOP -- DIAGRAMMENE ER FERDIGE!

TEST NO.:018   DATE :01-MAR-84
7.75%C2H2-AIR / AIR (.10 m) / 7.75%C2H2-AIR
IDF-SINTEF 15

.RUN HSDET2

     TEST NUMBER ? : <u>18</u>

     CHANNNEL NUMBER ? : <u>3</u>

     START READING AT TIME (Mic.Sec.) :<u>1500.0</u>

     STOP READING AT TIME (Mic.Sec.) :<u>2990.0</u>

     SAMPLE NUMBER FOR FOR THE MEAN VALUES :<u>5</u>

     DATO : 01-MAR-84

     KL.SLETT : 09:45:39

     KANAL NR. : 3
     SAMPLE RATE : 1
     DELAY TIME : 1
     STARTADR. : 0
     ANTALL MÅLEPUNKTER : 16383
 745
  7.643000

     Flere konverteringer J(a) ell. N(ei) :

STOP --

.RUN DETPL2

     TEST NUMBER ? : <u>18</u>

     CHANNEL NUMBER ? : <u>3</u>

PAUSE -- TYNN PENN & NYTT PAPIR?

     MORE CURVES ? : (Y/N)<u>N</u>

     STANDARD FIGUR TEXT ? : (Y/N)<u>Y</u>

     TAST INN TEKST I DIAGRAMMET (MAX.20 KARAKTER) :

<u>CH.3</u>

PAUSE -- POSISJONER PENNEN !
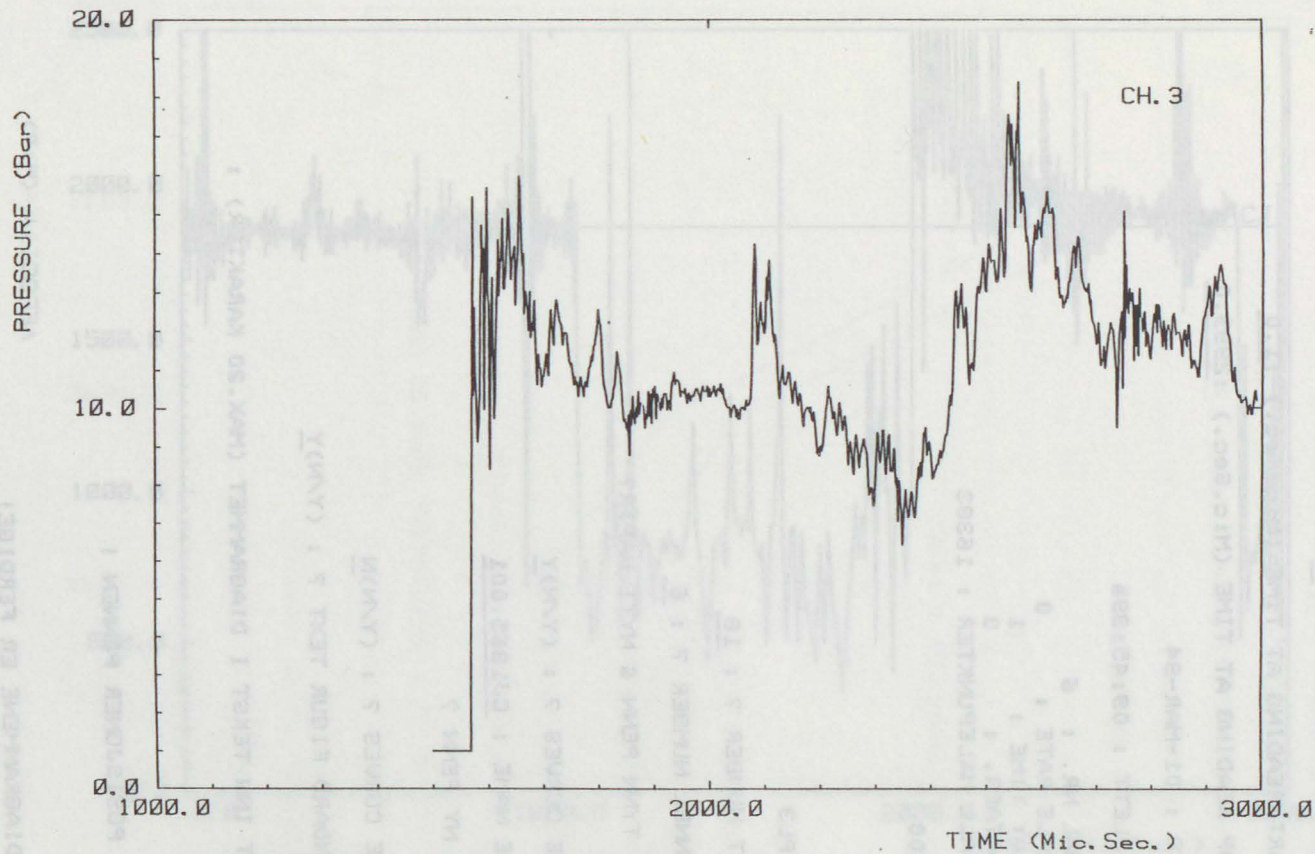
STOP -- DIAGRAMMENE ER FERDIGE!

PRESSURE (Bar)

20.0

CH. 3

10.0

0.0

1000.0   2000.0   3000.0

TIME (Mic.Sec.)

TEST NO.:018   DATE :01-MAR-84
7.75%C2H2-AIR /   AIR (.10 m) / 7.75%C2H2-AIR
IDF-SINTEF 15

```
.RUN HSDET3

      TEST NUMBER ? : 18

      CHANNNEL NUMBER ? : 6

      START READING AT TIME (Mic.Sec.) :1.0

      STOP READING AT TIME (Mic.Sec.) :2999.0

      DATO : 01-MAR-84

      KL.SLETT : 09:45:39ä

      KANAL NR. :   6
      SAMPLE RATE :      0
      DELAY TIME :      1
      STARTADR. :       0
      ANTALL MÅLEPUNKTER : 16383
  641
  0.9000000
STOP --

.

.RUN DETPL3

      TEST NUMBER ? : 18

      CHANNEL NUMBER ? : 6

PAUSE -- TYNN PENN & NYTT PAPIR?

      MORE CURVES ? : (Y/N)Y

      FILE NAME : CJ1865.001

PAUSE -- NY PENN ?

      MORE CURVES ? : (Y/N)N

      STANDARD FIGUR TEXT ? : (Y/N)Y

      TAST INN TEKST I DIAGRAMMET (MAX.20 KARAKTER) :

CJ

PAUSE -- POSISJONER PENNEN !

STOP -- DIAGRAMMENE ER FERDIGE!
```
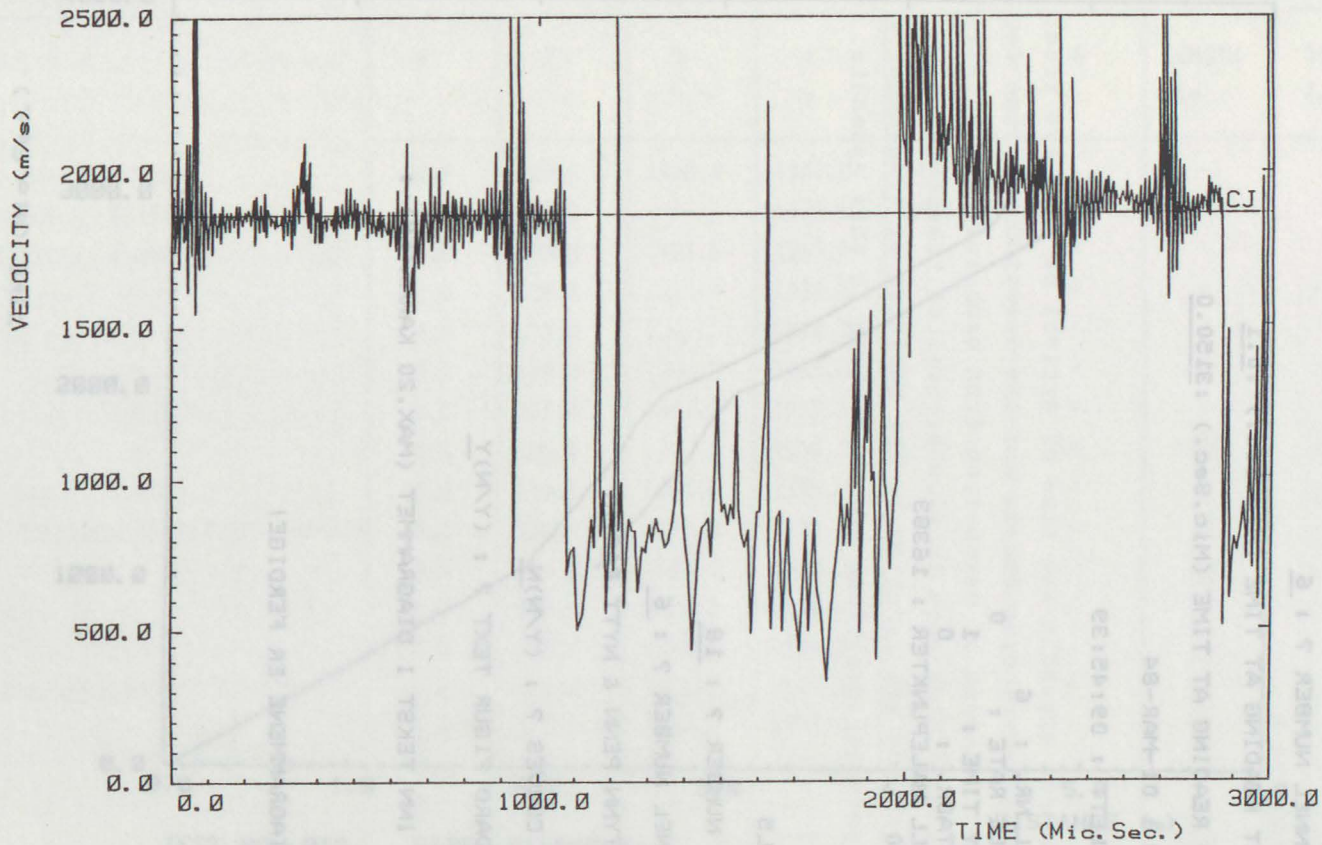
TEST NO.:018   DATE :01-MAR-84
7.75%C2H2-AIR /   AIR (.10 m) / 7.75%C2H2-AIR
IDF-SINTEF 15

```
.RUN HSDET6

     TEST NUMBER ? : 18

     CHANNNEL NUMBER ? : 6

     START READING AT TIME (Mic.Sec.) :0.1

     STOP READING AT TIME (Mic.Sec.) :3150.0

     DATO : 01-MAR-84

     KL.SLETT : 09:45:39


     KANAL NR. :   6
     SAMPLE RATE :        0
     DELAY TIME :       1
     STARTADR. :        0
     ANTALL MÅLEPUNKTER : 16383
 0.9000000
STOP --

.

.RUN DETPL5

     TEST NUMBER ? : 18

     CHANNEL NUMBER ? : 6

PAUSE -- TYNN PENN & NYTT PAPIR?

     MORE CURVES ? : (Y/N)N

     STANDARD FIGUR TEXT ? : (Y/N)Y

     TAST INN TEKST I DIAGRAMMET (MAX.20 KARAKTER) :


STOP -- DIAGRAMMENE ER FERDIGE!
```
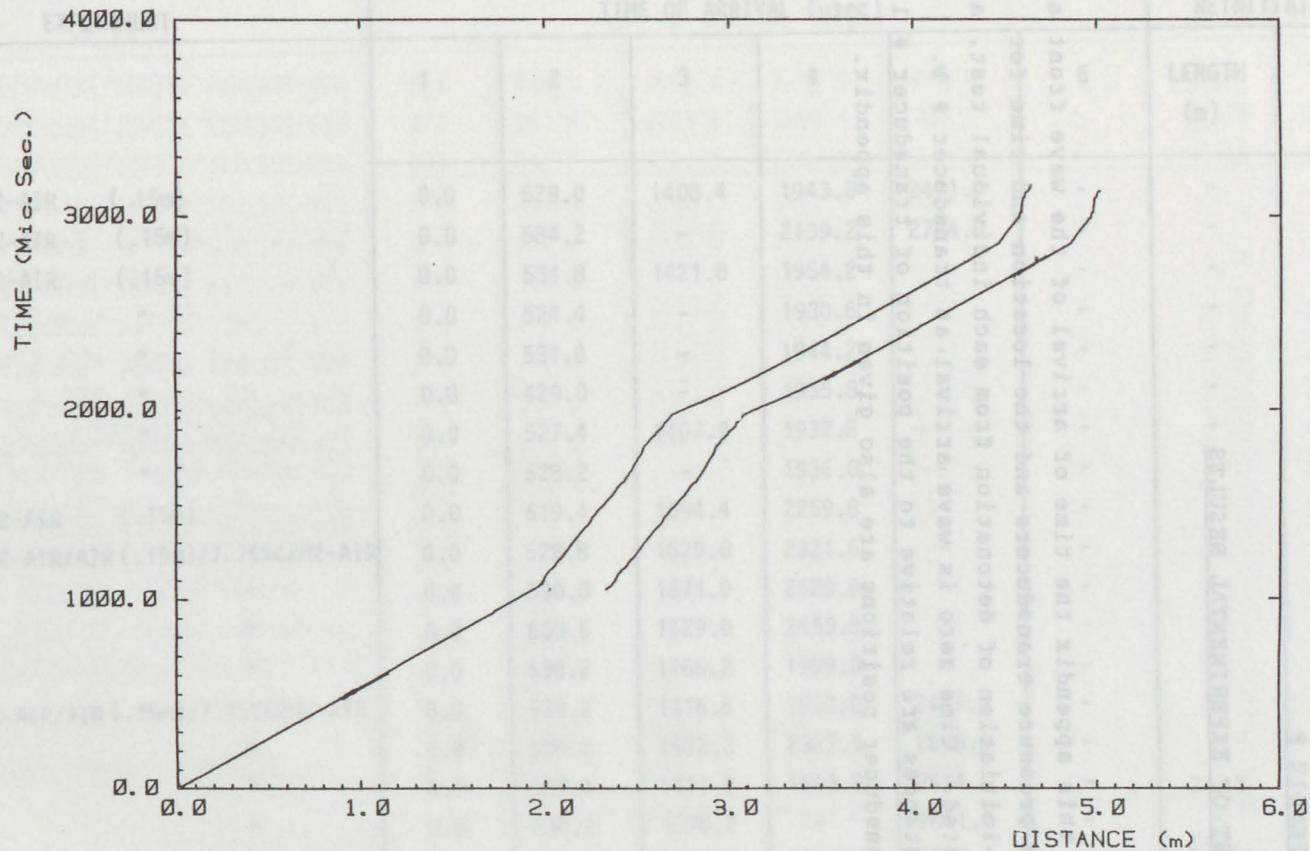
TEST NO.:010   DATE :01-MAR-84
7.75%C2H2-AIR / AIR (.10m) / 7.75%C2H2-AIR
IDF-SINTEF 15

APPENDIX F

LIST OF EXPERIMENTAL RESULTS

In this appendix the time of arrival of the wave front at
the pressure transducers and the location and time for
re-initiation of detonation from each individual test, are
listed. Time zero is wave arrival at transducer # 1.
Distances are relative to the position of transducer # 1.
Transducer positions are also given in this appendix.
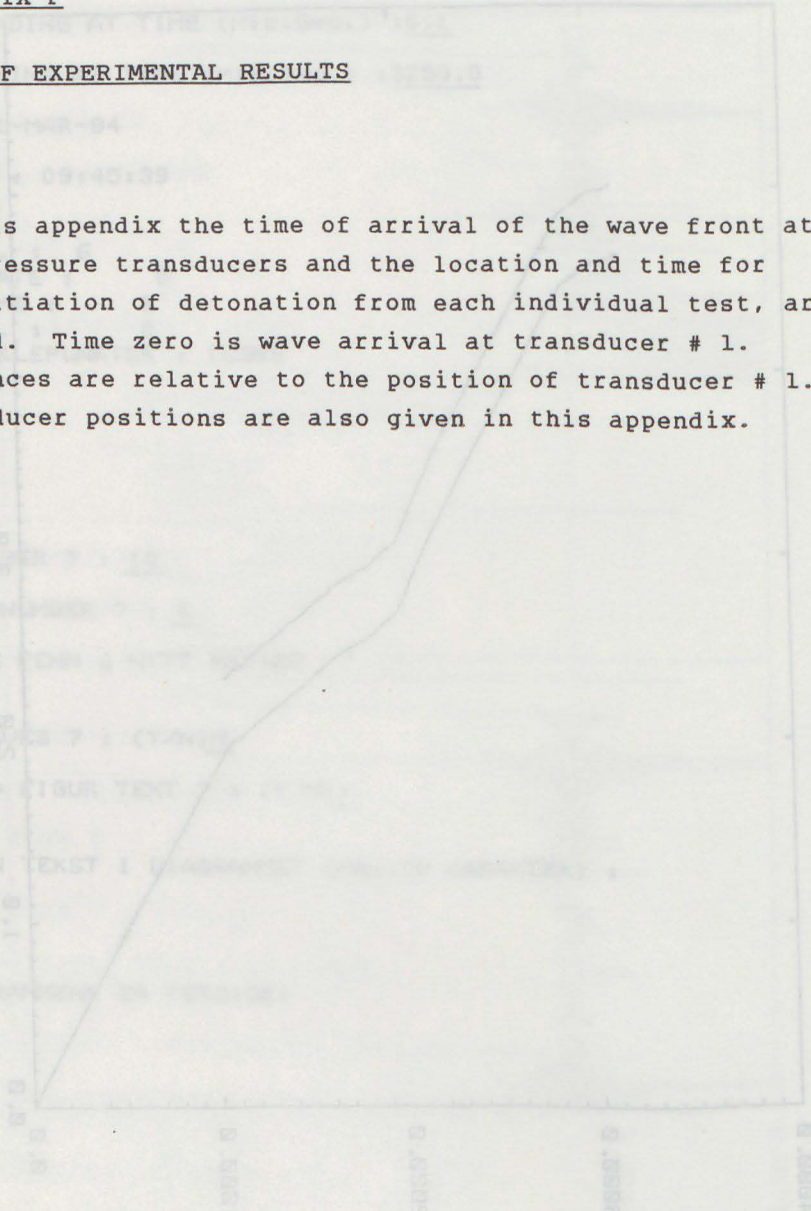
SHOT	EXPERIMENT	TIME OF ARRIVAL (μsec)						REINITIATION	
		1	2	3	4	5	6	LENGTH (m)	TIME (μsec.)
1	7.75% C2H2-AIR (.15m)	0.0	529.0	1408.4	1943.0	2471.0	-	-	-
2	5.07% C2H2-AIR (.15m)	0.0	584.2	-	2139.2	2724.8	-	-	-
3	7.75% C2H2-AIR (.15m)	0.0	531.8	1421.0	1954.2	-	-	-	-
4	" "	0.0	524.4	-	1930.6	-	-	-	-
5	" "	0.0	531.0	-	1944.2	-	-	-	-
6	" "	0.0	429.0	-	1935.8	-	-	-	-
7	" "	0.0	527.4	1407.0	1932.8	-	-	-	-
8	" "	0.0	528.2	-	1936.0	-	-	-	-
9	4.00% C2H2-AIR (.15m)	0.0	619.4	1694.4	2259.8	-	-	-	-
10	7.75% C2H2-AIR/AIR (.15m)/7.75%C2H2-AIR	0.0	528.8	1629.0	2321.6	-	-	-	-
11	" "	0.0	530.0	1671.0	2520.8	-	-	-	-
12	" "	0.0	530.6	1629.0	2455.8	-	-	-	-
13	" "	0.0	530.2	1466.2	1999.0	-	-	-	-
14	7.75%C2H2-AIR/AIR (.10m)/7.75%C2H2-AIR	0.0	530.2	1416.6	1950.0	2487.0	-	-	-
15	" "	0.0	530.2	1582.2	2327.0	2833.0	-	-	-
16	" "	0.0	529.4	1411.8	1943.8	2914.6	-	2.45	1310
17	" "	0.0	530.2	1570.2	-	2611.4	-	-	-
18	" "	0.0	530.2	1570.6	2213.4	2729.4	-	3.08	1970

SHOT	EXPERIMENT	TIME OF ARRIVAL (µsec)						REINITIATION	
		1	2	3	4	5	6	LENGTH (m)	TIME (µsec.)
19	7.75%C2H2-AIR(.10m)/7.75%C2H2-AIR	0.0	528.2	1567.8	2249.4	2756.2	-	3.31	2050
20	"	0.0	528.6	1565.0	2194.2	2708.6	-	3.13	1920
21	"	0.0	529.8	1569.4	2190.4	2703.6	-	3.03	1920
22	"	0.0	529.0	1510.2	2022.2	-	-	2.58	1450
23	"	0.0	531.4	1458.2	1955.8	-	-	2.43	1320
24	"	0.0	529.8	1571.8	2215.8	2725.4	-	3.24	1960
25	7.00%C2H2-AIR/AIR(.10m)/7.00%C2H2-AIR	0.0	540.2	1605.0	2475.4	3183.4	-	4.35	3020
26	"	0.0	539.0	1604.2	2473.0	3134.6	-	4.01	2860
27	7.37%C2H2-AIR/AIR(.10m)/7.37%C2H2-AIR	0.0	533.0	1585.8	2438.6	2979.8	-	3.83	2570
28	8.44%C2H2-AIR/AIR(.10m)/8.44%C2H2-AIR	0.0	521.8	1549.0	2052.2	2573.0	-	2.72	1560
29	9.14%C2H2-AIR/AIR(.10m)/9.14%C2H2-AIR	0.0	514.2	1508.6	1983.4	-	-	2.62	1470
30	6.53%C2H2-AIR/AIR(.10m)/6.53%C2H4-AIR	0.0	546.6	1624.2	2556.2	-	-	2.75	1580
31	5.91%C2H4-AIR/AIR(.10m)/5.91%C2H4-AIR	0.0	558.2	-	2586.6	-	-	*	*
32	5.29%C2H4-AIR/AIR(.10m)/5.29%C2H4-AIR	0.0	566.6	1671.0	2637.8	-	-	*	*
33	8.44%C2H4-AIR/AIR(.10m)/5.29%C2H2-AIR	0.0	521.0	1545.0	2052.6	2572.6	-	*	*
34	7.01%C2H2-AIR/AIR(.10m)/9.14%C2H2-AIR	0.0	540.2	1594.2	2101.0	2615.4	-	2.70	1600
35	7.01%C2H2-AIR/AIR(.10m)/7.73%C2H2-AIR	0.0	541.4	1607.4	2465.4	2999.8	-	4.04	2730
36	6.53%C2H4-AIR/AIR(.10m)/9.14%C2H2-AIR	0.0	548.2	1609.4	2124.6	2642.6	-		

SHOT	EXPERIMENT	TIME OF ARRIVAL (µsec)						REINITIATION	
		1	2	3	4	5	6	LENGTH (m)	TIME (µsec.)
37	4.66%C2H4-AIR/AIR(.10m)/9.14%C2H2-AIR	0.0	578.2	1686.6	2203.8	-	-	2.75	1780
38	6.53%C2H4-AIR/AIR(.10m)/7.73%C2H2-AIR	0.0	547.0	1608.6	2479.4	-	-	4.08	2900
39	6.53%C2H4-AIR/AIR(.10m)/8.44%C2H2-AIR	0.0	547.8	1613.0	2276.2	2785.4	-	3.33	2140
40	9.14%C2H2-AIR/AIR(.10m)/7.01%C2H2-AIR	0.0	515.4	1537.0	2328.6	2829.0	-	3.57	2290
41	9.14%C2H2-AIR/AIR(.10m)/7.73%C2H2-AIR	0.0	516.2	1534.0	2175.8	2690.2	-	3.12	1960
42	7.73%C2H2-AIR/AIR(.15m)/7.73%C2H2-AIR	0.0	530.6	1632.2	2515.8	3068.2	-	4.06	2790
43	9.14%C2H2-AIR/AIR(.15m)/9.14%C2H2-AIR	0.0	516.6	1582.2	2103.4	2619.8	-	2.87	1770
44	8.44%C2H2-AIR/AIR(.15m)/8.44%C2H2-AIR	0.0	524.6	1603.8	2311.0	2803.0	-	3.32	2160
45	7.37%C2H2-AIR/AIR(.15m)/7.37%C2H2-AIR	0.0	536.6	1645.4	2553.0	3393.4	-	4.65	3380
46	9.14%C2H2-AIR/AIR(.20m)/9.14%C2H2-AIR	0.0	516.6	1627.0	2507.8	3013.8	-	4.03	2710
47	8.79%C2H2-AIR/AIR(.20m)/8.79%C2H2-AIR	0.0	520.2	1648.6	2548.6	3179.0	-	4.28	2990
48	8.44%C2H2-AIR/AIR(.20m)/8.44%C2H2-AIR	0.0	522.2	1649.8	2549.4	-	-	420	2850
49	" "	0.0	523.0	1647.0	2351.0	-	-	3.41	2220
50	" "	0.0	525.4	1658.2	2391.0	2886.6	-	3.39	2250
51	" "	0.0	523.0	1647.4	2364.2	2856.6	-	3.29	2190
52	" "	0.0	525.0	1655.8	2474.6	2956.6	-	3.86	2540
53	" "	0.0	523.4	1643.0	2283.4	2804.6	-	3.32	2100
54	" "	0.0	523.8	1655.8	2417.8	2903.8	-	3.49	2300

SHOT	EXPERIMENT	TIME OF ARRIVAL (μsec)						REINITIATION	
		1	2	3	4	5	6	LENGTH (m)	TIME (μsec.)
55	8.44%C2H2-AIR/AIR(.20m)/8.44%C2H2-AIR	0.0	522.6	1655.8	2361.8	2860.6	–	3.42	2240
56	" "	0.0	523.0	1655.4	2555.4	3167.0	–	4.04	2890
57	" "	0.0	523.4	1651.8	2535.4	3103.0	–	4.13	2850
58	9.14%C2H2-AIR/AIR(.20m)/9.14%C2H2-AIR	0.0	515.8	1633.4	2155.0	2653.0	–	3.09	1820
59	7.73%C2H2-AIR/AIR(.20m)/7.73%C2H2-AIR	0.0	533.0	1681.0	2618.2	3502	–	4.74	3680
60	9.14%C2H2-AIR/AIR(.20m)/9.14%C2H2-AIR	0.0	518.2	1635.0	2476.2	3003.4	–	3.96	2670
61	8.44%C2H2-AIR/AIR(.20m)/8.44%C2H2-AIR	0.0	524.6	1657.8	2567.0	3245.4	–	3.85	2720
62	7.73%C2H2-AIR/AIR(.20m)/7.73%C2H2-AIR	0.0	531.4	1676.2	2620.2	–	–	4.76	3570
63	8.44%C2H2-AIR/AIR(.20m)/8.44%C2H2-AIR	0.0	524.2	1659.8	2526.2	–	–	4.22	2780
64	7.73%C2H2-AIR/AIR(.20m)/7.73%C2H2-AIR	0.0	530.6	1683.8	2584.2	3156.6	–	3.86	2750
65	" "	0.0	531.8	1687.8	–	3573.0	–	> 4.95	–
66	9.14%C2H2-AIR/AIR(.20m)/9.14%C2H2-AIR	0.0	517.0	1643.0	2531.4	3061.4	–	4.19	2820
67	9.14%C2H2-AIR/AIR(.20m)/9.14%C2H2-AIR	0.0	–	1641.4	2519.4	3061.8	–	4.02	2750
68	" "	0.0	518.2	1640.2	2512.6	2973.0	–	3.88	2590
69	" "	0.0	517.8	1637.4	2159.0	2676.6	–	2.87	1720
70	" "	0.0	515.8	1631.4	2149.4	2665.4	–	2.90	1720
71	" "	0.0	517.4	1637.8	2395	2882.6	–	3.36	2240

SHOT	EXPERIMENT	TIME OF ARRIVAL (μsec)						REINITIATION	
		1	2	3	4	5	6	LENGTH (m)	TIME (μsec.)
72	7.73%C2H2-AIR/AIR(.50m)	0.0	515.8	1190.6	1364.6	1974.6	4054.2	–	–
73	" "	0.0	612.2	1185.8	1358.2	1966.2	4044.6		
74	" "	0.0	531.8	1186.6	1359.4	1963.8	4028.6		
75	" "	0.0	528.6	1179.4	1349.8	1949.8	3998.2		
76	" "	0.0	531.4	1185.4	1353.8	1955.0			
77	" "	0.0	531.8	1186.2	1956.2	2930.6	4000.2		
78	9.14%C2H2-AIR/AIR(.50m)	0.0	515.8	1146.6	1904.6	2861.0	3906.2		
79	7.01%C2H2-AIR/AIR(.50m)	0.0	540.6	1205.0	1985.4	2974.6	4035.8		
80	4.79%C2H2-AIR/AIR(.50m)	0.0	590.6	1308.6	2144.6	3232.6	4411.4		
81	6.53%C2H4-AIR/AIR/(.50m)	0.0	545.8	1213.4	1993.8	3009.4	4109.8		
82	7.73%C2H2-AIR/AIR(.50m)	0.0	531.4	1184.6	1357.0	1953.0			
83	7.73%C2H2-AIR(.50m)	0.0	531.0	1145.0	1249.8	1593.8			
84	" "	0.0	532.0	1149.0	1254.6	1599.0			
85	7.73%C2H2-AIR/AIR(.50m)	0.0	532.6	1187.8	1361.0	1958.2			
86	" "	0.0	529.4	–	1353.8	1946.6			
87	" "	0.0	531.0	1184.6	1357.8	1951.4			

TRANSDUCER POSITION (m)

TRANSDUCER

SHOT	1	2	3	4	5	6
14-41	0.0	1.0	2.60	3.60	4.60	
1-13&42-44	0.0	1.0	2.65	3.65	4.65	
45-71	0.0	1.0	2.70	3.70	4.70	
72-76&82-87	0.0	1.0	2.15	2.35	3.0	5.00
77-81	0.0	1.0	2.15	3.00	4.00	5.00